ΕΛΛΗΝΙΚΗ ΔΗΜΟΚΡΑΤΙΑ
Εθνικόν και Καποδιστριακόν Πανεπιστήμιον Αθηνών
ΙΔΡΥΘΕΝ ΤΟ 1837

ΣΧΟΛΗ ΕΠΙΣΤΗΜΩΝ ΥΓΕΙΑΣ

ΤΜΗΜΑ ΦΑΡΜΑΚΕΥΤΙΚΗΣ

Τομέας Φαρμακευτικής Τεχνολογίας

ΔΙΠΛΩΜΑ ΜΕΤΑΠΤΥΧΙΑΚΩΝ ΣΠΟΥΔΩΝ «ΒΙΟΜΗΧΑΝΙΚΗ ΦΑΡΜΑΚΕΥΤΙΚΗ»

«ΑΝΑΛΥΣΗ ΦΑΡΜΑΚΟΚΙΝΗΤΙΚΩΝ ΔΕΔΟΜΕΝΩΝ ΜΕ ΧΡΗΣΗ ΤΗΣ ΑΡΧΗΣ ΤΟΥ ΠΕΠΕΡΑΣΜΕΝΟΥ ΧΡΟΝΟΥ ΑΠΟΡΡΟΦΗΣΗΣ ΚΑΙ ΔΙΑΛΥΣΗΣ ΜΕ ΕΜΦΑΣΗ ΣΕ ΦΑΡΜΑΚΑ ΒΙΟΑΠΑΛΛΑΓΗΣ (BIOWAIVERS)»

Διπλωματική Εργασία

ΣΙΜΙΤΟΠΟΥΛΟΣ ΑΝΤΩΝΙΟΣ, ΧΗΜΙΚΟΣ, 7452142206009

Αθήνα, 2024

ΕΛΛΗΝΙΚΗ ΔΗΜΟΚΡΑΤΙΑ
Εθνικόν και Καποδιστριακόν Πανεπιστήμιον Αθηνών
ΙΔΡΥΘΕΝ ΤΟ 1837

FACULTY OF HEALTH SCIENCES

DEPARTMENT OF PHARMACY

Sector of Pharmaceutical Technology

POSTGRADUATE DIPLOMA (M.Sc.) «INDUSTRIAL PHARMACY»

«ANALYSIS OF PHARMACOKINETIC DATA UTILIZING THE FINITE ABSORPTION FINITE DISSOLUTION TIME CONCEPTS WITH EMPHASIS ON BIOWAIVERS»

Dissertation

SIMITOPOULOS ANTONIOS, CHEMIST, 7452142206009

Athens, 2024

ΤΡΙΜΕΛΗΣ ΕΠΙΤΡΟΠΗ

Παναγιώτης Μαχαίρας, Ομότιμος Καθηγητής, Τμήμα Φαρμακευτικής ΕΚΠΑ

Παρασκευάς Δάλλας, Αναπληρωτής Καθηγητής, Τμήμα Φαρμακευτικής ΕΚΠΑ

Δημήτριος Ρέκκας, Καθηγητής, Τμήμα Φαρμακευτικής ΕΚΠΑ

Abstract

The concept of infinite time in oral drug absorption, rooted in early pharmacokinetics, was initially formulated by H. Dost in 1953, drawing on H. Bateman's 1908 function for nuclear isotope decay. This premise, assuming first-order kinetics, proved to be physiologically unsound over the decades, significantly impacting the evolution of oral pharmacokinetics, bioavailability, and bioequivalence metrics. The Finite Absorption Time (F.A.T.) concept emerged as a corrective paradigm, leading to the development of Physiologically Based Finite Time Pharmacokinetic (PBFTPK) models. This thesis delves into the theoretical underpinnings of the F.A.T. concept, exploring its application to several BCS Class I biowaiver drugs. By examining and classifying drugs based on F.A.T. values, this study sheds light on its potential applications in drug absorption research and regulatory guidelines. The findings underscore the F.A.T. concept's relevance in assessing drug input rates, stochastic mean absorption time calculations, population analyses, in vitro-in vivo correlations, and bioequivalence guidelines.

Furthermore, this research endeavors to extend the understanding of drug dissolution dynamics through the development of a Temporal Biopharmaceutic Classification System (T-BCS). The T-BCS links the Finite Dissolution Time (F.D.T.) and Mean Dissolution Time (M.D.T.) for Class I/III drugs and Mean Dissolution Time for saturation (M.D.T.s.) for Class II/IV drugs. Through graphical estimation or fitting dissolution models to experimental data, coupled with the dose-to-solubility ratio (q) normalized by the actual volume of dissolution medium (900 mL), this framework provides insights into drug behavior across different dissolution themes. This integrated approach not only enhances our understanding of drug absorption kinetics but also offers a systematic framework for classifying drugs based on dissolution dynamics, thus contributing to the refinement of drug development and regulatory practices.

I express my gratitude to Dr. Panos Macheras

for introducing me to the world of research and nurturing my curiosity.

Special thanks to my dear friends who supported me both emotionally

and research-wise in the programming Python segments, making this journey even more fulfilling.

Table of Contents

Chapter 1

Introduction

In our body, drugs exist in a dynamic state where various processes such as dissolution, absorption, distribution, metabolism, and elimination take place simultaneously. This means that a detailed study of the behavior of drugs within the body, considered as a set of pathways, is essential. Such a study is expected to present challenges that are further complicated by the heterogeneity of various factors tied to the physiological system, such as age, fed or fasted state, regional differences in the body and disease status [1]. Overcoming these challenges and the complexity of the biological system has become possible through the invention of pharmacokinetic models. These models simplify the human body and take into account only those processes that are pharmacokinetically significant for the considered drug and system. These models are considered reliable and therapeutically valuable when they show high correlations with $in\ vivo$ results. A proven and reliable pharmacokinetic model for a specific drug can be used to "predict" its movement, i.e., distribution and elimination in the body. This prediction is typically portrayed as a concentration (C) of the drug in the blood over time (t) (Figure 1.1), which allows for a proper design of therapeutic and dosing regimens [1].

1. Compartmental models

Depicting a complex organism with a ”black box” in the initial approach is undoubtedly imaginative. This ”black box” was later referred to as a compartment, and this term is widely used in pharmacokinetics to describe a space or area in the body where the drug’s concentration is uniform throughout its extent, an equilibrium of concentrations within the compartment is rapid or, at least, much faster than other kinetic processes are taking place between compartments. This implies that within the compartment, there is homogeneous drug diffusion, resulting in uniform concentration changes. According to the compartment’s definition, it is simple to assume that a realistic model of the organism should consist of more than one compartment and its physiological significance is understood when we contemplate three real spaces with defined volumes and individually uniform composition, specifically, the plasma, the total extracellular fluid, and the intracellular fluid. With this understanding, we arrive at the concept of multi compartment models, where the organism is considered to be composed of two or more compartments, each with its own characteristics [1].

In pharmacokinetics, however, one is usually unable to define each of the compartments independently unless the drug’s kinetics are ideally described by a multi-compartmental model. In such cases, it is assumed that the drug is distributed between a ”central” compartment counterpart to the blood and one or two (rarely more) ”peripheral” compartments corresponding to to the areas of drug selectivity, like tissues due to high lipophilicity or high protein binding. Naturally, the rate of transfer of the drug between compartments is almost always different in both directions. This is a result of the different characteristics of each compartment, reflecting different rates of drug passage. Through pharmacokinetics, it is possible to numerically estimate the characteristics of each of the compartments, such as their volumes, distribution and elimination rate constants, and micro-constants that link them with other said compartments. Only the one-compartment model can be autarkic [1].

1..1 The one-compartment model of disposition

In the context of pharmacokinetic modeling, it is emphasized that the organism’s unidirectional perception predominates in cases where the drug’s distribution phase is much faster than its elim-

ination. In cases where the unidirectional model is applied, changes that occur in the blood drug levels are reflected in corresponding fluctuations in tissue drug levels. This underscores the importance of understanding and studying the changes in blood drug levels, as in the unidirectional model, the entire variation reflects the general change in drug concentration in the body. The above observations easily lead to the conclusion that the study of the unidirectional model provides a comprehensive picture of the drug's entire journey within the organism. In practice, the determination of drug concentration in blood plasma or urine and the corresponding concentration-time profile is the most common way to represent the drug's path within the organism [1]. The rapid intravenous bolus administration results in the entry of the entire administered dose of the drug into the general circulation. According to the one-compartment model, all tissues will rapidly equilibrate in terms of drug concentration. Since intravenous drug administration implies total drug delivery to the general circulation and, moreover, at an "instantaneous" rate, bioavailability is defined to be 100% in this case. However, orally administered dosage forms undoubtedly present a much higher degree of problematic bioavailability than non-intravenous injections and suppositories. This is because oral administration involves greater variation due to the complexity of the routes prior to absorption: degradation, dissolution, etc [1].

1..2 The two-compartment model of disposition

The fundamental principle of the one-compartment model is the assumption of rapid establishment of drug concentration equilibrium throughout the body. However, this assumption often proves to be inapplicable in reality. There are many drugs for which the distribution phase is not so "instantaneous," or more accurately, not significantly shorter than the elimination phase. When these drugs are administered intravenously (IV bolus), they do not exhibit the classic exponential concentration decline associated with the one-compartment model. The shape of the curve that typically emerges is shown in the diagram below (Figure 1.1). Curves of this type lead to the conclusion that the drug follows a pharmacokinetic model described by the two-compartment model [1,(Chapter 9)]. The reduction in drug concentration in both compartments occurs at the same rate following the re-establishment of pseudo-equilibrium. As a result, the ratio of the drug quantity in the two compartments remains constant throughout the distribution phase, and the model behaves approximately as a unidirectional one. Therefore, it is natural, according to the information provided, that

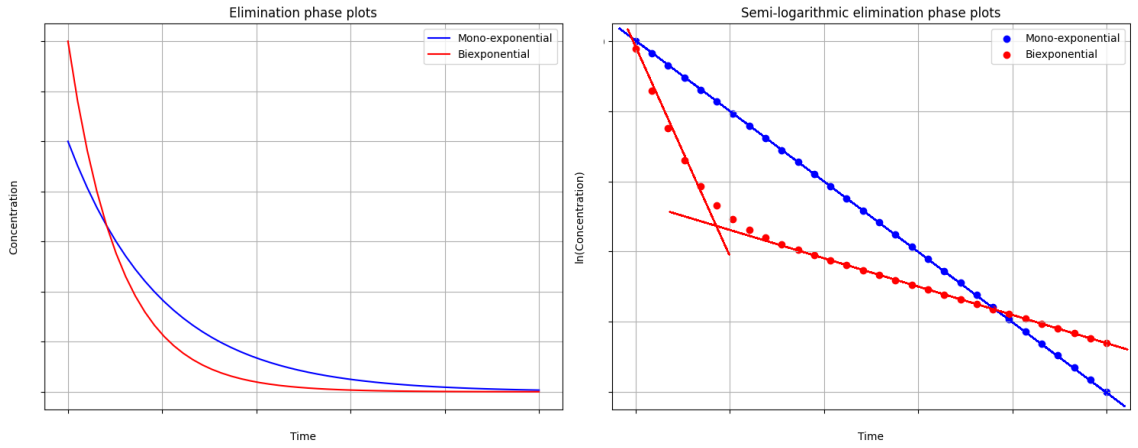

Figure 1.1: On the left side: Concentration - time profiles of drugs that follow one- (blue line) and two-compartment (red line) models of disposition. On the right side: Their corresponding semi-logarithmic depiction of the absorption data. The descending limb of the elimination phase can be described by a linear part in the one-compartment model, while for the two-compartment model two linear parts describe the elimination phase.

the decline in concentration after the re-establishment of pseudo-equilibrium follows the classical exponential decline [1].

To ascertain whether a drug follows one- or two-compartmental disposition, a close examination of the semi-logarithmic plot of natural logarithms of plasma concentrations versus time is conducted. If the semi-logarithmic plot resembles Figure 1.1, indicating that the descending limb related to the elimination phase can be accurately represented by a single linear segment, it strongly suggests that the drug adheres to a one-compartment model of disposition kinetics. Conversely, if the semi-logarithmic plot resembles Figure 1.1, it strongly indicates that the drug follows a two-compartment model of disposition. In both scenarios, the elimination rate constant parameter can be estimated by conducting linear fitting through the descending limb, where the negative slope corresponds to the elimination rate constant, k_{el}. Comparing the two diagrams/curves, it is evident that in the case of the one-compartment model, the entire administered drug quantity is instantly distributed throughout the body, and then the reduction in concentration occurs uniformly following the typical shape of the exponential curve. In contrast, in the case of the diagram for the two-compartment model, the initial portion of the rapid decline corresponds to the ”distribution phase” of the drug, which is subsequently followed by a slower decline in concentration, characterized as the ”elimination phase” [1].

2. The emergence of the Finite Absorption Time (F.A.T.) concept

The conventional analysis of oral drug absorption is based on the Bateman equation (Equation 1.1), which assumes one-compartment model of disposition utilizing first-order absorption and elimination rates [2]:

$$C = \frac{F * D * k_a}{V * (k_a - k_{el})} \left(e^{(-k_{el} * t)} - e^{(-k_a * t)} \right) \tag{1.1}$$

where C represents the drug concentration in the body (compartment), F is the bioavailable fraction of the dose (D), V is indicating the volume of distribution, and k_a and k_{el} are representing the absorption and elimination rate constants, respectively. Depending in the relative magnitude of the rate constants, classical ($k_{el} < k_a$) and flip-flop ($k_{el} > k_a$) cases can be encountered. In the extreme case where the two rate constants are equal (($k_{el} = k_a$)), the concentration-time curve is expressed as [2]:

$$C = \frac{F \cdot D}{V} \cdot k \cdot t \cdot e^{-k \cdot t} \tag{1.2}$$

The origin of Equation 1.1 can be traced back to 1908 when British mathematician Henry Bateman described the abundances and activities in a decay chain of three isotopes over time. Equation 1.1 models the time profile of the daughter isotope in a parent-daughter-granddaughter chain. Nearly fifty years later, German professor of pediatrics Friedrich Hartmut Dost adapted this equation for the purpose of pharmacokinetic analysis of blood data, assuming mono-compartmental distribution and first-order absorption and elimination rates. The similarity between the decay of the isotopes and the drug processes is evident, aligning the isotope chain with the journey the drug takes from the gastrointestinal (GI) tract to the blood and finally its elimination via renal and hepatic routes. Dost, in his 1953 monograph "$Der\ Blutspiegel$" (Blood levels), coined the term "pharmacokinetics" and referenced Equation 1.1. Despite its widespread use in oral drug absorption research, the physiological validity of Equations 1.1 and 1.2 is compromised by the unacknowledged assumption of infinite absorption time [2].

Oral drug absorption occurs within a defined timeframe, typically ranging from 0.5 to 10 hours, in contrast to the infinite time characteristic of the nuclear decay. Present-day software such as Simcyp®and Gastroplus®, along with relevant research papers, allow users to assign values for drug transit from the GI tract, addressing the unrealistic assumption of infinite absorption

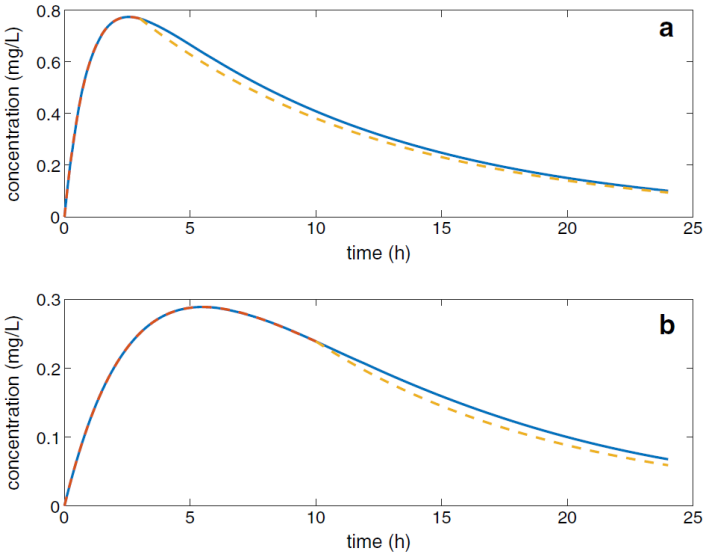

Figure 1.2: Simulated curves generated from Equation 1.1, [2].

time. Current regulatory guidelines for Class I drugs emphasize rapid and complete absorption, ensuring a fraction of dose absorbed greater than 0.90. Consequently, one anticipates the termination of the absorption phase for a Class I drug immediately after the time corresponding to the maximum concentration (C_{max}), indicating complete drug absorption. Conversely, heterogeneous drugs (Class II, III and IV) traversing the entire GI tract, generally undergo slow and incomplete absorption (fraction of dose absorbed less than 0.90). Intuitively, the termination of the absorption phase for Class II, III and IV drugs aligns with much lengthier duration that t_{max}, coinciding with the transit of the unabsorbed drug beyond the absorptive site in the GI tract [2].

Figure 1.2 illustrates simulated curves for a rapidly absorbed (Figure 1.2.A) and a slowly absorbed drug (Figure 1.2.B). These curves are generated from Equation 1.1 using absorption time periods of 3 and 10 hours for the fast and slowly absorbed drugs, respectively. Subsequently, a mono-exponential elimination phase initiates at 3 and 10 hours, respectively (dotted lines). The corresponding Bateman equation (Equation 1.1), using the same parameter values but without the discontinuation of the absorption phase, are overlaid in Figure 1.2 (continuous curves). A visual examination of Figure 1.2 indicates substantial similarity in the descending limbs of the curves in a pairwise comparison [2].

Clearly, when experimental data points are available and analyzed, the discontinuation of the

absorption phase followed by the elimination phase lacks justification. In other words, the physiologically reasonable finite drug absorption duration has been misinterpreted since the introduction of Equation 1.1 in 1953 for the pharmacokinetic analysis of oral data. Building on these logical deductions and the illustrated Figure 1.2, one can infer that Dost's erroneous adoption of Equation 1.1 for oral analysis has significantly impacted fundamental aspects of biopharmaceutics and pharmacokinetics [2].

For example, the integral of Equation 1.1 from zero to infinity, which corresponds to the area under the curve $(\mathrm{AUC})_0^\infty$, has not only been established as a measure for drug exposure but also as a metric of the drug's extent of absorption because of its proportionality:

$$(\mathrm{AUC})_0^\infty = \frac{FD}{k_{el}V} \tag{1.3}$$

Clearly, this relationship is inherently tied to the infinite duration of both first-order processes, drug absorption and elimination. Nevertheless, the current suggestions that $(\mathrm{AUC})_0^\tau$ (where τ signifies the finite duration of the absorption phase) is an appropriate metric for the drug's bioavailable fraction. Mathematically, $(\mathrm{AUC})_0^\tau$ can be calculated using Equation 1.4, [2]:

$$(\mathrm{AUC})_0^\tau = \frac{F * D * k_a}{V\left(k_a - k_{el}\right)}\left[\frac{1 - e^{(-k_{el}*\tau)}}{k_{el}} - \frac{1 - e^{(-k_a*\tau)}}{k_a}\right] \tag{1.4}$$

Equation 1.4 illustrates that the correlation between $(\mathrm{AUC})_0^\tau$ and the bioavailable fraction $(F * D)$ is maintained. However, the significance of both rate constants, k_a and k_{el}, should not be overlooked. While the integral of Equation 1.4 is directly proportional to bioavailability, it is not recommended for the estimation of F. Instead, its is prudent to us the well-established expression $F = \frac{CL \cdot AUC_0^\infty}{D}$ (CL = clearance) to estimate F, as it remains unaffected by when absorption ceases or if there are fluctuations during the absorption process as long as CL remains constant [2].

In the analysis of bioavailability/bioequivalence (BA/BE) data, the estimation of $(\mathrm{AUC})_0^\infty$ and $(\mathrm{AUC})_0^\tau$, along with their relative magnitudes, is closely tied to the biopharmaceutical properties of the drug. For BCS Class I compounds, this should not be a practical problem if actual

data beyond t_{max} are utilized to extrapolate the whole AUC. However, this becomes more of an issue for BCS Class II, III and IV drugs where it is crucial to measure blood plasma concentrations beyond the conclusion of absorption phase to accurately define the terminal elimination. For Class I drugs, the absorption phase typically terminates either at or shortly after the t_{max}. In the former scenario, the experimentally observed C_{max}, t_{max} of the study aligns with the termination of the absorption phase. On the other hand, for Class II, III and IV drugs, the duration of the absorption process (τ) is more prolonged. In such cases, the value of τ might exceed even $2t_{max}$, which corresponds to the inflection point of Equation 1.1. Analyzing concentration-time (C, t) data based on the concept of the finite duration of the absorption process necessitates the development of software for estimating τ. The corresponding data point (C_τ, τ) serves as a discontinuity point for a piece-wise function defined by two sub-functions: Equation 1.1 is applicable for $t \leq \tau$, while the one- or two-compartment model of disposition holds for $t > \tau$ [2].

Chapter 2

Theory

1. Navigating oral drug absorption: Properties, models and historical insights on the absorption rate constant

The oral route stands as the most commonly utilized approach for drug administration. Comprehensive research in this domain has unveiled that oral absorption of drugs hinges on two fundamental properties [3]:

1. The solubility of the drug and
2. The permeability of the drug through the GI epithelium

These scientific advancements have given rise to critical classifications, such as the Biopharmaceutic Classification System (BCS), the Biopharmaceutic Drug Disposition Classification System (BDDCS) and the formulation of regulatory guidelines by the Food and Drug Administration (FDA) and European Medicines Agency (EMA). These guidelines outline the scientific prerequisites for conducting or abstaining from bioequivalence studies, a crucial step in the approval process for generic drugs (I, II, III, IV). For instance, a drug classified as Class I (highly soluble and highly permeable) may qualify for biowaiver status, excluding it from bioequivalence studies. However, this exemption does not extent to Class II (low solubility/high permeability) and Class IV (low solubility and permeability) drugs. In the case of Class III drugs (high solubility/low permeability), a biowaiver status can be granted under specific conditions. Notably, Class I demonstrate extensive absorption (fraction of dose absorbed > 0.90), whereas for Class II, III and IV drugs,the fraction of dose absorbed is notably lower, falling below 0.90 [3].

Nonetheless, it is widely acknowledged that the absorption of orally administered drugs is a multifaceted process influenced not only by the inherent properties of the drug, but also various physiological aspects of the GI tract. These factors encompass:

1. Drug/formulation-dependent elements, such as:
   (a) drug physicochemical attributes (e.g., aqueous solubility, permeability, molecular size, aggregation/complexation, charge, pKa, H-bonding potential and crystal lattice energy)

(b) and formulation composition (e.g., dosage form, absorption enhancers and drug release)

2. System-dependent factors, including:

   (a) physiological parameters (e.g., gastric emptying, intestinal motility, intestinal pH, site-dependent permeability, intestinal content composition and disease state)

   (b) and biochemical parameters (e.g., metabolism, efflux transporters and active uptake transporters)

A critical aspect that holds paramount importance across all modeling approaches is the duration of the absorption process, which is usually shorter than the mean intestinal transit time. In many cases, users have the flexibility to assign a fixed value to this duration, such as 199 minutes, a choice that significantly influences the predictive capabilities of the model. However, in this vast array of pharmacokinetic, pharmacokinetic-pharmacodynamic and pharmacometric studies focusing on oral drug absorption, the rate of drug input is conventionally estimated using the absorption rate constant. This parameter, synonymous with the first-order rate of drug absorption, has historical significance dating back to 1953 when Dost introduced the term ”pharmacokinetics”. Worth noting is that this parameter implies an infinite absorption time, reflecting the prevailing understanding at the time of its introduction [3].

In 1910 Henry Bateman described, using Equation 1.1, the abundances and activities of the daughter-isotope in a decay chain of three isotopes i.e. mother, daughter, grand-daughter, as a function of time (Figure 2.1). Based on the similarity of the kinetic processes portrayed in Figure 2.1, Friedrich Hartmut Dost used that expression in 1953 to describe blood concentration C_b in the body at time t, assuming one-compartment model disposition with first-order absorption and elimination rates. In physics, thousands of experimental observations have shown that the first-order decay of isotopes is undoubtedly true. Similarly, the prevailing first-order character of the elimination rate of drugs has been verified in numerous pharmacokinetic studies. On the contrary, the

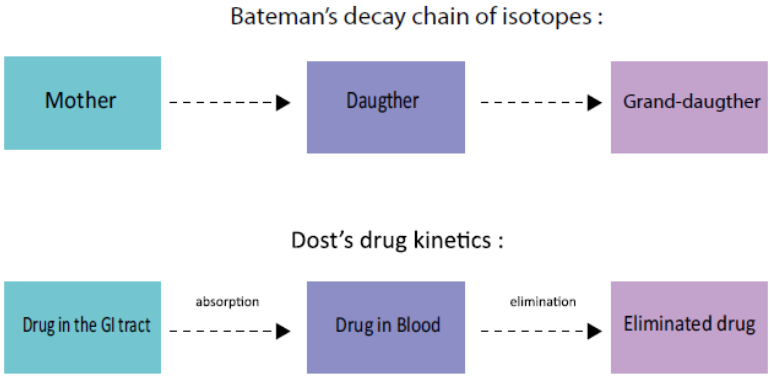

Figure 2.1: Henry Bateman's and Friedrich Hartmut Dost's kinetic considerations. Up: Bateman's mother, daughter, grand-daughter isotope chain of decay. Down: Dost's drug kinetics,[3].

infinite time of drug absorption is not physiologically sound since drugs are not absorbed beyond their absorptive sites in the GI tract. In fact, oral drug absorption takes place in a certain period of time in accordance with the biopharmaceutical properties of the drug as well as the physiological gastric, intestinal and colon transit times reported in the literature [3].

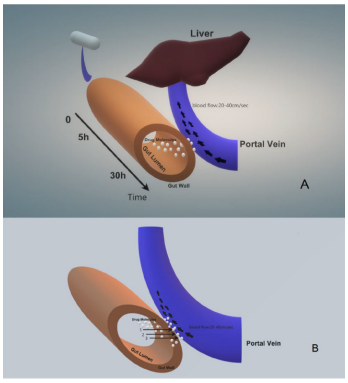

Figure 2.2: (A) Schematic depiction of the passive transfer of dissolved drug molecules (white spheres) from the GI lumen to the portal vein (also known as vena cava). The blood flow in the portal vein is 20-40 cm/s ensuring sink conditions. The physiological time limits 5 and 30 hours for completion of drug absorption in the small intestine and the colon, respectively are shown on the time axis. (B) Enlargement of the region gut wall-portal vein for the drug transfer; the arrows indicate up to three successive input rates for the dissolved drug molecules,[4].

2. Unraveling the dynamics of passive drug absorption. Biopharmaceutical and Pharmacokinetic considerations

Fundamentally, drugs traverse the GI membranes primarily through passive diffusion. Fick's laws of diffusion provide a framework for understanding the flux of solutes, such as drugs, undergoing classical diffusion. A straightforward way of examination involves a drug solution with two distinct regions of concentration: C_{GI} at the absorption site in the GI lumen and C_b denoting the blood concentration at the GI membrane that separates the two regions. The driving force propelling the drug transfer is the drug concentration gradient existing between these two regions [4]. According to Fick's fundamental model of absorption under sink conditions, the concentration remains relatively low due to the physiological factors, Figure 2.2.A: The absorption of drugs under sink conditions has been widely and effectively utilized in physiologically based pharmacokinetic (PBPK) modeling [3,4]. Consequently, the rate of penetration can be expressed as follows:

$$Rate\ of\ penetration\ =\ P(SA) * (C_{GI} - C_b) \tag{2.1}$$

where P is the permeability of the drug expressed in velocity units (length/time) and SA is the surface area of the membrane in $(length)^2$ units. The seer size of the body tends to maintain sink

conditions, in which C_b is much smaller than C_{GI}, therefore:

$$Rate\ of\ penetration\ =\ P(SA) * (C_{GI}) \tag{2.2}$$

Equation 2.2 can be written in terms of drug amount, A_{GI}, assuming that the volume of fluid at the absorption site, V_{GI}, remains relatively constant:

$$Rate\ of\ penetration\ =\ P(SA) * \frac{A_{GI}}{V_{GI}}\ =\ k_a * A_{GI} \tag{2.3}$$

where k_a is the absorption rate constant expressed in $(time)^{-1}$ units. In all pharmacokinetic textbooks, the classical analysis of one-compartment starts from Equation 2.3, assuming a first-order decrease of the amount of drug:

$$\frac{dA_{GI}}{dt}\ =\ -k_a * A_{GI} \tag{2.4}$$

which upon integration from $t = 0$, $A_{GI} = FD$ to $t = t$, $A_{GI} = A_{GI}$ one obtains:

$$A_{GI}(t)\ =\ FD * e^{-k_a * A_{GI}} \tag{2.5}$$

Equation 2.5 can be further coupled with the differential equation which describes the change of drug concentration in the blood (C_b), leading to Equation 1.1.

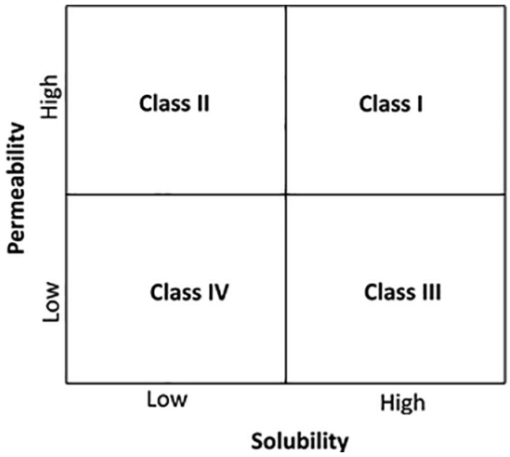

Figure 2.3: Biopharmaceutics Classification System (BCS) presented in a Cartesian spatial perspective,[12]

3. Development of mathematical models grounded in the F.A.T. concept

Crucial to the process of oral drug absorption, is the dissolution of the drug in the GI fluids. In this context, we reassess the rate of drug penetration for the different drug classes (I-IV) by incorporating the dissolution process into the fundamental Equation 2.2. Besides, the pharmacokinetic considerations are grounded in a one-compartment model of disposition, assuming, for simplicity, the absence of a first-pass effect; which mean that the fraction of the dose that is absorbed is equal to the bioavailable fraction[3].

3..1 Models for Class I drugs

In the case of Class I drugs (high solubility/high permeability), the rate of permeation is elevated as per Equation 2.2 and Figure 2.4. Whether administered as a drug solution or a solid formulation, these drugs are not bound by limitations due to either dissolution or permeability. Consequently, the combination of a high permeability coefficient (P) alongside with a substantial surface area $(SA)_i$ in the small intestine, results in a swift and complete absorption, as depicted in Figure 2.4. Therefore, this rapid absorption can be efficiently approximated using a constant rate of drug penetration [3].

$$, Rate\ of\ penetration\ =\ P(SA)_i\ C_{GI}\ =\ k_I\ =\ \frac{F_i D}{\tau_i}\ =\ \frac{D}{\tau_i} \tag{2.6}$$

where k_I denotes the constant penetration rate (mass/time) for Class I drugs, F_i is the fraction of the dose that is absorbed in the stomach and the small intestine and τ_i is the duration of the initial absorption phase. Since Class I drugs are fully absorbed, F_i = 1 may be used in Equation 2.6. Accordingly, the change of drug concentration $C_b\ (t)$ for Class I drugs is:

$$\frac{V_d dC}{dt}\ =\ k_I - k_{el} C_b V_d\ =\ \frac{D}{\tau_i} - k_{el} C_b V_d \tag{2.7}$$

Plausibly, the small intestine is the major site that the absorption phase takes place for Class I drugs while is also evident that absorption always ceases in much shorter time than 4.86 h; which is the sum of gastric and small intestinal transit times (Figure 2.4). Upon integration, for t from 0 to t and for C_b from 0 to C_b, Equation 2.7 gives [3]:

$$C_b(t)\ =\ \frac{D}{\tau_i}\frac{1}{V_d k_{el}}(1 - e^{-k_{el}\ t}) \tag{2.8}$$

Upon termination at time $t\ =\ \tau_i$, the drug concentration is equal to Equation 2.8. The change in drug concentration that is taking place beyond time τ_i can be described by the following equation [3]:

$$\frac{dC_b}{dt}\ =\ -k_{el}(C_b) \tag{2.9}$$

which upon integration for $t\ =\ \tau_i$, $C_b\ =\ (C_b)_{\tau_i}$ and $t->\infty$, $C_b\ =\ 0$ leads to Equation 2.10 describing the elimination phase:

$$C_b(t)\ =\ (C_b)_{\tau_i} * e^{-k_{el}(t-\tau_i)} \tag{2.10}$$

3..2 Models for Class II, III and IV drugs

For low soluble/highly permeable (Class II), high soluble/low permeable (Class III) and low soluble/low permeable (Class IV) drugs, the rate of drug penetration is low. For Class II drugs, this is so, since $C_{GI,\ max}$ value of Equation 2.2 cannot be higher than the low saturation solubility C_s , of

the drug in the GI fluids. In contrast, for Class III drugs, this is the result of a low permeability, P_l being the rate limiting step for the absorption process, while for Class IV drugs, this is a combined effect of low C_{GI} and P_l values. Therefore, the rate of gastric and small-intestinal penetration for Class II, III and IV drugs is similar to that depicted in Equation 2.6, [3]:

$$(Rate\ of\ penetration)\ =\ P(SA)_i C_s\ =\ k_j\ =\ \frac{F_i D}{\tau_i} \tag{2.11}$$

where k_j denotes the constant penetration rate for Class II-IV drugs and j = II, III and IV. Accordingly, the change of drug blood concentration C_b as a function of time assuming one-compartment model for Class II-IV drugs is:

$$\frac{V_d dC}{dt}\ =\ k_j\ -\ k_{el} C_b V_d \tag{2.12}$$

Similarly, assigning their respective constant penetration rates k_{II} , k_{III} and k_{IV} , one can approximate the gastric and small-intestinal penetration rates as per Equations 2.6 and 2.7. It should be noted, that these derived equations roughly operate for no more than 4.86 h, which is as we previously mentioned, the sum of the gastric and small intestine transit times, [3].

The passage of those drugs to the colon via the ileocecal valve, which separates the large from the small intestine, can either result in the termination of drug absorption or the significant reduction of the drug penetration rate, since in the colon the effective surface area SA_c is much smaller and the amount of unabsorbed drug at the ileocecal valve is equal to $1 - F_i D$, [3]:

$$(Rate\ of\ penetration)_{j,\,c}\ =\ P(SA)_c\, C_s\ =\ k_{j,\,c}\ =\ \frac{(1 - F_i)D}{\tau_c - \tau_i}\lambda \tag{2.13}$$

where j can either be II, III or IV, τ_c denotes the termination of the absorption in the colon, λ is a coefficient ($0\ <\ \lambda\ <\ 1$) associated with the reduction of the penetration rate due to the small surface area in the colon, SA_c compared to SA_i. As a result, the change of drug blood concentration C_b as a function of time assuming one-compartment model disposition for Class II, III and IV drugs during the drug passage through the colon is [3]:

$$\frac{V_d dC}{dt}\ =\ k_{j,\,c} - k_{el} C_b V_d \tag{2.14}$$

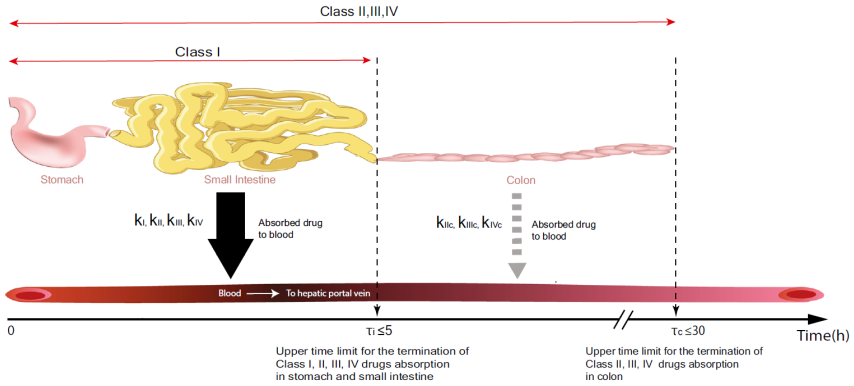

Figure 2.4: A schematic representation of the drug absorption model, which relies on the transit times of the drug along the GI tract. For Class I drugs, the completion of absorption ceases in a shorter time than the sum of the stomach and small intestine transit times (4.86 h). For Class II-IV drugs, the limited overall absorption can be continued beyond the ileocecal valve and lasts not more than the whole gut transit time (29.81 h). The thick arrow shows the major site of drug absorption; the small intestine, while the dashed arrows indicate the potentially limited drug absorption that takes place at the colon,[3].

This equation roughly holds from 4.86 h until the time needed for the drug to reach the non-absorptive sites of the colon, τ_c, but certainly shorter than 20.28 or 31.95 h i.e. the colon transit time for a single-unit or multi-unit formulation, respectively, Figure 2.4. At time τ_c absorption ceases and beyond this time point the drug is only eliminated from the body. Hence, the drug concentration decreases in a way similar to Equation 2.10:

$$C_b(t) \;=\; (C_{b_c})_{\tau_c} * e^{-k_{el}(t-\tau_c)} \tag{2.15}$$

To recount the fundamental expressions based on the one-compartment model, we have Equation 1.1 for $t \;\leq\; \tau$ and a more comprehensive version of Equations 2.10 and 2.15, that holds for $t \;>\; \tau$, [3]:

$$C_b(t) \;=\; C_b(\tau)e^{-k_{el}(t-\tau)} \tag{2.16}$$

Time τ, can either signal passage of drug beyond the absorptive sites or pinpoint completion of the absorption process.

While the models were initially developed based on a one-compartment model of disposition, similar equations can be derived assuming a two-compartment model. For example, the following equations do not assume any absorption from the colon,but correspond to two-compartment model

drugs. [3]:

$$\frac{V_d dC}{dt} = k_1 - (k_{12} - k_{10})C_b V_d + k_{21} C_b V_d \qquad for\ 0 < t \leq \tau_i \tag{2.17}$$

$$\frac{dC_b}{dt} = -(k_{12} - k_{10})C_b + k_{21} C_2 \qquad for\ t > \tau_i \tag{2.18}$$

Here, k_{12}, k_{10} and k_{23} are the microconstants of the two-compartment model, C_2 is the drug concentration in the peripheral compartment and k_1 can either be k_I , k_{II} , k_{III} *or* k_{IV} depending in the class [3].

4. Physiologically Based Finite Time Pharmacokinetic (PBFTPK) models - Implications and applications

Thus far, the theoretical segment regarding oral drug absorption has relied on [5]:

1. the finite absorption time concept
2. the physiologically based transit times reported in the literature and
3. the basic drug properties, namely, solubility and permeability, which have been adopted by the regulatory authorities as the key factors controlling oral drug absorption.

Given the physiological significance of the finite absorption time models that were developed, the term "Physiologically Based Finite Time Pharmacokinetic" (PBFTPK) models was coined. For drugs following linear disposition kinetics, we coin the term $p-PBFTPK-m$, where p is the number of the successive input rates 1, 2, 3 and m takes the values 1 and 2 denoting the disposition characteristics of the drug, namely, one- or two-compartmental disposition. For metabolized drugs following non-linear Michaelis-Menten disposition kinetics, the term $p-PBFTPK-m(MM)$ was coined [4].

The model based on Equations 1.1 and 2.16 will now be called $(PBFTPK)_1$, while the subscript 1 denotes that the model maintains the first-order character of the absorption rate. If the model maintains a zero-order character instead, a 0 subscript is used and the model is called $(PBFTPK)_0$. In their work, Chryssafidis et al. (2021), explored the drug blood concentration at time τ, as well as the partial areas under the curve $[AUC]_0^\tau$ and $[AUC]_\tau^\infty$ prior to and beyond the termination of the drug's absorption at time τ, respectively, as metrics for the drug's extent of absorption. On top of that, noteworthy is their application of $(PBFTPK)_0$ and $(PBFTPK)_1$ models on oral concentration-time data exclusively for the estimation of the absolute bioavailability [5].

The development of bioavailability metrics both for the extent and rate of absorption was based upon the parameters $[AUC]_0^\infty$, C_{max} and t_{max}, which are all derived from the fundamental

Equation 1.1 [5].

$$[AUC]_0^\infty = \frac{FD}{V_d k_{el}} = \frac{FD}{CL} \tag{2.19}$$

$$t_{max} = \frac{1}{k_a - k_{el}} ln\left(\frac{k_a}{k_{el}}\right) \tag{2.20}$$

$$C_{max} = \frac{FD}{V_d}\left(\frac{k_a}{k_{el}}\right)^{\left(-\frac{k_{el}}{k_a - k_{el}}\right)} \tag{2.21}$$

4..1 $(PBFTPK)_0$ models

For the one-compartment model, Equation 2.22 was used to describe the drug blood concentration-time profile for $t \leq \tau$ assuming termination of the absorption process at time τ, [5].

$$C_b(t) = \frac{FD}{\tau}\frac{1}{V_d k_{el}}\left(1 - e^{-k_{el}*t}\right) \tag{2.22}$$

while for $t > \tau$, Equation 2.16 applies. The drug blood concentration $C_b(\tau)$ for the one-compartment $(PBFTPK)_0$ *model* is derived from Equation 2.22 by replacing $t = \tau$:

$$C_b(t) = \frac{FD}{\tau}\frac{1}{V_d k_{el}}\left(1 - e^{-k_{el}*\tau}\right) \tag{2.23}$$

while the partial areas $[AUC]_0^\tau$ and $[AUC]_\tau^\infty$ can be derived upon integration of Equations 2.22 and 2.16, respectively.

$$[AUC]_0^\tau = [AUC]_0^\infty\left(1 - \frac{1 - e^{-m*ln2}}{m * ln2}\right) \tag{2.24}$$

$$[AUC]_\tau^\infty = [AUC]_0^\infty\frac{1}{m * ln2}\left(1 - e^{-m*ln2}\right) \tag{2.25}$$

where m is the ratio $\tau/t_{1/2}$, while $k_{el} = ln2/t_{1/2}$, where $t_{1/2}$ is the half-life during the elimination phase. One can easily show that the sum of Equations 2.24 and 2.25 leads back to Equation 2.19.

A hypothetical curve corresponding to the same dose administered as an IV bolus would follow the same pattern for $t \geq \tau$ and ultimately lead to [5]:

$$[AUC_{IV}]_0^\infty = [AUC]_0^\infty\frac{1}{k_{el}\tau}\left(e^{k_{el}t} - 1\right) \tag{2.26}$$

Taking into consideration that in either a test or a reference formulation administered orally, the absolute bioavailability equals to [5,6]:

$$F = \frac{[AUC]_0^\infty}{[AUC_{IV}]_0^\infty} = \frac{k_{el}\,\tau}{e^{k_{el}\,\tau} - 1} \tag{2.27}$$

where F is the fraction of the dose absorbed, since both oral and IV data rely on a single orally administered dose to an individual. However, as was previously mentioned, if the first-pass effect is insignificant, F describes the bioavailable fraction that reaches the body.

4..2 $(PBFTPK)_1$ models

Now, for the drugs that follow first-order kinetics the corresponding models rely upon Equations 1.1 and 2.16 by replacing $t = \tau$.

$$C_b(\tau) = \frac{FDk_a}{V_d(k_a - k_{el})}\left(e^{-k_{el}\tau} - e^{-k_a\tau}\right) \tag{2.28}$$

In a similar pattern, we derive the respective AUC expressions for the oral and hypothetical IV curves:

$$[AUC]_0^\tau = \frac{FD}{V_d k_{el}} - \frac{FDk_a}{V_d(k_a - k_{el})}\left(\frac{e^{-k_{el}\tau}}{k_{el}} - \frac{e^{-k_a\tau}}{k_a}\right) \tag{2.29}$$

$$[AUC]_\tau^\infty = \frac{C_b(\tau)}{k_{el}} = \frac{FDk_a}{V_d k_{el}(k_a - k_{el})}\left(e^{-k_{el}\tau} - e^{-k_a\tau}\right) \tag{2.30}$$

$$[AUC]_0^\infty = \frac{FD}{V_d k_{el}}\left(1 - e^{-k_a\tau}\right) \tag{2.31}$$

and are able to calculate the absolute bioavailability:

$$F = \frac{[AUC]_0^\infty}{[AUC_{IV}]_0^\infty} = \left(1 - \frac{k_{el}}{k_a}\right)\frac{1 - e^{-k_a\,\tau}}{1 - e^{-(k_a - k_{el})\tau}} \tag{2.32}$$

The difference between the quantity of Equation 2.31 and the required value of $\frac{FD}{V_d k_{el}}$ is attributed to the discrepancy that the drug ceases to be absorbed beyond time τ and the mathematical representation of a first-order absorption process, which theoretically continues indefinitely. Specifically, the expression in the parenthesis (Equation 2.31) is directly tied to absorption characteristics, namely k_a and τ. The influence of this term diminishes as k_a and τ assume higher values, as shown in Fig-

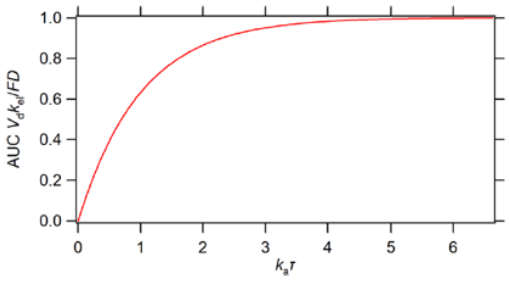

Figure 2.5: Plot of $[AUC]_0^\infty k_{kel} V_d/FD$ as a function of k_a and τ, Equation 2.31. The term in the ordinate axis is dimensionless,[5].

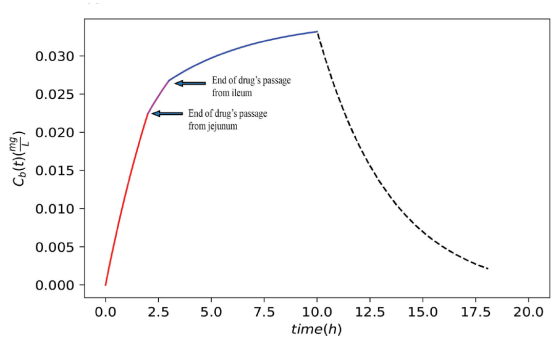

Figure 2.6: $C_b(\tau)$ curve for a drug exhibiting three successive constant rates for absorption in the jejunum (1.4 mg/h), ileum (1.0 mg/h) and colon (0.8 mg/h). The duration of the absorption process in those regions are 2, 1 and 7 hours, respectively, [3].

ure 2.7, [5] While it is acknowledged that under $in\ vivo$ conditions more than one constant input rate may operate successively, this section specifically concentrates on the simplest scenario — the one-compartment model with a constant input rate and first-order elimination. Nevertheless, the principles elucidated in this section can be adjusted and extended to models incorporating multiple input rates, [4]. Owing to the anatomical and physiological features of the GI tract, drugs with varied biopharmaceutical properties such as solubility, permeability and ionization, may manifest one, two, or three consecutive input rates, as illustrated in Figure 2.2.A. Figure 2.6 depicts a representative scenario of a drug showcasing variations in regional permeability. Simulated in this example are three consecutive input rates observed in the jejunum, ileum and the colon, [5]. For example, if two constant input rates operate successively under $in\ vivo$ conditions, Equation 2.22 is replaced by:

$$C_b(t) = \frac{F_1 D}{\tau_1} \frac{1}{V_d k_{el}} \left(1 - e^{-k_{el} * t}\right) \quad for \quad 0 < t \leq \tau_1 \tag{2.33}$$

and Equation 2.18 is replaced by:

$$C_b(t) \;=\; C_b(\tau_1)e^{-k_{el}(t-\tau_1)} \;+\; \frac{F_2 D}{\tau_2}\frac{1}{V_d k_{el}}\left(1-e^{-k_{el}(t-\tau_1)}\right) \quad for \quad \tau_1 \le t \le \tau_2 \tag{2.34}$$

$$C_b(t) \;=\; C_b(\tau_1 \;+\; \tau_2)e^{-k_{el}(t-\tau_1-\tau_2)} \quad for \quad t > \tau_1+\tau_2 \tag{2.35}$$

In a similar pattern, if three constant input rates operate successively under $in\ vivo$ conditions, we employ once more Equation 2.33 but this time, Equation 2.18 needs to be replaced by three expressions instead of two: The first is, again Equation 2.34, that now holds for $\tau_1 < t \le \tau_1+\tau_2$, the second is an extended version of Equation 2.35:

$$C_b(t) \;=\; C_b(\tau_1 \;+\; \tau_2)e^{-k_{el}(t-\tau_1-\tau_2)} \;+\; \frac{F_3 D}{\tau_3}\frac{1}{V_d k_{el}}\left(1-e^{-k_{el}(t-\tau_1-\tau_2)}\right) \quad \tau_1+\tau_2 < t \tag{2.36}$$

and the third:

$$C_b(t) \;=\; C_b(\tau_1 \;+\; \tau_2 \;+\; \tau_3)e^{-k_{el}(t-\tau_1-\tau_2-\tau_3)} \quad \tau_1+\tau_2+\tau_3 < t \tag{2.37}$$

In that same study, Chryssafidis et al. (2021) applied the $(PBFTPK)_0$ and $(PBFTPK)_1$ models on concentration-time data from orally administered drugs in order to facilitate a comparative study between the two and then re-examine some well known rate and exposure metrics.

4..3 $(PBFTPK)_0$ and $(PBFTPK)_1$ models: A visual comparison

Figures 2.7 and 2.8 demonstrate $(PBFTPK)_0$ and $(PBFTPK)_1$ models respectively. In Figure 2.7, a zero-order absorption process with one (2.7.A) and two (2.7.B) successive input rates are depicted, where the termination of the absorption process, τ, leads to $C_{max} \;=\; C_b(\tau)$. For these two cases, this equality implies that C_{max} is not a steady-state value described by Equation 2.21 but rather correspond to the termination of drug input, as described by Equation 2.23. In some cases, when a very highly soluble and permeable drug (Class I and possibly biowaivers) is studied, these type of $C_b \;-\; t$ profiles similar to Figures 2.7.A and 2.7.B can indicate the completion, and not simply the termination, of the absorption process. Figures 2.7.C and 2.7.D show two examples with two and three successive input rates, respectively. In both cases, termination of drug absorption

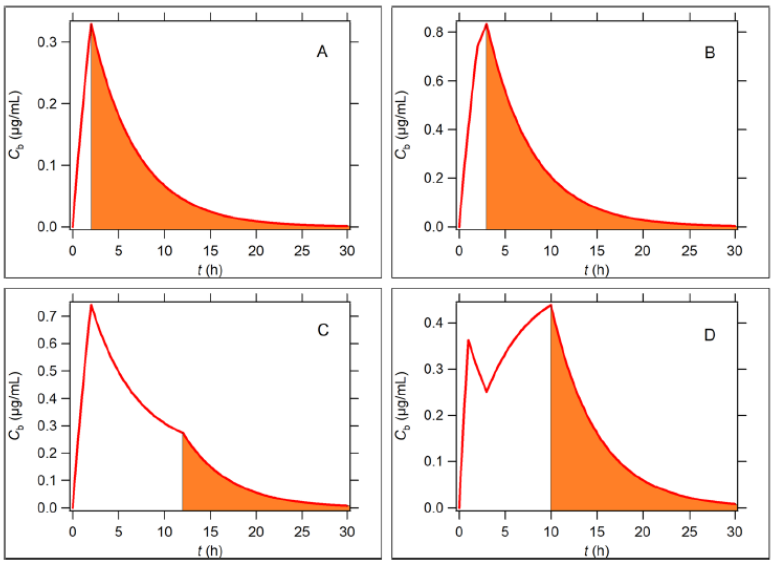

Figure 2.7: Concentration $versus$ time curve for $(PBFTPK)_0$ models. In all cases, k_{el} and V_d were set to constant values. Absorption and elimination phase was generated using Equations 2.16, 2.22, 2.29-2.33, [5]

takes place in the colon (as implied by τ values longer than t_{max} and the schematic of Figure 2.4) [5]. In Figure 2.7.C, C_{max} is higher than $C_b(\tau)$ ($C_{\text{max}} > C_b(\tau)$), as the cessation of drug absorption lies in the descending portion of the elimination limb of the curve. Figure 2.7.D depicts a simulated example with three constant input rates causing fluctuations in drug concentration during the absorption/elimination phase. The second, lower input rate may be associated with a lower segmental permeability and/or partial drug precipitation. Consequently, the observed concentration maximum C_{max} is higher than the second peak ($C_b(\tau)$), likely linked to drug re-dissolution and/or higher intestinal permeability. Once again, C_{max} is not a steady-state value described by Equation 2.21; in fact, C_{max} corresponds to an "equilibrium" point in the complex absorption phenomena in the small intestine [5].

In Figure 2.8, simulated curves derived from the $(PBFTPK)_1$ models are illustrated for three distinct cases with varying finite absorption durations, deviating from the classical first-order absorption. The curve corresponding to the lower absorption rate constant, k_a, 0.1 h^{-1} in Figure 2.8.A, clearly demonstrates that as the absorption duration decreases, the curve profile tends to differ significantly from the classical top curve. In 2.8.B and 2.8.C, as k_a and τ increase, the curves tend to coinside with the classical top curve, something that substantiates Equation 2.31 and Figure 2.8 [5].

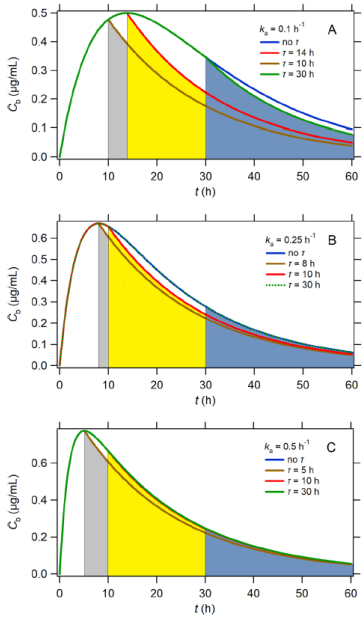

Figure 2.8: Truncated Bateman drug concentration profiles with A: k_a=0.1 h^{-1}, k_{el}=0.05 h^{-1} and termination times 10 h (gray), 14 h (yellow) and 30 h (blue); B: k_a=0.25 h^{-1}, k_{el}=0.05 h^{-1} and termination times 8 h (gray), 10 h (yellow) and 30 h (blue); C: k_a=0.5 h^{-1}, k_{el}=0.05 h^{-1} and termination times 5 h (gray), 10 h (yellow) and 30 h (blue), [5].

4..4 Comparison between the rate metrics (C_{max}, t_{max}) and $(C_b(\tau), \tau)$

Comparison of these rate metrics involves historical associations with the use of C_{max} as a measure of absorption rate, deriving from Equation 1.1 as a steady-state value. Despite its use as a bioavailability rate parameter, Equation 2.21 highlights the dependence of C_{max} on the extent of absorption. Nevertheless, C_{max} continues to be employed as a rate parameter in bioequivalence guidelines, with its numerical value depicting the peak concentration of the drug in the blood. Over the past decades, concerns have been raised leading to the suggestion of alternative metrics and methodologies. As Equation 2.23 suggests, in $(PBFTPK)_0$ models, $C_b(\tau)$ is directly proportional to the input rate $\frac{FD}{\tau}$, making it an ideal parameter. Additionally, the inclusion of time τ emphasizes the termination of the absorption process which is a fundamental characteristic of the $(PBFTPK)_0$ models. Conceptually, various C_{max} and $C_b(\tau)$ may or may not align in actual practice, given that $C_{max} \geq C_b(\tau)$, as depicted in Figure 2.4 When equality holds, a straightforward derivation form the $(PBFTPK)_0$ model can be made [5]:

$$Rate\ in = \frac{V_d C_b}{dt} = \frac{FD}{\tau} - k_{el} C_b V_d = 0 \tag{2.38}$$

$$C_b(\tau) \;=\; C_{max} \;=\; \frac{FD}{\tau * CL} \tag{2.39}$$

This equality signifies the termination or completion of the absorption phase at time τ, while C_{max} or $C_b(\tau)$ remains proportional to both the input rate and the extent of absorption.
However, it's important to note that C_{max} or $C_b(\tau)$ does not represent the asymptotic limit of a zero-order absorption process followed by a first-order elimination, typically observed in continuous intravenous infusion. In other words, the $(C_b(\tau), \tau)$ data point is a discontinuity point linked to [5]:

1. the conclusion of the input process (no more drug available for absorption)
2. a sudden change in drug solubility (e.g., precipitation)
3. a shift in drug permeability (e.g., altered regional permeability due to pH changes), or
4. the drug's transit beyond absorptive sites

In the $(PBFTPK)_1$ models, the termination of absorption at time τ can result from either the completion of drug absorption or the passage of the drug beyond absorptive sites. The corresponding value of $C_b(\tau)$ (Equation 2.27) is always equal to or smaller than the experimental C_{max}, as illustrated in Figure 2.8. However, it's crucial to recognize that the experimental values for $(C_b(\tau)$ and τ in $(PBFTPK)_1$ models are not steady-state values, unlike C_{max} (Equation 2.21) and t_{max} (Equation 2.20), respectively. Instead, the pair $(C_b(\tau), \tau)$ represents a discontinuity time point [5].

4..5 Comparison of the exposure metrics $[AUC]_0^\infty$ versus $[AUC]_0^\tau$ and $[AUC]_\tau^\infty$

Comparison of exposure metrics is crucial in bioavailability and bioequivalence studies generally for assessing safety and efficacy, obtaining regulatory approval, establishing interchangeability, ensuring consistency in drug performance and maintaining quality assurance. Undoubtedly, the golden standard for measuring the extent of absorption is $[AUC]_0^\infty$. This metric holds true for $(PBFTPK)_0$ models, where the sum of Equations 2.24 and 2.25 aligns with Equation 2.19. Despite the fact that Equation 2.24 illustrates that $[AUC]_0^\tau$ is only a fraction of $[AUC]_0^\infty$, its magnitude is determined solely by the quantity m, representing the ratio of the duration of the absorption to

the elimination half-life. Consequently, the significance of $[AUC]_0^\tau$ for $(PBFTPK)_0$ models does not align with the conventional concept of partial areas used as indicators for the initial rate of exposure. Moreover, $[AUC]_0^\tau$ for $(PBFTPK)_1$ models is dependent on τ (Equation 2.29) while $[AUC]_0^\infty$ is also dependent on τ (Equation 2.31). Therefore, for both $(PBFTPK)_0$ and $(PBFTPK)_1$ models, the typical role of partial areas is not applicable due to the involvement of τ in the calculations. According to Equation 2.25, $[AUC]_\tau^\infty$ is proportional to the fraction of the dose absorbed, which is in the general circulation at time τ. This proportionality is particularly valuable in bioequivalence studies when the duration of the absorption process is short or very short, and the absorption phase data exhibit high variability. This scenario is often encountered with inhalers and nasal products. For these formulations, the test-reference comparison can be based on the area $[AUC]_\tau^\infty$, which is proportional to the fraction of the dose absorbed that is in the general circulation at time τ, [5].

4..6 Estimation of absolute bioavailability from oral data

For drugs obeying one-compartmental disposition with any number of input rate kinetics lasting for a τ period of time, an estimate for F can be also derived from the areas under the curve corrected in terms of dose [5]:

$$F = \frac{[AUC]_{0,oral}^\infty Dose}{[AUC]_{0,hypoth.IV}^\infty FDose} \tag{2.40}$$

where $[AUC]_{0,hypoth.IV}^\infty$ corresponds to the area of the hypothetical curve projected after an IV bolus administration of the same dose derived from the back extrapolation of the elimination phase experimental data beyond time τ of the oral dose, (Figure 2.9). Its numerical value can be calculated from the ratio $\frac{e^{y-intercept}}{k_{el}}$, where the y-intercept on the lnC axis corresponds to the back extrapolated regression line with slope $-k_{el}$. The integral $[AUC]_{0,oral}^\infty$ can be calculated using the trapezoidal rule for the experimental oral data. Solving Equation 2.31 in terms of F, we get [5]:

$$F^2 = \frac{[AUC]_{0,oral}^\infty}{[AUC]_{0,hypoth.IV}^\infty} \tag{2.41}$$

The positive root of Equation 2.41 provides an estimate for F. In their study, Chryssafidis et al., used Equation 2.41 for the estimation of F of theophylline formulations and the results were very similar to those from Equations 2.27 and 2.32.

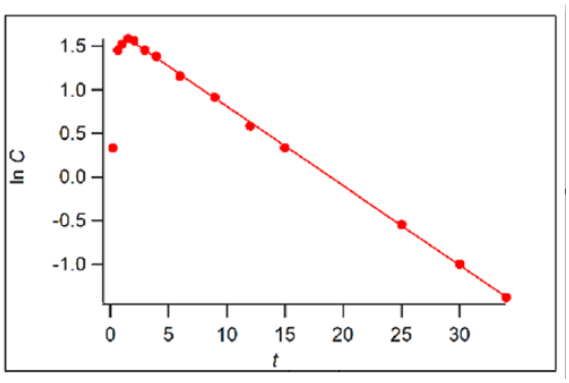

Figure 2.9: Semi-logarithmic concentration-time plots of a drug that follow one-compartmental disposition (theophylline), [5]

5. F.A.T. concept: The ”Columbus egg” of modern Pharmacokinetics

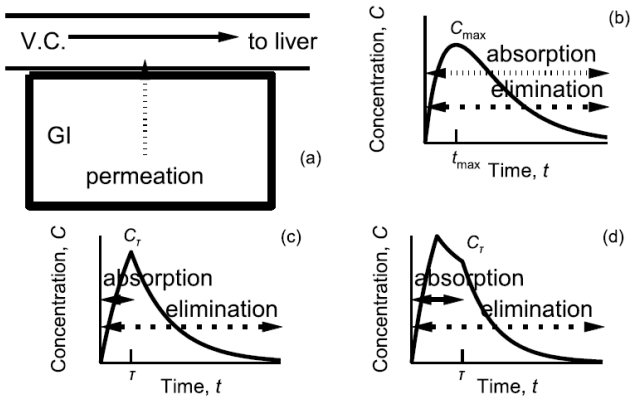

Figure 2.10: (A) The passive drug absorption of drug molecules (vertical arrow) from the GI tract to the blood in vena cava always takes place under sink conditions, resulting in constant drug input rate to the liver. (B) According to the established view, drug absorption and elimination operate concurrently from zero to infinity. (C,D) According to the F.A.T. concept, drug absorption and elimination operate concurrently from zero to τ, while only elimination continues to infinity. Two different profiles can be observed with (C) $t_{max} = \tau$ and (D) $t_{max} < \tau$. Such behaviours have been observed in a number of drugs including paracetamol, cyclosporin [Chryssafidis et al., 2022] and axitinib [Alimpertis et al., 2022] formulations, respectively, [8].

As is evident, the concept of the finite absorption time induces a transformative shift in the understanding of oral drug absorption, and absorption in general as a topic. This is elucidated in Figure 2.10.A, which illustrates the underlying processes within the GI membrane/vena cava region that support the F.A.T. concept. Figure 2.10.A is deemed a ”Columbus egg” because, despite the microscopic processes being unknown at the inception of pharmacokinetics with Dost, they have been well understood for several decades. Recently, it has been established that the high blood flow in the vena cava (20-40 cm/s), which ensure sink conditions in the system, is actually five orders of magnitude greater than the typical estimates of drug effective permeability ($10^{-4}\ cm/s$) [8]. Consequently, the rate of drug appearance in the liver is the result of this flow rate and the fact that the concentration of the drug is changing along with the permeability in a linear fashion. Plausibly, the constant drug entry in the liver ceases either when the drug is completely absorbed before passing from the absorptive site in the intestine or when dissolved/undissolved drug particles move beyond the absorptive sites, predominantly located in the small intestine. Beyond time τ, only drug elimination is in effect, as shown in Figures 2.10.B, 2.10.C and 2.10.D, [8].

The development and successful application of the the BPFTPK models on a number of oral drug absorption data not only provided a mathematical framework for the grounding of the F.A.T. concept, but also managed to show potency in the estimation of the absolute bioavailability of highly soluble and permeable drugs (Class I) e.g., theophylline, solely through oral absorption data [5,7]. In their follow-up study, Tsekouras and Macheras (2021) re-examined digoxin bioavailability using data published prior to the grounding of the term, in comparison with a bioequivalence study conducted under the light of FDA guidelines in 2002. The original study stated that "… when measured by peak serum digoxin concentration as well as by area under the serum digoxin concentration–time curve, the bioavailability of digoxin appeared to be higher in the fasting state than in the fed state. However, when measured by cumulative five day urinary excretion of digoxin bioavailability was identical in both conditions". The same result was quoted by looking at the ratio of pertinent AUCs; in fact, by applying the trapezoidal rule we get $\frac{[AUC_{fasted}]_0^1}{[AUC_{fed}]_0^3} = 0.76/0.8345 = 0.90$. This finding implies that digoxin absorption concludes at 1 and 3 hours in the fasted and fed state, respectively, aligning with the finite absorption time concept. In essence, this observation underscores the salience of AUC calculation up to the point of termination of drug absorption as reliable indicator of digoxin's extent of absorption [9].

In a different study, Alimpertis et al.(2022), attempted to establish a non-compartmental methodology, under the framework of the F.A.T. concept, for evaluating bioequivalence. The study employed data from a pilot bioequivalence study of two axitinib test formulations. The fitting results achieved through the application of the PBFTPK models consistently outperformed those obtained from conventional one- and two-compartment models that utilize first-order absorption kinetics. On top of that, the results emphasized the significance of $[AUC]_0^\tau$ as an promising metric for estimating the extent of drug absorption. Consequently, the utilization of $[AUC]_0^\tau$ in bioequivalence assessment aligns seamlessly with the physiologically grounded FAT concept, reinforcing the conceptual coherence of their approach [10].

6. Novel dimensions in $in\ vitro-\ in\ vivo$ correlations through the F.A.T. concept

In the early stages of Biopharmaceutics and Pharmacokinetics, Wagner and Nelson introduced a fundamental concept involving percent absorbed versus time plots. These plots have been widely employed for the depiction of the entry rate into the general circulation, for drugs that follow one-compartment disposition kinetics. Furthermore, these plots have been proven valuable for the estimation of the first-order absorption rate constant, k_a. Later, Loo and Riegelman expanded this framework to encompass two-compartment model drugs as well. In the late 1970s, a numerical deconvolution method emerged as an alternative for calculating drug input rates, with numerous applications detailed in literature since then [11].

The creation of the percent absorbed versus time plots constitutes a fundamental aspect of the $in\ vitro-in\ vivo$ correlations (IVIVC), a crucial element in the development and approval of drug products and formulations. The FDA categorizes IVIVC into levels A, B, C, and Multiple C based on the type of data used to establish the relationship and its ability to predict the plasma concentration profiles of a dosage form. Level A represents a comprehensive point-to-point relationship between $in\ vitro$ release and $in\ vivo$ absorption. Successful IVIVC for a range of formulations, implies that $in\ vitro$ dissolution tests can be a substitute for additional bioequivalence studies that take place during the production and modification of diverse formulations. In some instances, achieving a ”level A” IVIVC involves the % absorbed profile essentially mirroring the $in\ vivo$ dissolution profile, aligning point by point with $in\ vitro$ dissolution data. All these techniques have been integrated into pharmacokinetics over the past six decades. However, recent demonstrations have challenged the physiological soundness of the infinite absorption time concept that is inherently likened to the absorption rate constant, governing drug's absorption. The first-order absorption notion significantly impacts all calculations related to constructing percent absorbed versus time plots, critical components of IVIVC plots [11].

Recent analysis of oral drug absorption data utilizing the finite absorption time concept and the physiologically based pharmacokinetic models, have yielded meaningful and reliable estimates for the duration of the drug absorption process and its corresponding input rates. The PBFTPK model differential equations are rooted in the principles of passive drug absorption under sink

conditions lasting for a finite absorption time. For each of the four Biopharmaceutics Classification System (BCS) drug classes, the input rate is linked with the limiting property, such as solubility or permeability. In instances of complex drug absorption, more than one input rate is observed. Under the light of these findings, Alimpertis et al. (2023) attempted to reevaluate the percent absorbed versus time plots within the framework of the finite absorption time concept. The modifications that were made to the classical approaches, took into consideration the cessation of drug absorption, represented by τ, corresponding to the F.A.T. [11].

6..1 Percent absorbed $versus$ Time plots

Creating these curves is a pivotal element for the development of IVIVC. All methodologies employed by Wagner-Nelson, Loo-Riegelman and deconvolution techniques utilize $[AUC]_0^\infty$ for normalization purposes. For example, Equation 2.42 provides the fraction of dose absorbed up to time t, $[AUC]_0^t$, in alignment with the Wagner-Nelson framework.

$$\frac{A_t}{A_\infty} = \frac{C_t + k_{el}\int_0^t C\,dt}{k_{el}\int_0^\infty C\,dt} = \frac{C_t + k_{el}[AUC]_0^\infty}{k_{el}[AUC]_0^t} \tag{2.42}$$

where A_t is the amount of drug absorbed up to time t, A_∞ is the amount that is absorbed at infinite time, and k_{el} the elimination rate constant that is very well established until this point. Under the finite time notion, the absorption process terminates at time τ as we've discussed so far, therefore, Equation 2.42 should be modified accordingly into Equation 2.43, where the area $[AUC]_0^\infty$ and the amount of drug absorbed at infinite time A_∞ is replaced by the amount of drug absorbed by the time absorption has been completed A_τ. C_τ is added in the denominator for mass balance purposes

$$\frac{A_t}{A_\tau} = \frac{C_t + k_{el}\int_0^\infty C\,dt}{k_{el}\int_0^\tau C\,dt} = \frac{C_t + k_{el}[AUC]_0^\infty}{C_\tau + k_{el}[AUC]_0^\tau} \qquad for\ t \leq \tau \tag{2.43}$$

which for one input rate, transforms to a more simplified form:

$$\frac{A_t}{A_\tau} = \frac{t}{\tau} \qquad for\ t \leq \tau \tag{2.44}$$

$$\frac{A_t}{A_\tau} = 1 \qquad for\ t > \tau \tag{2.45}$$

For two-compartment model drugs, Loo and Riegelman proposed the method described in Equation 2.46 for the calculation of the fraction of dose absorbed up to time t, which is symbolized by t_n:

$$\frac{A_{t_n}}{A_\infty} = \frac{C_{1_{t_n}} + C_{2_{t_n}} + k_{el}\int_0^{t_n} C_1\,dt}{k_{el}\int_0^{\infty} C_1\,dt} = \frac{C_{1_{t_n}} + C_{2_{t_n}} + k_{el}[AUC]_0^{t_n}}{k_{el}[AUC]_0^{\infty}} \tag{2.46}$$

where $C_{1_{t_n}}$ is the concentration of the drug in the central compartment and $C_{2_{t_n}}$ is the respective concentration in the peripheral compartment. $C_{2_{t_n}}$ can be calculated as:

$$C_{2_{t_n}} = \frac{k_{12}}{k_{21}} C_{1_{t_{n-1}}} \left[1 - e^{-k_{21}\Delta t}\right] + \frac{k_{12}\Delta C_1 \Delta t}{2} + C_{2_{t_{n-1}}} e^{-k_{21}\Delta t} \tag{2.47}$$

where t_n is the sampling time of the sample n, t_{n-1} the sampling time of the sample before n, $n-1$, $C_{1_{t_{n-1}}}$ is the concentration of the drug in the central compartment at time t_{n-1}, k_{12} and k_{21} are the disposition micro-constants, ΔC_1 equals to $C_{1_{t_n}}$ - $C_{1_{t_{n-1}}}$, and Δt is equal to t_n - t_{n-1}.

Equation 2.46 can now be written in accord with the finite absorption time concept. Again, Equations 2.44 and 2.45 holds for a single input stage:

$$\frac{A_{t_n}}{A_\tau} = \frac{C_{1_{t_n}} + C_{2_{t_n}} + k_{el}[AUC]_0^{t_n}}{C_{1_\tau} + C_{2_\tau} + k_{el}[AUC]_0^{\tau}} \qquad for\ t \leq \tau \tag{2.48}$$

In view of all the above, Alimpertis et al., developed a computer based approach for the estimation of τ, utilizing cyclosporin experimental data (Figure 2.12), by calculating the fraction A_t/V_d (V_d being the volume of distribution) as a function of time, using combinations of experimental data points from the two segments of the bilinear plot. In Figure 2.12, the continuous line connects the points that correspond to the apparent absorbed concentrations (numerators from Equation 2.42 and 2.46 divided by V_d) and the dashed lines correspond to the absorption profiles based on the finite absorption time (Equations 2.44 and 2.45). The ascending part of the curve determines the sloping line, and the average of remaining data points defines the level of the horizontal line. Their intersection determines the end of the absorption stage, i.e., τ. According to this methodology, the determination of the intersection point depends on the choice of which points

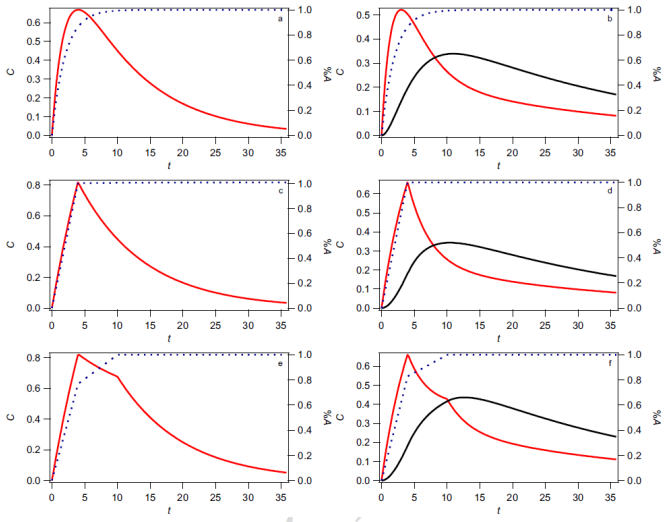

Figure 2.11: Simulated oral pharmacokinetic data showing drug concentration, C, in the blood (red line) and in the peripheral compartment (where pertinent, black line) and percent of the drug absorbed (dashed blue line) using one-(a,c,e) and two-(b,d,f)compartment models based on first-order infinite time absorption (a,b) and infinite zero- or first-order absorption (c-f), [11].

belong to the first segment and which ones to the second one. The intermediate point is allowed to be part of both segments. The best choice is determined by the sum of squares of deviations from the two lines, χ^2. The partitioning of the data is scanned in search of the minimum value of this sum. The values of χ^2 for this data set are presented in Figure 2.13. Also included is the associated value of the absorption time, τ, and its associated uncertainty, σ_τ. The minimum χ^2 value coincides with the τ value with the lowest uncertainty. The values for τ, slope and plateau level at the least value of χ^2 are taken as the optimum values [11].

The results derived from the adjustments made to the Wagner-Nelson and Loo-Riegelman equations, incorporating the finite absorption time concept, extend beyond the realm of percent absorbed $versus$ time plots. These findings indeed pave the way for much broader applications of the finite time framework across the entire spectrum of biopharmaceutic-pharmacokinetic, pharmacometric studies, and regulatory science in the domain of oral drug absorption studies[11].

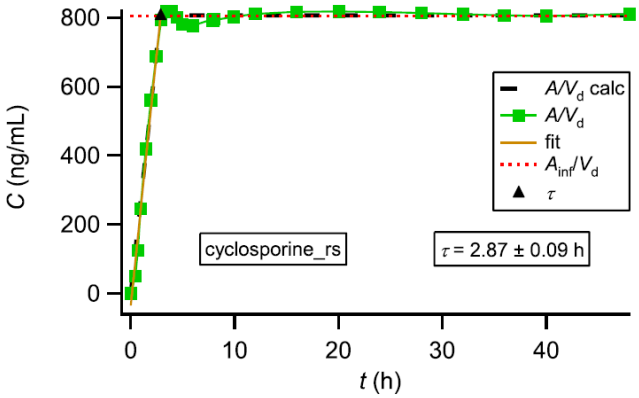

Figure 2.12: Percent absorbed (expressed as apparent absorbed concentration) $versus$ time plot (green squares and solid line) for cyclosporine. Optimum partitioning of the data in two segments was found at $i = 8$ as seen in Figure 2.13. The intersection of the two straight segments corresponds to the termination of cyclosporine absorption. For this example, the optimum estimate for $\tau = 2.87 \pm 0.09h$. The black triangle denotes the termination of drug absorption. The black dashed line is the simulation based on the model (Equation 2.48). The brown solid line is the fit of Equation 2.48 to the ascending segment data; the red dotted lines are the average level of the plateau values, [11].

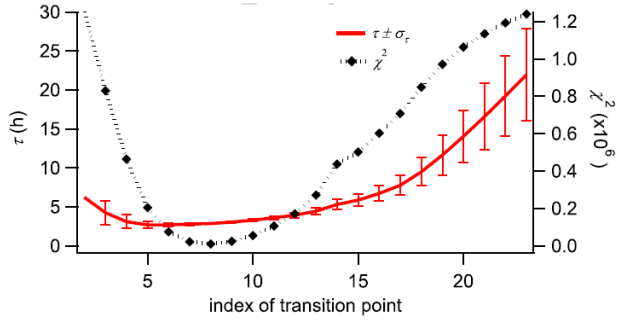

Figure 2.13: Investigation of the effect of partitioning of cyclosporine apparent absorbed concentration in rising and plateau segments. Shown are the values (and associated errors) for τ, (red solid line) as well as χ^2 values (black dotted line) as a function of index of point where the two segments meet. The minimum value for χ^2 determines the optimum selection of the transition point [11]

.

Chapter 3

Methods

1. Analysis of the absorption data

Our analysis commenced with the acquisition of oral absorption data from solid drug formulations, with a primary focus on Class I or borderline Class I biowaiver drugs. This preference was rooted in their predictable characteristics and nature of these compounds, including high aqueous solubility, high permeability, and a fraction dose absorbed, F_a, exceeding 0.9. Additionally, the extensive accessibility of absorption data in the literature, derived from bioequivalence and bioavailability studies, contributed to the selection of this BCS Class in order to lay the groundwork for understanding and applying the F.A.T. concept and the PBFTPK models, providing a basis for addressing less predictable Classes. Moreover, Class I drugs are commonly associated with obtaining biowaiver status, offering valuable insights into biowaivers from the other classes.

Upon gathering a substantial amount of Class I oral absorption data, primarily from the corresponding biowaiver monographs, a digitization process was undertaken to render the data adaptable for subsequent analysis.

The initial step involved investigating whether the drugs adhere to a one- or two-compartment model of disposition. Utilizing either Igor programming language through the PBFTPK software developed by Thekouras and Macheras, or Python programming language, $ln(C)$ versus time (t) plot were created for all drug's absorption data, focusing on the descending limb that corresponds to the elimination phase of the drug. Linear fitting of the data points on the descending limb facilitated the determination of the compartmental profile, under the light of Figure 1.1. The estimated $(-slope)$ values enabled the determination of the elimination rate constant, (k_{el}), for drugs following one-compartment models of disposition, while for drugs that follow a two-compartment model the respective constants are denoted as α and β, instead.

Proceeding to curve fittings, the PBFTPK models were employed within the Igor programming environment. The PBFTPK software utilized user-defined functions and a versatile built-in least squares algorithm, accommodating restrictions to parameter values, statistical weights, data sub-sets, covariance matrix calculations, and graphical representation of results. Given the complex nature of the model equations and the intricate shape of the resulting χ^2 hypersurface in parameter space, the determination of initial trial parameter values necessitated manual adjust-

ments. Each data set underwent fittings using various models, including the classical Bateman equation (Equation [1.1]), zero-order kinetics/one-compartmental (Equations 2.22, 2.33 - 2.35 for one- and two-successive input rates, respectively) and two-compartmental models, and first-order/one-compartmental (Equation 2.28) and two-compartmental models. Adjusting the total duration of the simulation, in accord with the experimental data, is crucial. Also, setting various sound initial guesses for the pharmacokinetic parameters, namely the absorption and elimination constants (k_a and k_{el}) respectively, the micro-constants in the cases of two-compartmental disposition ($k_{10} - k_{12} - k_{21}$) and the various input rates (FD/τ), we can obtain the best possible fitting for each of the data sets using the statistical R^2 as a primary guide.

Model selection was executed through the application of the Akaike Information Criterion (A.I.C.), providing a measure to compare the goodness of fit among different models. A.I.C. is particularly useful when dealing with a finite sample size, as it helps balance the trade-off between the goodness of fit and the complexity of a model.

$$A.I.C. = N * ln(\chi^2) + 2p \tag{3.1}$$

where N is the number of the total data points, χ^2 signifies the goodness of fit and it is provided alongside with each fitting, and p denotes the number of parameters of each model. Despite A.I.C. being a valuable tool, other considerations were factored in before finalizing the model selection, such as the literature information about the compartmental model, the coefficient of determination, R^2, and the overall visual appearance of the curve fitting

Moving to the subsequent computational phase we leverage Equations 2.27, 2.32, and 2.41 to ascertain the absolute bioavailability, denoted as F, across various models. Employing Equation 2.27 for the zero-order/one-compartment model with a singular input rate ($(PBFTPK)_0$), we utilize estimates of the elimination rate constant, k_{el}, and the duration of absorption, τ, derived from fitting procedures. This enables the calculation of absolute bioavailability. Similarly, for the first-order/one-compartment model with a single input rate ($(PBFTPK)_1$), we apply Equation 2.32. In that case, estimates of the elimination rate constant, k_{el}, the absorption phase duration, τ, and the absorption rate constant, k_a, are utilized to once again determine absolute bioavailability. Regarding Equation 2.41, a preliminary step involves determining the $y - intercept$ on semi-logarithmic

plots (Figure 2.9) through digitization (specifically, the back extrapolation method applicable only to drugs conforming to the one-compartment model). Subsequently, leveraging the $-slope$ values, k_{el}, obtained from this analysis, facilitates the calculation of the concentration corresponding to the initiation of intravenous administration. This approach enables the computation of the area under the hypothetical curve after a iv administration, thereby allowing for the determination of absolute bioavailability based solely on oral data.

Similar to the approach taken by Tsekouras et al.([4]) in their 2022 study, this modeling methodology enables the exploration of potential relationships between biopharmaceutic properties, such as solubility and permeability, and various pharmacokinetic parameters. This exploration extends to evaluating relationships among different pharmacokinetic parameters. The rationale behind this lies in the fact that the kinetics of a drug's passive absorption under sink conditions can be elucidated by the rate of penetration. One method for investigating possible relationships, involves creating a correlation plot by graphing values for a set of parameters on an x-y Cartesian system. In our study, we specifically plotted partial areas under the curve $(AUC)_0^\tau$, utilizing fitting estimations for the termination of the absorption phase, against the elimination rate constant k_{el} (for one-compartment model drugs) or β (for two-compartment model drugs). Subsequently, by applying linear regression and fitting a linear curve through the data points, we can assess the existence of a correlation between these two parameters by analyzing the slope of the curve.

Finally, percent absorbed versus time plots were simulated using the PBFTPK software based on the F.A.T. concept, aiming to determine the amount of drug absorbed, identify the duration of the absorption process, τ, and evaluate the predictive accuracy in comparison to PBFTPK models.

2. Analysis of the dissolution data

Dissolution profiles of biowaivers, Class I, II, III, and IV drugs were extracted from their respective literature monographs, articles and subsequently digitized to facilitate analysis. Our analytical focus encompassed three distinctive metrics: F.D.T. (τ_d) and M.D.T. for Class I and III drugs and M.D.T.s. for Class II and IV drugs. These metrics were computed through four distinct methods: one involving graphical analysis employing the trapezoidal rule, another employing the Noyes-Whitney equation, a third utilizing the Weibull function and a fourth one utilizing the reaction-limited model of dissolution.

For the graphical analysis, the computational methodology was inaugurated by a graphical approach to ascertain the F.D.T. metric. A plot depicting % dissolved against time was crafted to articulate the dissolution profile. Essential to this process was the identification of two critical time junctures: the first where % dissolved indicated a value below 100%, succeeded by the subsequent point at which % dissolved surpassed the 100% threshold. A judicious application of linear interpolation was then employed to deduce the precise temporal instant at which % dissolved attained complete dissolution, thereby characterizing the F.D.T. Similarly, for the calculation of the M.D.T. and M.D.T.s., utilizing the dissolution profiles, we assessed the area (ABC) bounded by the dissolution curve and a line parallel to the time-axis aligned with the plateau, Figure 2. This area (ABC) was subsequently divided by the % dissolved magnitude corresponding to the plateau, Equation 2.51, thus yielding the M.D.T. for Classes I and III, as well as the M.D.T.s. for Classes II and IV. Since BCS is based on the minimum solubility across the physiological pH range, for each compound the lowest solubility at its corresponding pH was utilized in the calculations.

For the remaining three models, we systematically performed curve fitting procedures to analyze the experimental data. We employed the equations specified in Table 4.8 for the Noyes-Whitney and Weibull models and utilized Equation 2.67 for the reaction-limited model of dissolution. These curve fitting analyses were executed within the Python programming environment, particularly employing the SciPy library. The outcome of the curve fittings provided us with parameter estimates, which were subsequently utilized to calculate the M.D.T., M.D.T.s., and F.D.T. (τ_d). In contrast, for the reaction-limited model, explicit expressions for these parameters were unavailable, and as a result, we resorted to numerical methods for the computation of M.D.T. and

M.D.T.s. Specifically, for the numerical computation for the reaction-limited model time parameters, Equation 2.67 was adapted by incorporating the D/V (dose of drug/volume of dissolution medium (900 mL) ratio of each drug to generate the corresponding $W(t)$ curve, which illustrates the cumulative amount of dissolved drug over time. This curve was subsequently integrated according to Equation 2.50 to determine the M.D.T. and M.D.T.s. values, using the corresponding parameter estimates derived from the curve fittings.

Chapter 4

Results and Discussion

1. Results of the analysis of the absorption data

Table 4.1 provides a comprehensive overview of the drugs under investigation, listing their names and corresponding classification in the Biopharmaceutics Classification System (BCS) based on their respective monographs and various literature sources. Notably, drugs marked with an asterisk (*) have been classified in more than one BCS classes [23]. The table reveals either purely Class I (characterized by high aqueous solubility and intestinal permeability) or borderline Class I classification, possibly due to dose scaling and ionization phenomena.

Table 4.1: BCS Class I biowaiver drugs and their classification. Drug names/formulations and their corresponding BCS classification are displayed. Dual or triple classifications are noted according to their respective monographs and further literature [13-22] (classification derived from [23] is marked with an asterisk *).

Drug Name/Formulation	BCS Classification
Amitriptyline Hydrochloride	Class I/II
Amoxicillin Trihydrate	Class I/II/IV*
Acetylsalicylic Acid	Class I/III
Bisoprolol Fumarate	Class I
Cephalexin Monohydrate	Class I
Doxycycline Hyclate	Class I
Fluconazole	Class I/III*
Levetiracetam	Class I
Ondansetron	Class I
Acetaminophen (Paracetamol)	Class I/III/IV*

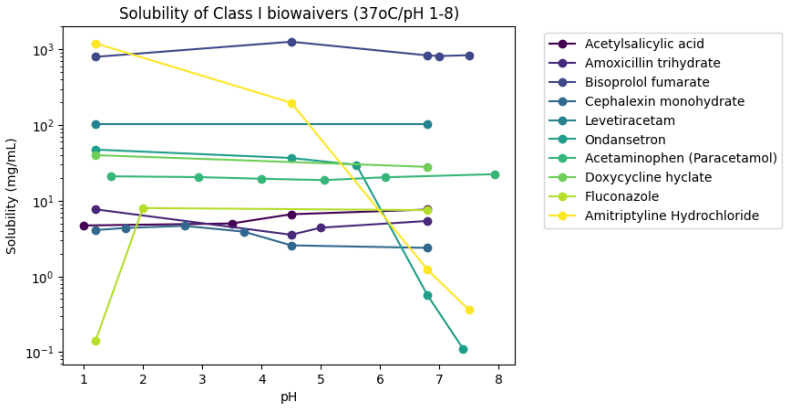

Figure 4.1: pH-Dependent Drug Solubility Profile: Illustrating variations in solubility for Class I biowaiver drugs across pH 1-8 at 37°C.

In Figure 4.1, we depict the solubility profiles of the drugs enumerated in Table 4.1 across a pH range of 1 to 8 at 37 $^{\circ}C$, [24 - 49]. This visualization aims to elucidate potential dose/solubility ratios substantiating their placement in distinct BCS classes. Most of the drugs exhibit relatively constant solubility within this pH range. However, exceptions are observed, particularly in ondansetron and amitriptyline hydrochloride, which demonstrate decreasing solubility patterns, and fluconazole, which exhibits increasing solubility as a function of pH. It is noteworthy that these three compounds are physicochemically characterized as weak bases and the decreasing solubility of ondansetron and amitriptyline hydrochloride towards higher pH, albeit still on the acidic side of the pH scale, could be attributed to their weak basic nature. In the case of fluconazole, additional factors influencing solubility need consideration. Intriguingly, the biowaiver monograph for fluconazole suggests that a biowaiver may be recommended for immediate-release (IR) dosage forms under specific conditions, including the presence of fluconazole in polymorphic form II or III, demonstrating high solubility. Furthermore, it emphasizes limitations in excipient selection to those approved in International Conference on Harmonisation (ICH) countries, used in typical amounts, and requiring both test and comparative dosage forms to rapidly dissolve or maintain rapid dissolution profiles throughout the shelf life across various pH conditions (1.2, 4.5, and 6.8). Notably, solubility values reported for polymorphic form III align with these criteria.

The entirety of the elimination phase data was subjected to analysis using a semi-logarithmic plot (Figure 4.2). Notably, with the exception of amitriptyline hydrochloride and cephalexin, all plots exhibit linearity, and the regression coefficients (R^2) – embedded within each plot along the elimination rate constant, k_{el} (h^{-1}), confirm the adherence of the majority of elimination data to a one-compartment model of disposition (R^2 exceeding 0.99 in most of the cases), aligning with the implications of Figure 1.1. The elimination constant, k_{el}, is delineated by the negative slope of the linearly fitted segments (red line) and the intersection of the extrapolated linear portion (blue line) with the y-axis corresponds to the natural logarithm of the hypothetical intravenous administered dose equivalent to the same oral administration, C_0. Beyond furnishing essential pharmacokinetic parameters, these semi-logarithmic plots offer valuable insights into potential models that may yield optimal fitting, particularly discerning between one- and two-compartment models of disposition. Subsequent to the aforementioned analysis, Table 4.2 encapsulates the elimination rate constant values, accompanied by their corresponding standard deviations and the disposition model sorting solely based upon the R^2 values derived from each regression depicted in Figure 4.2.

Table 4.2: Presents Class I biowaiver drugs alongside their derived elimination rate constants, k_{el}, (h^{-1}) from Figure 4.2, and indicates compartmental model classification based on the linearity of the elimination phase of the semi-logarithmic plots (one- or two-compartment) basen on the R^2 values.

Drug Name	k_{el} (h^{-1}) ($\pm SD$)	Compartmental Model	R^2
Amitriptyline Hydrochloride	0.095873 $\pm$ 0.014486	Two-compartment	0.96915
Amoxicillin Trihydrate	0.24353 $\pm$ 0.0099005	One-compartment	0.99616
Acetylsalicylic Acid	0.2549 $\pm$ 0.016449	One-compartment	0.98914
Bisoprolol Fumarate	0.062384 $\pm$ 0.0018785	One-compartment	0.9949
Cephalexin Monohydrate (fasted)	0.21308 $\pm$ 0.020738	One-compartment	0.98212
Cephalexin Monohydrate (fed)	0.20211 $\pm$ 0.0096901	One-compartment	0.98992
Doxycycline Hyclate	0.059961 $\pm$ 0.0025197	One-compartment	0.98746
Fluconazole	0.032918 $\pm$ 0.0010793	One-compartment	0.9953
Levetiracetam (fasted)	0.11496 $\pm$ 0.0035217	One-compartment	0.99546
Levetiracetam (fed)	0.12872 $\pm$ 0.0050471	One-compartment	0.99414
Ondansetron	0.13911 $\pm$ 0.000031331	One-compartment	0.9963
Acetaminophen (Paracetamol)	0.18695 $\pm$ 0.011097	One-compartment	0.99311

The relationship between Biopharmaceutics Classification System (BCS) classes and pharmacokinetic models is not strict, meaning that a BCS Class I drug doesn't necessarily follow a specific pharmacokinetic model. However, it is often observed that drugs with favorable biopharmaceutical properties, such as those in BCS Class I, may exhibit characteristics consistent with a one-compartment model of disposition. This is because drugs in this class typically are hydrophilic and not moving to peripheral tissues.

According to the guidelines of the FDA (U.S. FDA, 2017), a drug substance is considered "highly soluble" if the highest dose strength can be dissolved in $\leq$ 250 mL of aqueous media at a pH from 1 to 6.8 and a temperature of 37°C ± 1°C. For a drug dose higher than the highest dose strength additional data are required. "High permeability" is granted if the fraction of dose absorbed reaches 85% or more, of the dose administered, based on a mass balance determination or compared to a referred iv dose. On top of that, due to that nature, these drugs tend to exhibit absolute bioavailability values > 0.90, which makes them ideal for assessing a new pharmacokinetic model.

One of the reasons that a drug can appear in more than one Biopharmaceutic Classification System (BCS) classes can be described as a concept of drug migration based on dose scaling is known as "dose-dependent BCS classification." This phenomenon implies that the biopharmaceutical behavior of a drug undergoes changes at different dose levels, resulting in variations in its BCS classification. At lower doses, a drug might exhibit characteristics conducive to complete absorption, allowing it to be classified, for example, as BCS Class I, where both solubility and permeability are high. However, as the dose increases, solubility limitations may become more pronounced, potentially leading to a shift in classification to Class II (low solubility, high permeability), III (high solubility, low permeability) or even Class IV (low solubility, low permeability). This concept was extensively explored by Charkoftaki et. al [50]., where they created a dose-dependent BCS (DDBCS). According to that framework, drugs are classified based on their fraction of dose absorbed values, depending on their administered dose in three distinct regions. Drugs with F≥0.90 are completely absorbed (obviously, typical BCS Class I drugs belong to this region). Drugs with limited absorption, F≤0.20, like Class IV and drugs like Class II and III with 0.2<F<0.9. They further explain that Class II drugs may also be classified as completely absorbed (F $\geq$ 0.90) depending on the administered dose (doses $\leq dose_{critical}$) and behave like Class I; and thus biowaiver status can be granted. On the contrary, BCS Class I drugs may behave as BCS

Class II drugs for doses > $dose_{critical}$ and classified in the middle region. One particular example from the drugs of Table 4.1 is amoxicillin which belongs to [50] Class I for doses up to 875 mg, to Class II with 1000 mg, and to Class IV for even higher doses.

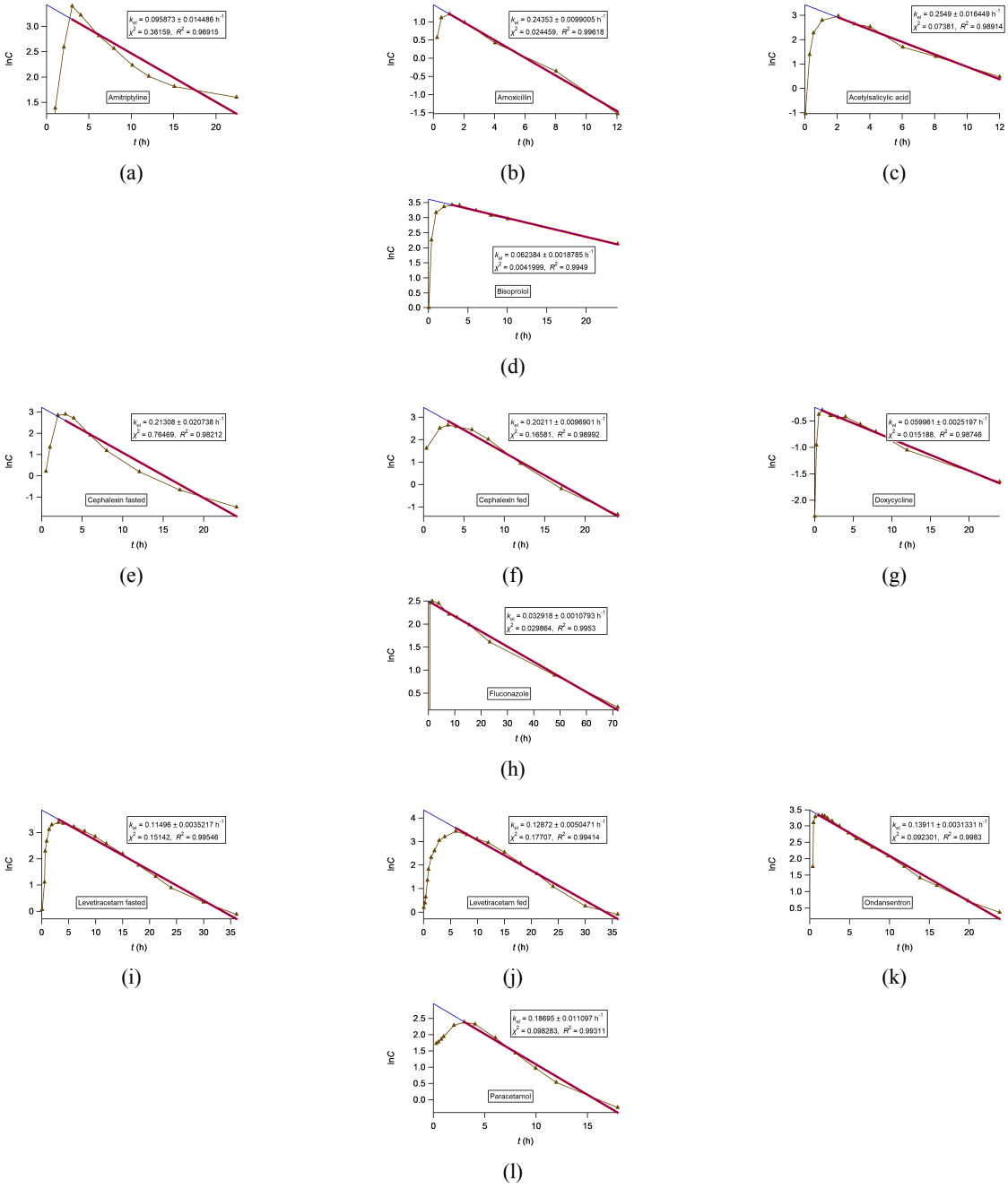

Figure 4.2: Semi-logarithmic representation of Class I biowaiver drugs: Employing linear regression on the descending limb data points to ascertain the slope, facilitating the extraction of k_{el} (elimination rate constant).

Table 4.3: Pharmacokinetic Fitting Model Abbreviations. Listed abbreviations are used in the Pharmacokinetic fitting models derived from Igor software and accompanying tables and figures for subsequent analysis. The second column provides the full form of each abbreviation, elucidating the meaning behind the model designations.

Models (abbreviations)	Models (full form)
fo	Classical Bateman
fot $[(PBFTPK)_1]$	Finite Bateman, finite/first-order/one-compartment
$zot1$ $[(PBFTPK)_0]$	Finite/zero-order/one-compartment (1 τ)
$zot2$	Finite/ zero-order/ one-compartment/ two-input stages (2 τ)
$zwt1\_k$	Finite/ zero-order/ two-compartment & peripheral in k_s
$zwt2\_k$	Finite/ zero-order/ two-compartment & peripheral in k_s / two-input stages
fwt_k	Finite/ first-order/ two-compartment (k_{12}, k_{el})

Following the preliminary analysis, several extensive unrestricted non-linear least squares curve fittings were conducted, encompassing various Physiologically Based Finite Time Pharmacokinetic (PBFTPK) models as well as the Bateman equation. The elucidation of fitting model abbreviations utilized in the Igor programming software, pivotal for subsequent figures and ensuing discussion, is detailed in Table 4.3. This table serves as a reference for the diverse models employed and provides corresponding explanations.

Figures 4.3 - 4.14 present the outcomes of the curve fittings for the drugs delineated in Table 4.1. Exceptional fits are discernible across the majority of the datasets, as attested by the R-squared values annotated above each fitting. Adjacent to each fitting, a legend is presented, furnishing crucial pharmacokinetic parameters such as the input rate constant (FD/V_d, μg/ml or mg/ml), elimination and absorption rate constants, k_{el} and k_a, respectively, (h^{-1}) in the context of one-compartment models, with first-order absorption.. For two-compartment models, micro-constants k_{10}, k_{12}, and k_{21}, (h^{-1}), model parameters α and β, (h^{-1}) and absorption duration, τ, (h) are detailed, with similar information provided for two-stage models (τ_1, τ_2). Statistical parameters, are presented alongside these parameters, providing a comprehensive overview of the precision and reliability of the derived values.

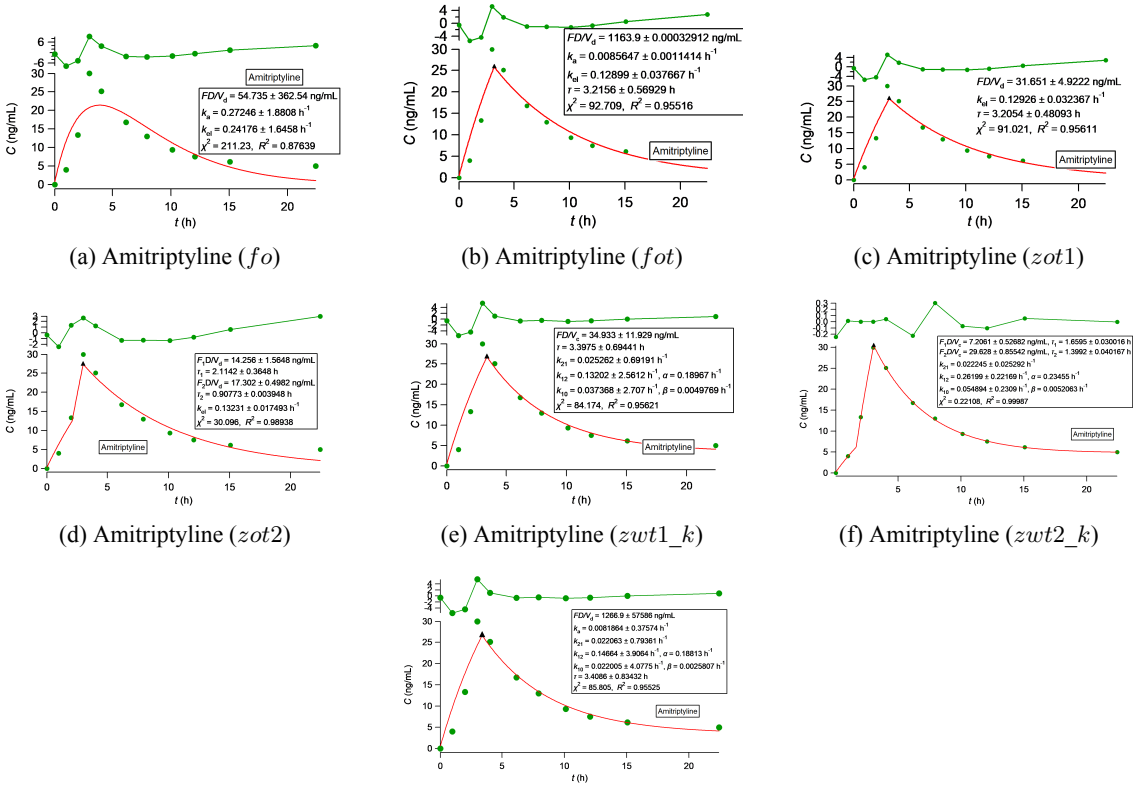

(a) Amitriptyline (fo)

(b) Amitriptyline (fot)

(c) Amitriptyline ($zot1$)

(d) Amitriptyline ($zot2$)

(e) Amitriptyline ($zwt1\_k$)

(f) Amitriptyline ($zwt2\_k$)

(g) Amitriptyline (fwt_k)

Figure 4.3: Curve fittings using the classical Bateman equation (4.3a) and the PBFTPK models (4.3b-4.3g) for amitriptyline hydrochloride oral absorption data [40]. Table 4.3 serves as a key for this figure.

(a) Amoxicillin Trihydrade (fo)

(b) Amoxicillin Trihydrade (fot)

(c) Amoxicillin Trihydrade ($zot1$)

(d) Amoxicillin Trihydrade ($zot2$)

(e) Amoxicillin Trihydrade ($zwt1\_k$)

(f) Amoxicillin Trihydrade (fwt_k)

Figure 4.4: Curve fittings using the classical Bateman equation (4.4a) and the PBFTPK models (4.4b-4.4f) for amoxicillin trihydrate oral absorption data [41]. Table 4.3 serves as a key for this figure.

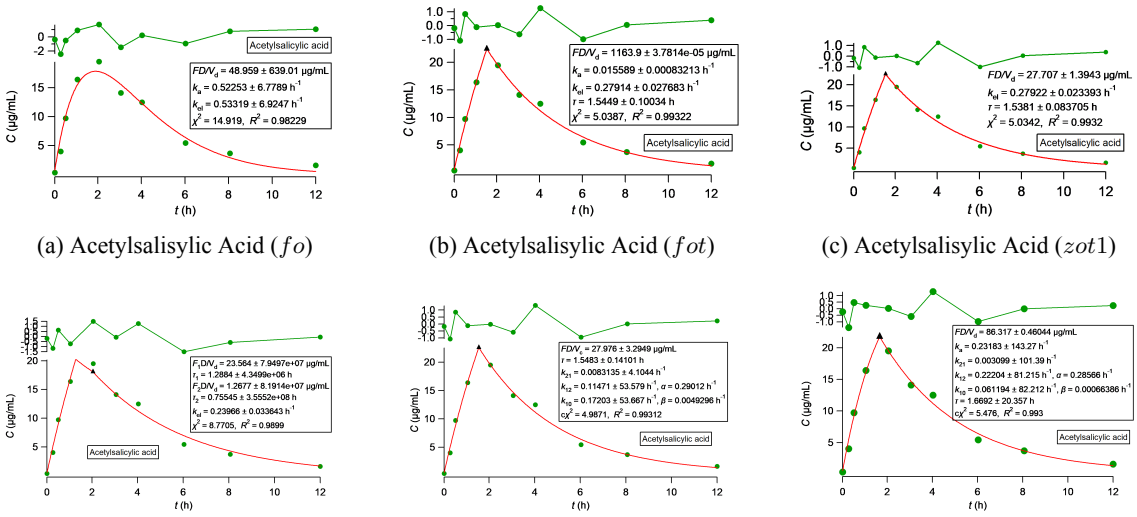

(a) Acetylsalisylic Acid (fo) (b) Acetylsalisylic Acid (fot) (c) Acetylsalisylic Acid ($zot1$)

(d) Acetylsalisylic Acid ($zot2$) (e) Acetylsalisylic Acid ($zwt1\_k$) (f) Acetylsalisylic Acid (fwt_k)

Figure 4.5: Curve fittings using the classical Bateman equation (4.5a) and the PBFTPK models (4.5b-4.5f) for Acetylsalisylic Acid oral absorption data [42].

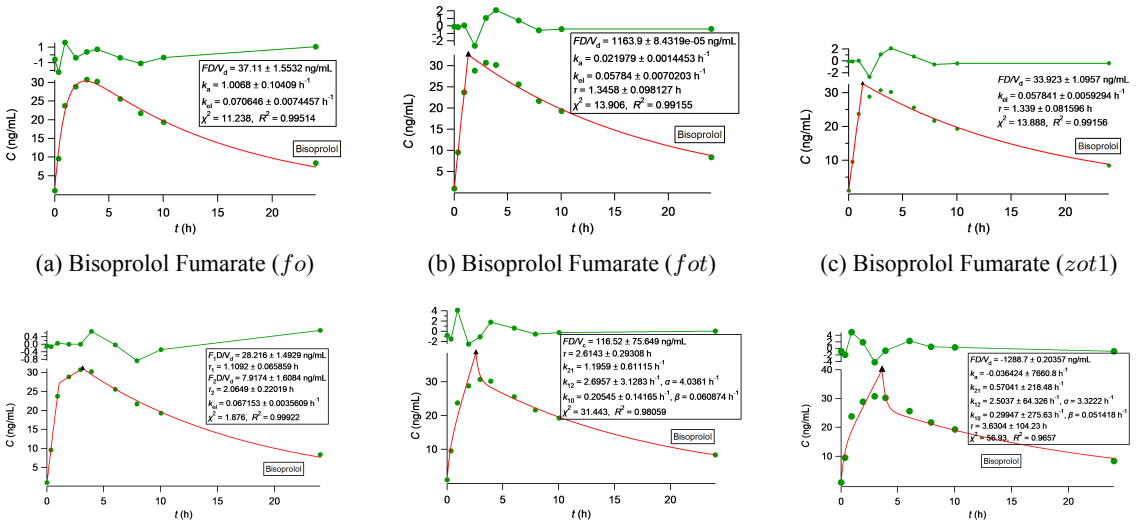

(a) Bisoprolol Fumarate (fo) (b) Bisoprolol Fumarate (fot) (c) Bisoprolol Fumarate ($zot1$)

(d) Bisoprolol Fumarate ($zot2$) (e) Bisoprolol Fumarate ($zwt1\_k$) (f) Bisoprolol Fumarate (fwt_k)

Figure 4.6: Curve fittings using the classical Bateman equation (4.6a) and the PBFTPK models (4.6b-4.6f) for bisoprolol fumarate oral absorption data [43]. Table 4.3 serves as a key for this figure.

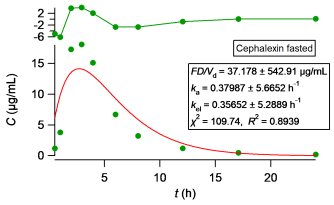

(a) Cephalexin Monohydrate (fasted) (fo)

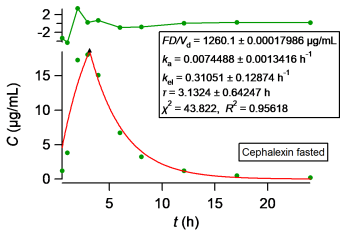

(b) Cephalexin Monohydrate (fasted) (fot)

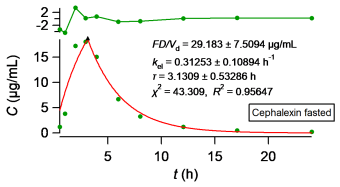

(c) Cephalexin Monohydrate (fasted) ($zot1$)

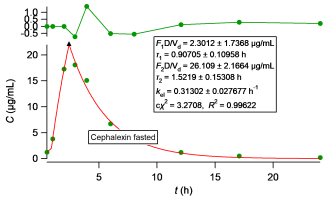

(d) Cephalexin Monohydrate (fasted) ($zot2$)

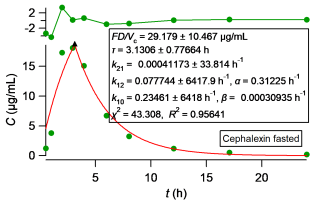

(e) Cephalexin Monohydrate (fasted) ($zwt1\_k$)

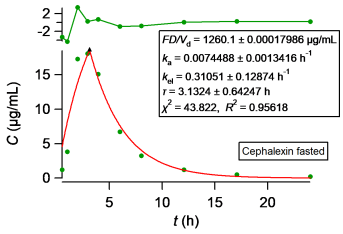

(f) Cephalexin Monohydrate (fasted) (fwt_k)

Figure 4.7: Curve fittings using the classical Bateman equation (4.7a) and the PBFTPK models (4.7b-4.7f) for cephalexin monohydrate (fasted) oral absorption data [44]. Table 4.3 serves as a key for this figure.

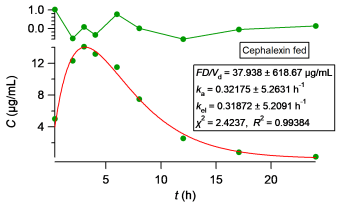

(a) Cephalexin Monohydrate (fed) (fo)

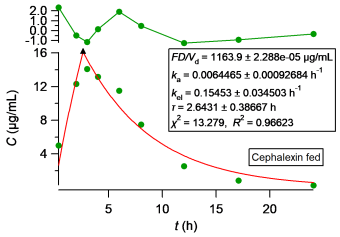

(b) Cephalexin Monohydrate (fed) (fot)

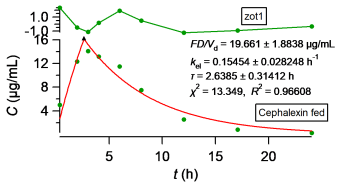

(c) Cephalexin Monohydrate (fed) ($zot1$)

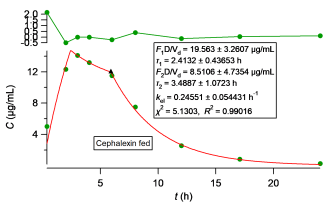

(d) Cephalexin Monohydrate (fed) ($zot2$)

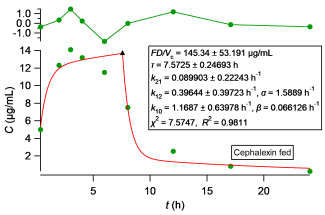

(e) Cephalexin Monohydrate (fed) ($zwt1\_k$)

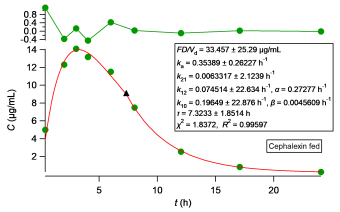

(f) Cephalexin Monohydrate (fed) (fwt_k)

Figure 4.8: Curve fittings using the classical Bateman equation (4.8a) and the PBFTPK models (4.8b-4.8f) for cephalexin monohydrate (fed) oral absorption data [44]. Table 4.3 serves as a key for this figure.

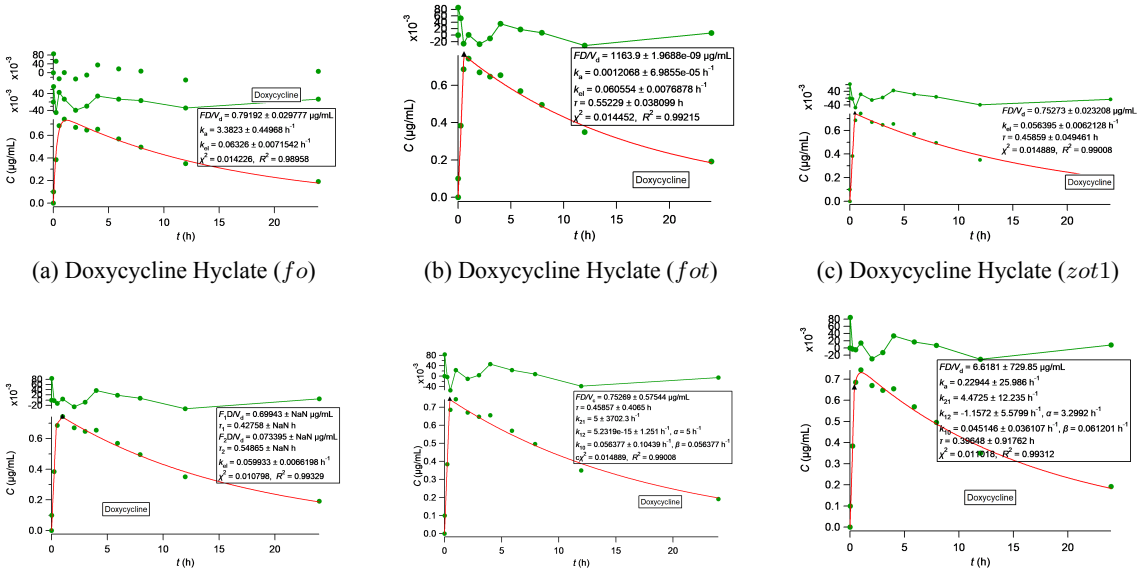

(a) Doxycycline Hyclate (fo) (b) Doxycycline Hyclate (fot) (c) Doxycycline Hyclate ($zot1$)

(d) Doxycycline Hyclate ($zot2$) (e) Doxycycline Hyclate ($zwt1\_k$) (f) Doxycycline Hyclate (fwt_k)

Figure 4.9: Curve fittings using the classical Bateman equation (4.9a) and the PBFTPK models (4.9b-4.9f) for doxycycline hyclate oral absorption data [45]. Table 4.3 serves as a key for this figure.

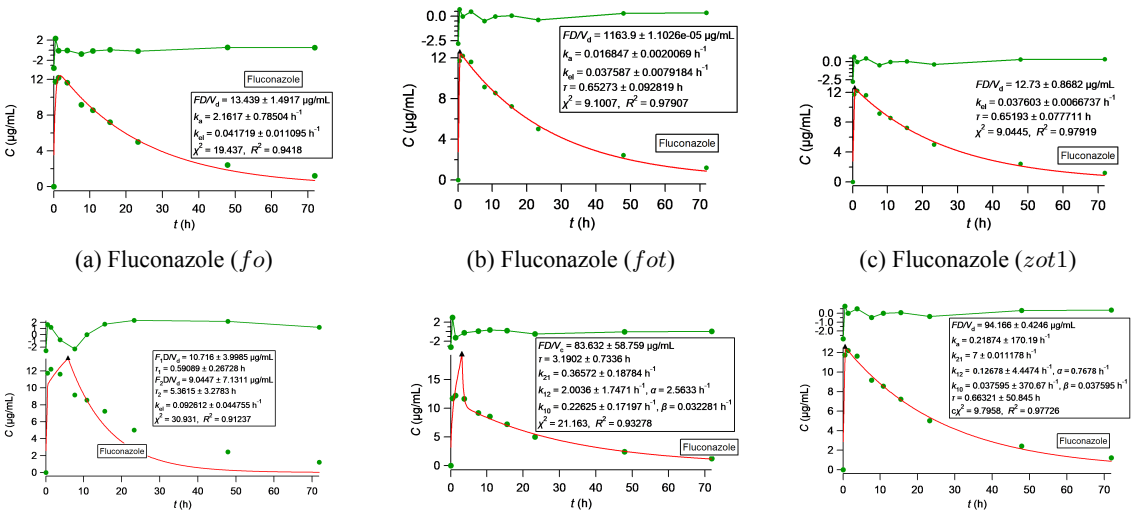

(a) Fluconazole (fo) (b) Fluconazole (fot) (c) Fluconazole ($zot1$)

(d) Fluconazole ($zot2$) (e) Fluconazole ($zwt1\_k$) (f) Fluconazole (fwt_k)

Figure 4.10: Curve fittings using the classical Bateman equation (4.9a) and the PBFTPK models (4.10b-4.10f) for fluconazole (fasted) oral absorption data [46]. Table 4.3 serves as a key for this figure.

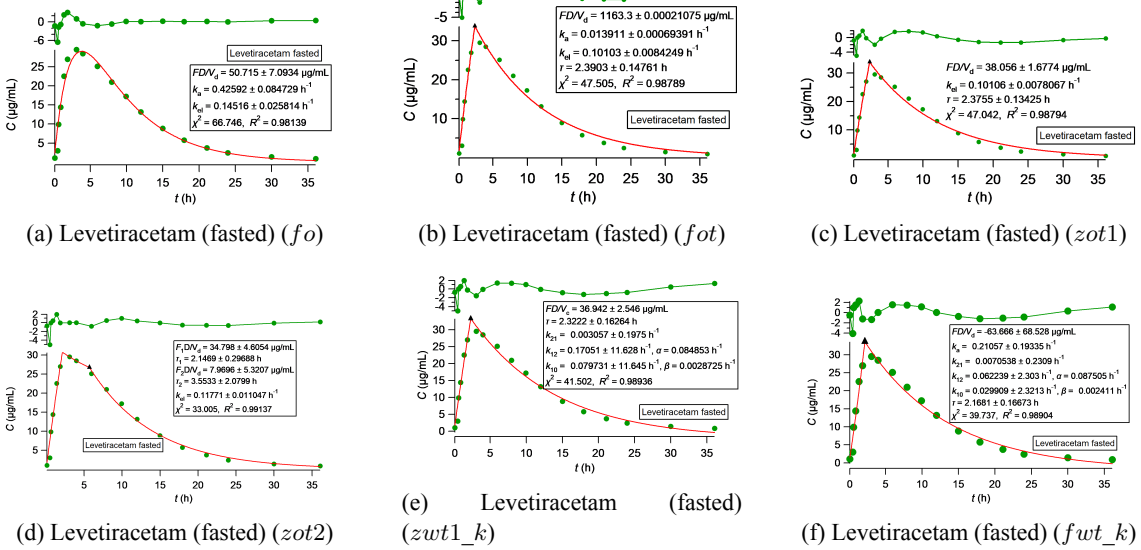

(a) Levetiracetam (fasted) (fo) (b) Levetiracetam (fasted) (fot) (c) Levetiracetam (fasted) ($zot1$)

(d) Levetiracetam (fasted) ($zot2$) (e) Levetiracetam (fasted) ($zwt1\_k$) (f) Levetiracetam (fasted) (fwt_k)

Figure 4.11: Curve fittings using the classical Bateman equation (4.11a) and the PBFTPK models (4.11b-4.11f) for levetiracetam (fasted) oral absorption data [47]. Table 4.3 serves as a key for this figure.

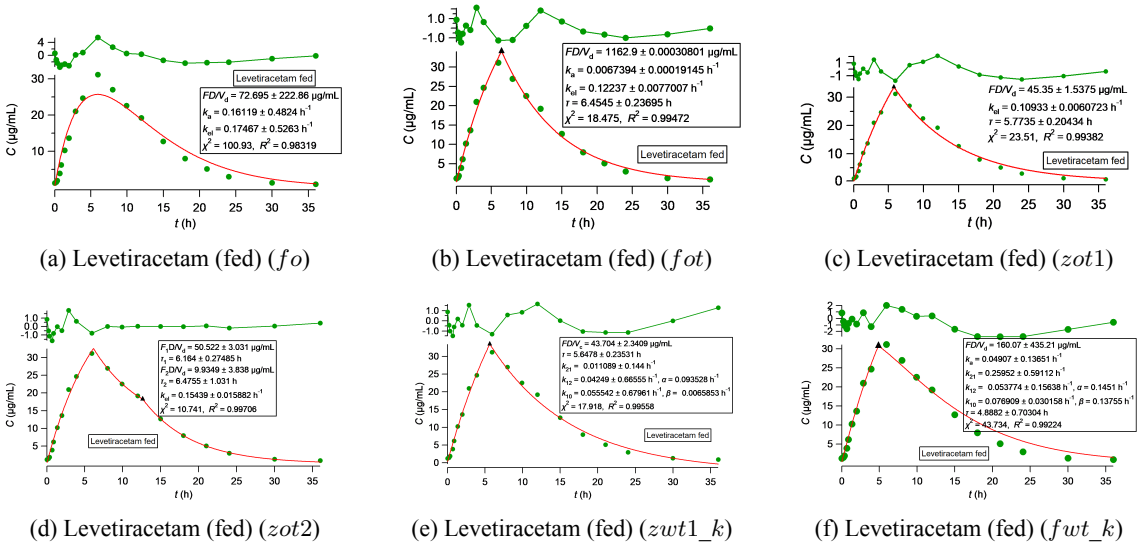

(a) Levetiracetam (fed) (fo) (b) Levetiracetam (fed) (fot) (c) Levetiracetam (fed) ($zot1$)

(d) Levetiracetam (fed) ($zot2$) (e) Levetiracetam (fed) ($zwt1\_k$) (f) Levetiracetam (fed) (fwt_k)

Figure 4.12: Curve fittings using the classical Bateman equation (4.12a) and the PBFTPK models (4.12b-4.12f) for levetiracetam (fed) oral absorption data [47]. Table 4.3 serves as a key for this figure.

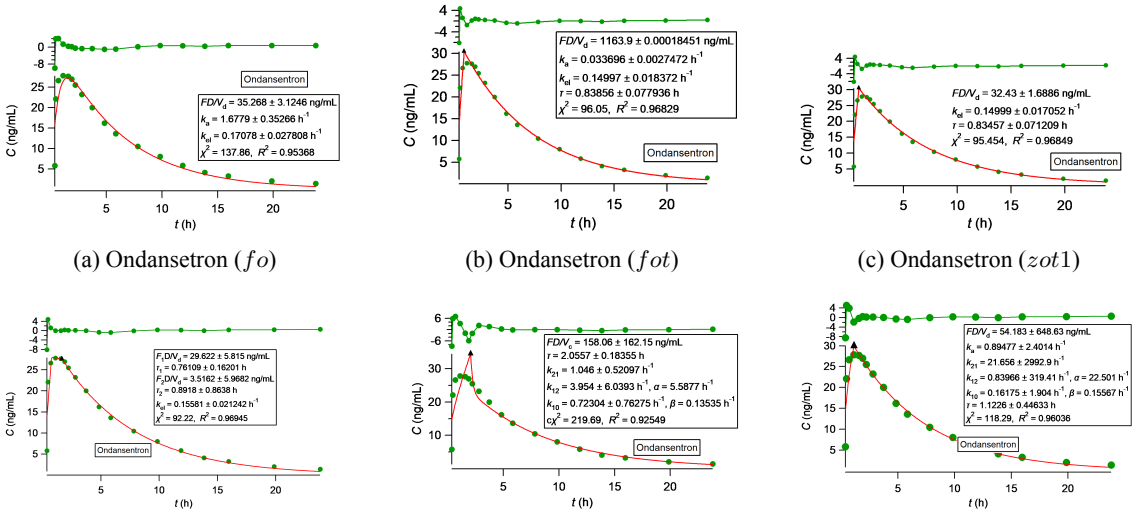

(a) Ondansetron (fo) (b) Ondansetron (fot) (c) Ondansetron ($zot1$)

(d) Ondansetron ($zot2$) (e) Ondansetron ($zwt1\_k$) (f) Ondansetron (fwt_k)

Figure 4.13: Curve fittings using the classical Bateman equation (4.13a) and the PBFTPK models (4.13b-4.13f) for ondansetron oral absorption data [48]. Table 4.3 serves as a key for this figure.

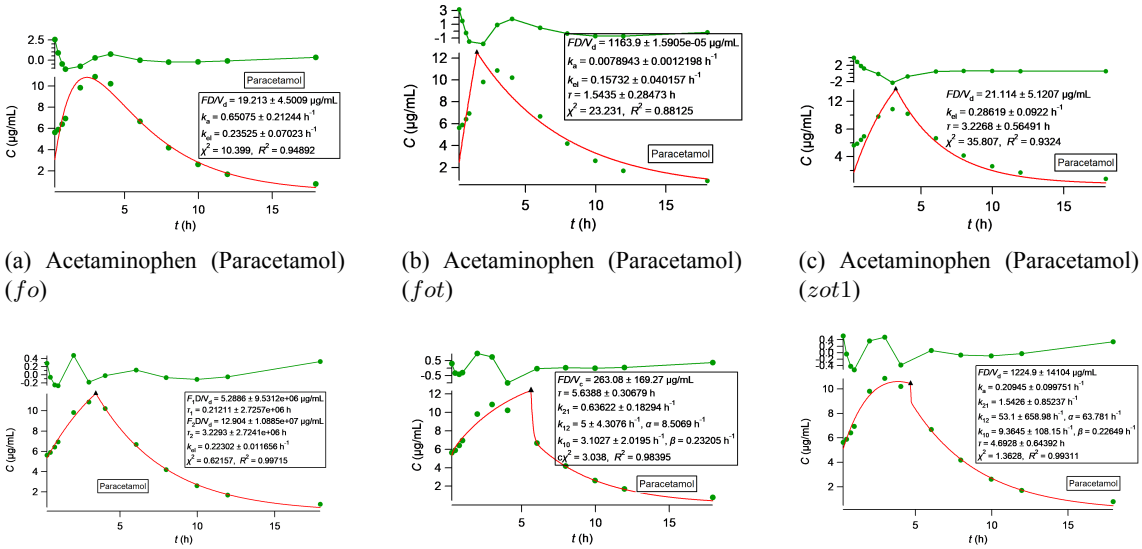

(a) Acetaminophen (Paracetamol) (fo) (b) Acetaminophen (Paracetamol) (fot) (c) Acetaminophen (Paracetamol) ($zot1$)

(d) Acetaminophen (Paracetamol) ($zot2$) (e) Acetaminophen (Paracetamol) ($zwt1\_k$) (f) Acetaminophen (Paracetamol) (fwt_k)

Figure 4.14: Curve fittings using the classical Bateman equation (4.14a) and the PBFTPK models (4.14b-4.14f) for acetaminophen (paracetamol) oral absorption data [49]. Table 4.3 serves as a key for this figure.

Table 4.4 consolidates a comprehensive listing of the drugs delineated in Table 4.1, accompanied by their respective abbreviations for the Physiologically Based Finite Time Pharmacokinetic (PBFTPK) models, as delineated in Table 4.3. The estimated absorption duration, τ (h), is provided for each drug-model pairing, with specific delineation of τ_1 (h) and τ_2 (h) in instances where the model comprises two successive input stages. Furthermore, the R^2 from each fitting and the Akaike Information Criterion, (AIC), computed according to Equation 3.1, explicated in the methods section, are presented for each model for the purposes of model selection. The lowest AIC value and the highest R^2 value for each drug-model pair is highlighted with purple and blue, respectively, in Table 4.4.

Table 4.4: Estimated absorption duration and model metrics. The absorption process endpoints, τ, and τ_1/ τ_2 (for 2-stage input models) (h) derived from the model curve fittings seen in Figures 4.1 - 4.14, are listed. R^2 and AIC values for each model, with the highest R^2 highlighted in blue and the lowest AIC in purple for optimal model selection, are also present.

Drug Name	PBFTPK model	τ (± SD) (h)	τ_1 (± SD) (h)	τ_2 (± SD) (h)	AIC	R^2
Amitriptyline Hydrochloride [40]	fo	-	-	-	64.88242346	0.87639
	fot	3.2156±0.037667	-	-	57.82412111	0.95516
	zot1	3.2054±0.48093	-	-	55.62199274	0.95611
	zot2	-	2.1142±0.3648	0.90773±0.003948	47.448315	0.98938
	zwt1_k	3.3975±0.69441	-	-	62.76174693	0.95621
	zwt2_k	-	1.6595±0.030016	1.3992±0.040167	1.398462828	0.99987
	fwt_k	3.4086±0.83432	-	-	64.97285008	0.95525
Amoxicillin Trihydrate [41]	fo	-	-	-	-11.11121836	0.9924
	fot	0.62397±0.05115	-	-	-8.850176932	0.99411
	zot1	0.62375±0.03622	-	-	-10.80478209	0.99408
	zot2	-	0.64233±0.05657	7.9409±5.4008	-8.244775832	0.99458
	zwt1_k	0.79088±0.0947	-	-	10.93935884	0.98643
	fwt_k	3.8271±2.8345	-	-	10.32578061	0.98562
Acetylsalicylic Acid [42]	fo	-	-	-	33.02635568	0.98229
	fot	1.5449±0.10034	-	-	24.17148112	0.99322
	zot1	1.5381±0.083705	-	-	22.16254626	0.9932
	zot2	-	1.2884±4.3499	0.75545±3.5552	31.71393817	0.9899
	zwt1_k	1.5483±0.14101	-	-	30.06854578	0.99312
	fwt_k	1.6692±20.357	-	-	33.00374907	0.993
Bisoprolol Fumarate [43]	fo	-	-	-	30.19300893	0.99514
	fot	1.3458±0.098127	-	-	34.32320402	0.99155
	zot1	1.339±0.081596	-	-	32.31025158	0.99156
	zot2	-	1.1092±0.065859	2.0649±0.22019	16.29141851	0.99922
	zwt1_k	2.6143±0.29308	-	-	48.48176383	0.98059
	fwt_k	3.6304±104.23	-	-	56.41822443	0.9657
Cephalexin Monohydrate (fasted) [44]	fo	-	-	-	52.98113932	0.8939
	fot	3.1324±0.64247	-	-	45.80135974	0.95618
	zot1	3.1309±0.53286	-	-	43.68360466	0.95647
	zot2	-	0.90705±0.10958	1.5219±0.15308	21.85034603	0.99622
	zwt1_k	3.1306±0.77664	-	-	51.68337375	0.95641
	fwt_k	3.1324±0.64247	-	-	26.62259459	0.95618
Cephalexin Monohydrate (fed) [44]	fo	-	-	-	13.96765768	0.99384
	fot	2.6431±0.38667	-	-	31.27565456	0.96623
	zot1	2.6385±0.31412	-	-	29.32297328	0.96608
	zot2	-	2.4132±0.43653	3.4887±1.0723	24.71647723	0.99016
	zwt1_k	7.5725±0.24693	-	-	32.22332372	0.9811
	fwt_k	7.3233±1.8533	-	-	21.47418406	0.99597

Drug Name	PBFTPK model	τ (± SD) (h)	τ_1 (± SD) (h)	τ_2 (± SD) (h)	AIC	R^2
Doxycycline Hyclate [45]	fo	-	-	-	-45.03220803	0.98958
	fot	0.55229±0.038099	-	-	-42.84306959	0.99215
	zot1	0.45859±0.04946	-	-	-44.48559112	0.99008
	zot2	-	0.42758	0.54865	-44.34073217	0.99329
	zwt1_k	0.45857±0.4065	-	-	-36.48559112	0.99008
	fwt_k	0.39648±0.91762	-	-	-38.09869976	0.99312
Fluconazole [46]	fo	-	-	-	35.67178466	0.9418
	fot	0.65273±0.09282	-	-	30.08351334	0.97907
	zot1	0.65193±0.07771	-	-	28.02156838	0.97919
	zot2	-	0.59089±0.26728	5.3615±3.2783	44.31758917	0.91237
	zwt1_k	3.1902±0.7336	-	-	44.52254374	0.93278
	fwt_k	0.66321±50.845	-	-	38.81953722	0.97726
Levetiracetam (fasted) [47]	fo	-	-	-	81.6160987	0.98139
	fot	2.3903±0.14761	-	-	77.4950294	0.98789
	zot1	2.3755±0.13425	-	-	75.3187348	0.98794
	zot2	-	2.1469±0.29688	3.5533±2.0799	72.9398632	0.99137
	zwt1_k	2.3222±0.16264	-	-	81.0633491	0.98937
	fwt_k	2.1681±0.16673	-	-	82.2810894	0.98904
Levetiracetam (fed) [47]	fo	-	-	-	93.6741169	0.98319
	fot	6.4545±0.23695	-	-	63.4119509	0.99472
	zot1	5.7735±0.20434	-	-	65.9910914	0.99382
	zot2	-	6.164±0.27485	6.4755±1.031	55.1072957	0.99706
	zwt1_k	5.6478±0.23531	-	-	68.8303101	0.99558
	fwt_k	4.8882±0.70304	-	-	87.7843908	0.99224
Ondansetron [48]	fo	-	-	-	94.6722962	0.95368
	fot	0.83856±0.07794	-	-	90.16764	0.96829
	zot1	0.83457±0.07121	-	-	88.0556002	0.96849
	zot2	-	0.76109±0.16201	0.8918±0.8638	91.4351865	0.96945
	zwt1_k	2.0557±0.18355	-	-	111.059914	0.92549
	fwt_k	1.1226±0.44633	-	-	101.916506	0.96036
Acetaminophen (Paracetamol) [49]	fo	-	-	-	34.1005158	0.94892
	fot	1.5435±0.28473	-	-	45.7458511	0.88125
	zot1	3.2268±0.56491	-	-	48.9377209	0.9324
	zot2	-	0.21211±0.27257	3.2293±0.27241	4.29391908	0.99715
	zwt1_k	0.21211±0.27257	-	-	27.3343929	0.98395
	fwt_k	4.6928±0.64392	-	-	19.7144969	0.99311

Upon initial examination of Figures 4.3 - 4.14 and the corresponding model selection parameters in Table 4.4, a discernible trend emerges, underscoring the superior fitting performance of Physiologically-Based Finite Time Pharmacokinetic (PBFTPK) models over the classical Bateman equation. Specifically, for each drug product/formulation, a PBFTPK model consistently yielded the best fit, as evidenced by R^2 values exceeding 0.99 in the majority of cases. Notably, in nine out of the twelve datasets, the Akaike Information Criterion (AIC) aligns harmoniously with the R^2 values, meaning that the model boasting the lowest AIC value coincided with the one exhibiting the highest R^2 value, thereby reinforcing its standing as the preferred model for achieving an ideal fit. In cases where the AIC and R^2 did not entirely concur, the R^2 consistently favored a PBFTPK model. Notably, the classical Bateman equation demonstrated optimal AIC values due to its inherent simplicity and omission of data errors, i.e, no statistical weights were used.

It is noteworthy that every PBFTPK model identified as either the best or optimally fitting adhered to zero-order pharmacokinetics, with the exception of the dataset involving cephalexin monohydrate under fed conditions, which predominantly followed first-order pharmacokinetics. Additionally, only two datasets, namely amitriptyline hydrochloride and cephalexin monohydrate (under fed conditions), conformed to a two-compartment model of disposition. In contrast, all other datasets adhered to a one-compartment model of disposition, thereby corroborating the findings outlined in Table 4.2.

In Table 4.5, columns encompassing crucial pharmacokinetic parameters extracted from Figures 4.3 - 4.14 are presented. Specifically, absorption and elimination rate constants, k_a and k_{el} (h^{-1}), respectively, derived from fittings utilizing the $(PBFTPK)_0$ and $(PBFTPK)_1$ models are detailed. Concomitant with these parameters is the corresponding absolute bioavailability, F, calculated through Equations 2.27 and 2.32, respectively.

Table 4.5: The bioavailable fraction (F) for each drug listed in Table 4.1 is presented, calculated using the elimination and absorption rate constants, k_{el} and k_a, (h^-1), respectively, from the $(PBFTPK)_0$ and $(PBFTPK)_1$ fittings (corresponding to Equations 2.27 and 2.32) in Figures 4.3 - 4.14. The corresponding rate constants are also enlisted in the table.

Drug Name	PBFTPK model	k_a (h^{-1})	k_{el} (h^{-1})	F
Amitriptyline Hydrochloride [40]	fot	0.008±0.001	0.128±0.0376	0.81 ± 0.26
	zot1	-	0.12926±0.032367	0.8071±0.2356
Amoxicillin Trihydrate [41]	fot	0.005±0.0003	0.246±0.0339	0.925 ± 0.159
	zot1	-	0.2469±0.024093	0.9250±0.1050
Acetylsalicylic Acid [42]	fot	0.015±0.0008	0.279±0.027	0.8 ± 0.1
	zot1	-	0.27922±0.023393	0.8006±0.0800
Bisoprolol Fumarate [43]	fot	0.021±0.001	0.0578±0.00702	0.962 ± 0.15
	zot1	-	0.057841±0.0059294	0.9618±0.1147
Cephalexin Monohydrate (fasted) [44]	fot	0.0074±0.0013	0.311±0.128	0.592 ± 0.294
	zot1	-	0.31253±0.10894	0.5893±0.2286
Cephalexin Monohydrate (fed) [44]	fot	0.0064±0.00092	0.1545±0.0345	0.81 ± 0.25
	zot1	-	0.15454±0.028248	0.8099±0.1767
Doxycycline Hyclate [45]	fot	0.0012±6.9855E-5	0.0605±0.00768	0.98 ± 0.15
	zot1	-	0.056395±0.0062128	0.9871±0.1522
Fluconazole [46]	fot	0.0168±0.002	0.0375±0.00779	0.988 ± 0.275
	zot1	-	0.037603±0.0066737	0.9878±0.2112
Levetiracetam (fasted) [47]	fot	0.0139±0.00069	0.101±0.0084	0.89 ± 0.1
	zot1	-	0.10106±0.0078067	0.8848±0.0847
Levetiracetam (fed) [47]	fot	0.0067±0.00019	0.122±0.0077	0.66 ± 0.05
	zot1	-	0.10933±0.0060723	0.7174±0.0472
Ondansetron [48]	fot	0.0336±0.0027	0.15±0.018	0.94 ± 0.16
	zot1	-	0.14999±0.017052	0.9387±0.1334
Acetaminophen (Paracetamol) [49]	fot	0.0078±0.0012	0.157±0.0402	0.88 ± 0.31
	zot1	-	0.28619±0.0922	0.6083±0.2231

Table 4.5 demonstrates that estimates derived from both $(PBFTPK)_0$ and $(PBFTPK)_1$ models yield comparable bioavailable fractions, F, utilizing Equations 2.27 and 2.32, respectively. Noteworthy exceptions include levetiracetam (under fed conditions) where F was found to be 0.66 for the $(PBFTPK)_0$ model and, slightly higher, 0.72 for the $(PBFTPK)_1$ model, and acetaminophen (paracetamol) with F values of 0.88 and 0.61, respectively. Additionally, the variance in F between the fasted and fed states for cephalexin monohydrate and levetiracetam underscores the notable food effect of these drugs [17,20]. Despite this, the analysis affirms that for Class I and borderline Class I drugs, whose absorption predominantly concludes in the small intestine, both $(PBFTPK)_0$ and $(PBFTPK)_1$ modes allow for the estimation of F. This achievement is not possible using the classical approach based on the Bateman equation.

However, a word of caution is warranted when applying this method, as many drugs exhibit a two-compartment model of disposition. This limitation should be taken into consideration when assessing the results from the amitriptyline hydrochloride and cephalexin monohydrate (under fed conditions) datasets.

Similarly, Table 4.6 compiles parameters extracted from the semi-logarithmic plots featured in Figure 4.2. Alongside these parameters, the corresponding absolute bioavailability, F, calculated using Equation 2.41 for each drug, are presented.

Table 4.6: The bioavailable fraction (F) as calculated from Equation 2.41 is presented for each Table 4.1 drug. The elimination rate constant, k_{el}, (h^{-1}) and y-intercepts from the semi-logarithmic plots in Figure 4.2, as well as the $[AUC]_0^\infty$ from the corresponding oral data and hypothetical IV curves for each drug, are also presented.

Drug Name	$[AUC]_{0,oral}^{\infty}$	y-intercept	k_{el} (h^{-1})	$[AUC]_{0,iv-hyp}^{\infty}$	F^2	F
Amoxicillin Trihydrate [41]	15.81094451	1.4655172	0.24353	17.77925522	0.889292	0.943023
Acetylsalicylic Acid [42]	94.4769402	3.4217252	0.2549	120.1341659	0.786429	0.886808
Bisoprolol Fumarate [43]	437.9017731	3.6296296	0.062384	604.3031928	0.724639	0.851257
Cephalexin Monohydrate (fasted) [44]	93.27504558	3.2129278	0.21308	116.6310341	0.799745	0.894284
Cephalexin Monohydrate (fed) [44]	117.3624136	3.4680851	0.20211	158.7020072	0.739514	0.85995
Doxycycline Hyclate [45]	9.76937852	-0.2418033	0.059961	13.09535554	0.746019	0.863724
Fluconazole [46]	329.3831895	2.5	0.032918	370.0860915	0.890018	0.943408
Levetiracetam (fatsed) [47]	351.4197476	3.8518519	0.11496	409.5352324	0.858094	0.926334
Levetriracetam (fed) [47]	383.2916107	4.3298969	0.12872	589.9351858	0.649718	0.806051
Ondansetron [48]	108.8691885	3.5	0.13911	238.0522749	0.457333	0.676264
Acetaminophen (Paracatamol) [49]	72.7231441	2.96	0.18695	103.2253103	0.704509	0.83935

Equation 2.41 is applicable exclusively to drugs conforming to a one-compartment model of disposition. While this was evident from the outset for amitriptyline hydrochloride, as indicated in Table 4.2, a note of caution is warranted for cephalexin monohydrate under fed conditions due to new insights gleaned from Table 4.4. Unlike the scenario observed with theophylline in [5], only amoxicillin trihydrate, fluconazole, and levetiracetam under fed conditions yielded somewhat congruent results with those derived from equations 2.27 and 2.32.

Finally, in Table 4.7, the absolute bioavailability values (F) obtained through the three distinct methods and documented in the preceding tables (Tables 4.5 and 4.6) are systematically compared with the absolute bioavailability of each drug, as documented in their respective monographs in the literature. Additionally, the fraction of these values attributable to the first-pass effect is explicitly outlined. Values with dark green highlights indicate the highest F values, whereas those with blue highlights correspond to the lowest calculated F values.

Table 4.7: The bioavailable fractions from Tables 4.5 and 4.6, are presented in comparison to literature values for each drug. Additionally, the fraction attributable to the first-pass effect is also provided.

Drug name	F reported in the literature	F due to first-pass effect	F (Eq.2.27)	F (Eq. 2.32)	F (Eq.2.41)
Amitriptyline Hydrochloride [40]	0.9	0.48	0.8077	0.8071	-
Amoxicillin Tryhydrate [41]	0.894 - 0.97	0.26	0.925	0.925	0.943
Acetylsalicylic Acid [42]	0.68 - 0.85	0.2	0.8005	0.8006	0.8868
Bisoprolol Fumarate [43]	0.9	0.1 - 0.15	0.9618	0.9618	0.851
Cephalexin Monohydrate (fasted) [44]	0.8 - 0.9	<0.1	0.5924	0.5893	0.894
Cephalexin Monohydrate (fed) [44]	0.8 - 0.9	<0.1	0.8101	0.8099	0.85995
Doxycycline Hyclate [45]	0.9 - 1	<0.05	0.9834	0.9871	0.8637
Fluconazole [46]	0.9	0.11	0.9878	0.9878	0.9434
Levetiracetam (fasted) [47]	0.95	0.24	0.8847	0.8848	0.9263
Levetiracetam (fed) [47]	0.95	0.24	0.6584	0.7174	0.806
Ondansetron [48]	0.5 - 0.7 (healthy)/0.85 - 0.87(cancer patients)	0.3 - 0.4	0.9387	0.9387	0.676
Acetaminophen (Paracetamol) [49]	0.62 - 0.89	0.25 - 0.3	0.8837	0.6083	0.839

An absolute bioavailability less than 100% indicates that not all the administered drug reach systemic circulation unchanged. The first-pass effect is a crucial consideration in drug development, affecting the choice of administration route and dosage forms to optimize therapeutic effectiveness. For amoxicillin trihydrate, all three methods for calculating F yield results within the range found in the literature [14]. However, Equation 2.41 provides a slightly higher value for F compared to the other two methods. Conversely, for acetylsalicylic acid, all three equations yield results within the literature range [15]. Notably, in this case, the F calculated from Equation 2.41 is slightly lower, bordering the lower limit, in contrast to the F values derived from the other two equations. In the case of bisoprolol fumarate, F estimates from Equations 2.27 and 2.32 surpass the reported literature value [16] ($0.9618 > 0.90$), suggesting a potential issue with the prediction of τ [5]. Conversely, the F calculated from Equation 2.41 is slightly lower than the reported value (0.851). For cephalexin monohydrate under fasted conditions, Equation 2.41 provides an F within the literature range [17]. In the fed state, all three equations yield F values consistent with literature reports. In the case of doxycycline hyclate, F values from Equations 2.27 and 2.32 align with reported literature values [18], while Equation 2.41 underperforms. For fluconazole, all three models yield F values exceeding the reported literature values [19], with Equation 2.41 providing the closest approximation. Once again this is possibly due to an issue with the prediction of τ [5]. In both states (fed and fasted) of levetiracetam, all three methods fail to meet the reported literature F values [20]. However, in both cases, Equation 2.41 yields the closest approximation among the three. For ondansetron [21], Equation 2.41 provides an F value within the reported range for healthy patients, while Equations 2.27 and 2.32 yield F values closer to the range reported for cancer patients. Lastly, for acetaminophen (paracetamol), all three equations yield F values within the reported literature range [22]. In conclusion, while each method demonstrated varying accuracy across different drugs, Equation 2.41 often provided F values within or closest to the reported literature values. However, caution is advised, and the choice of method should consider the specific characteristics of each drug and the limitations of the respective equations, in particular if first-pass effect is operating.

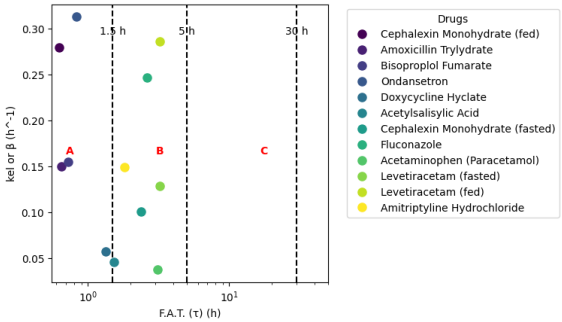

Figure 4.15: Estimated absorption duration, F.A.T. (h) f, plotted against the elimination rate constant k_{el} (h^{-1}) for one-compartment or β (h^{-1}) for two-compartment model drugs. Grouping limits (1.5, 5, and 30 h) delineated by vertical dashed lines categorize the various formulations into three possible sections (A, B, C), offering a comprehensive view of drug absorption dynamics and formulation distinctions.

The current analysis relies on the F.A.T. concept and allows the estimation of τ, which can characterize each drug given as an IR formulation. This is so since τ is conceptually associated with the fundamental biopharmaceutical properties of solubility and permeability. Intuitively, drugs and IR formulations can be classified as

1. rapidly absorbing, $\tau < 1.5$ h,
2. medium absorbing, $1.5 \leq \tau < 5$ h and
3. slow absorbing, $5 \leq \tau < 30$ h

For the first two categories, drug absorption takes place only in the small intestine, while for the third category, colon absorption is also operating. Figure 4.15 shows the proposed three categories (A,B, and C), a framework towards a Biopharmaceutic-Pharmacokinetic Classification System (BPCS). All estimates for τ are coupled with the corresponding estimate for drug's elimination rate constant k_{el} or β for drugs obeying one- or two-compartment model kinetics, respectively. Visual inspection of Figure 4.15 shows that almost all the drugs are positioned in category A and B, i.e., their absorption terminates in less than 5 h which mean that they are indeed absorbed in the small intestine.

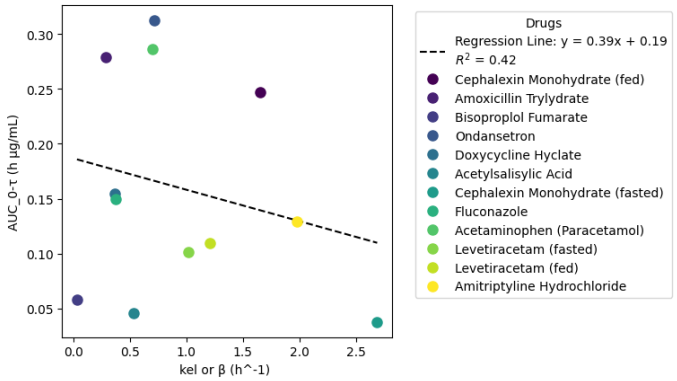

Figure 4.16: Correlation Plot: A comprehensive view of the relationship between Area Under the Curve (AUC), (h*μg/mL) from 0 until the end of the absorption phase, τ (h) and the elimination rate constant k_{el} (h^{-1}). Each data point is color-coded, with Class I biowaiver labels positioned above. The figure includes a linear fitted curve obtained through weighted regression, and the corresponding equation detailed in the legend. The R^2 was found to be 0.4124.

According to Equation 2.24 $[AUC]_0^\tau$ increases when k_{el} decreases. As shown in Figure 4.16, this trend is indeed observable. It should be emphasized that the partial area $[AUC]_0^\tau$ is used today as an early exposure metric; however, what it represents, under the prism of the F.A.T. concept is the fundamental extent of the absorption metric since it is linearly related (as Equation 2.24) with the dose absorbed in time τ, namely, the end of the absorption phase. Caution should be exercised with the use of Figure 4.16 since the volume of distribution of the drugs is different and thus AUC values should be corrected accordingly.

Figures 4.17 - 4.28 depict the percent-absorbed versus time plots as discussed earlier towards the end of Chapter 2. The continuous lines connect the points that correspond to the apparent absorbed concentration and the dashed lines show the absorption profiles based on the F.A.T. The ascending part of the curve determines the slopping line, and the average of remaining data points define the horizontal line. As stated before, their intersection determines the end of the absorption process, i.e., τ.

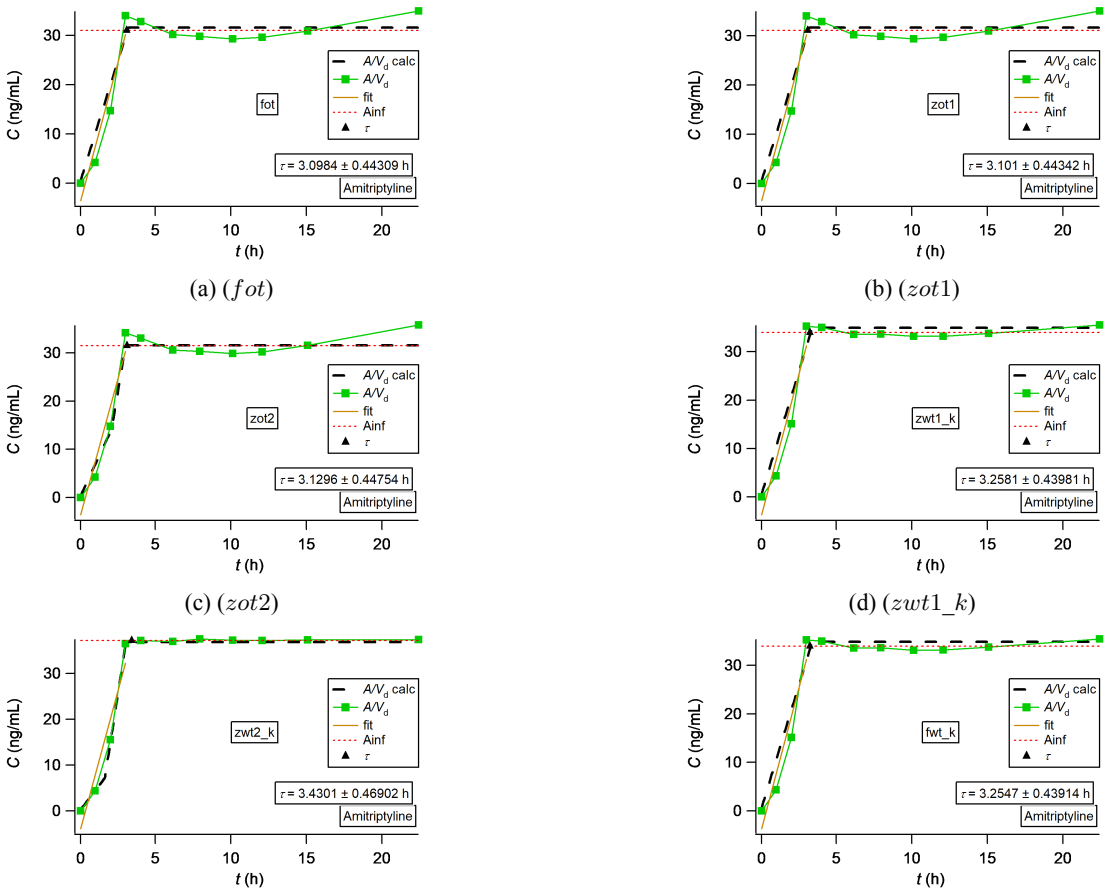

(a) (fot) (b) $(zot1)$

(c) $(zot2)$ (d) $(zwt1\_k)$

(e) $(zwt2\_k)$ (f) (fwt_k)

Figure 4.17: Percent absorbed (expressed as apparent absorbed concentration) $versus$ time plot (green squares and solid line) for amitriptyline hydrochloride derived from the various PBFTPK model fittings [40]. The black triangles denote the termination of drug absorption, i.e., τ. The black dashed line is the simulation based on the modified models, while the solid brown line is the fit of this model to the ascending limb data. The dashed red lines are the average levels of the plateau values.

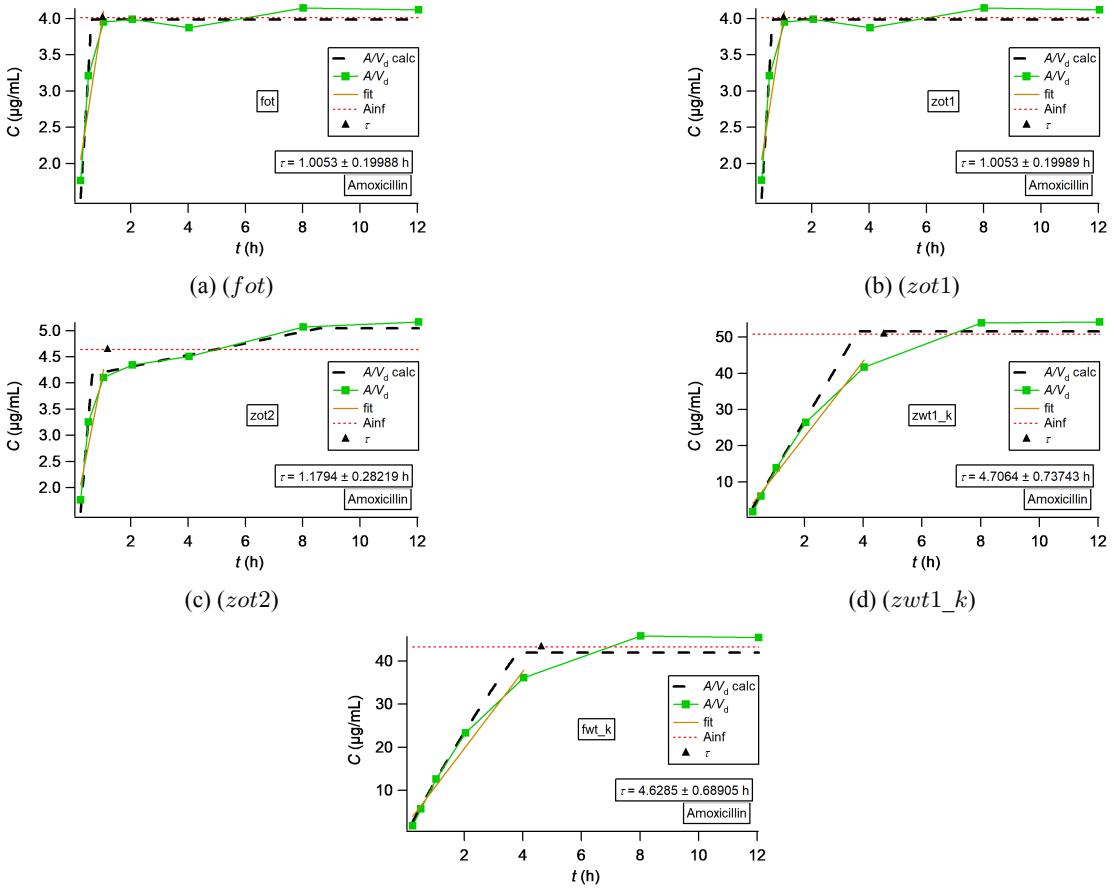

(a) (fot)

(b) $(zot1)$

(c) $(zot2)$

(d) $(zwt1\_k)$

(e) (fwt_k)

Figure 4.18: Percent absorbed (expressed as apparent absorbed concentration) $versus$ time plot (green squares and solid line) for amoxicillin trihydrate derived from the various PBFTPK model fittings [41]. The black triangles denote the termination of drug absorption, i.e., τ. The black dashed line is the simulation based on the modified models, while the solid brown line is the fit of this model to the ascending limb data. The dashed red lines are the average levels of the plateau values.

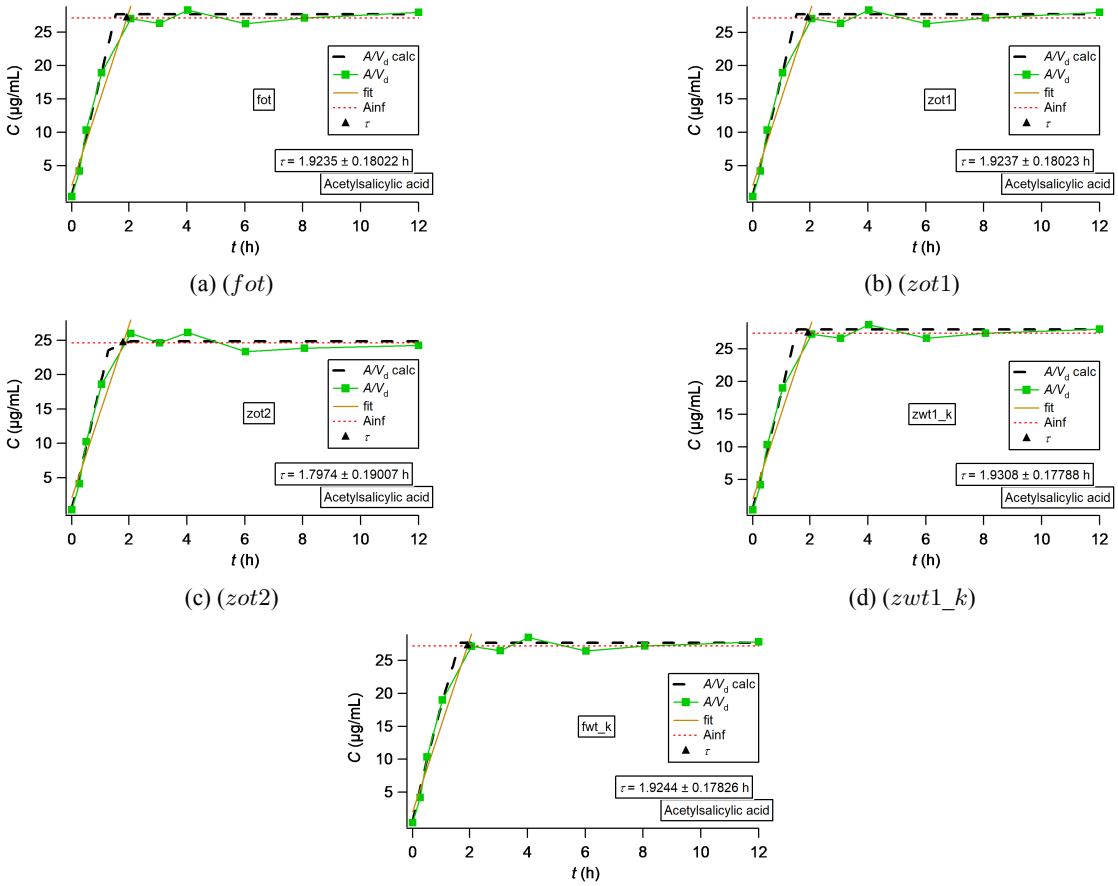

(a) (fot) (b) $(zot1)$

(c) $(zot2)$ (d) $(zwt1\_k)$

(e) (fwt_k)

Figure 4.19: Percent absorbed (expressed as apparent absorbed concentration) $versus$ time plot (green squares and solid line) for acetylsalysilic acid derived from the various PBFTPK model fittings [42]. The black triangles denote the termination of drug absorption, i.e., τ. The black dashed line is the simulation based on the modified models, while the solid brown line is the fit of this model to the ascending limb data. The dashed red lines are the average levels of the plateau values.

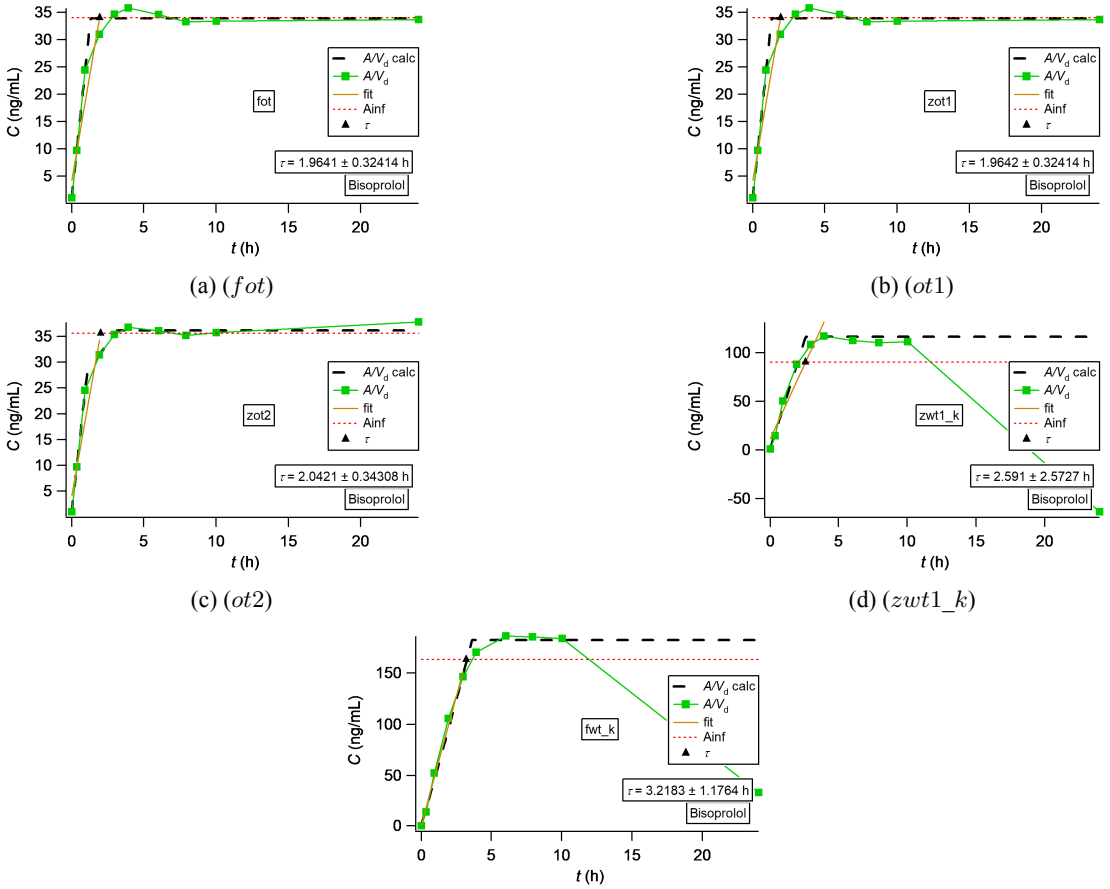

(a) (fot) (b) $(ot1)$

(c) $(ot2)$ (d) $(zwt1\_k)$

(e) (fwt_k)

Figure 4.20: Percent absorbed (expressed as apparent absorbed concentration) $versus$ time plot (green squares and solid line) for bisoprolol fumarate derived from the various PBFTPK model fittings [43]. The black triangles denote the termination of drug absorption, i.e., τ. The black dashed line is the simulation based on the modified models, while the solid brown line is the fit of this model to the ascending limb data. The dashed red lines are the average levels of the plateau values.

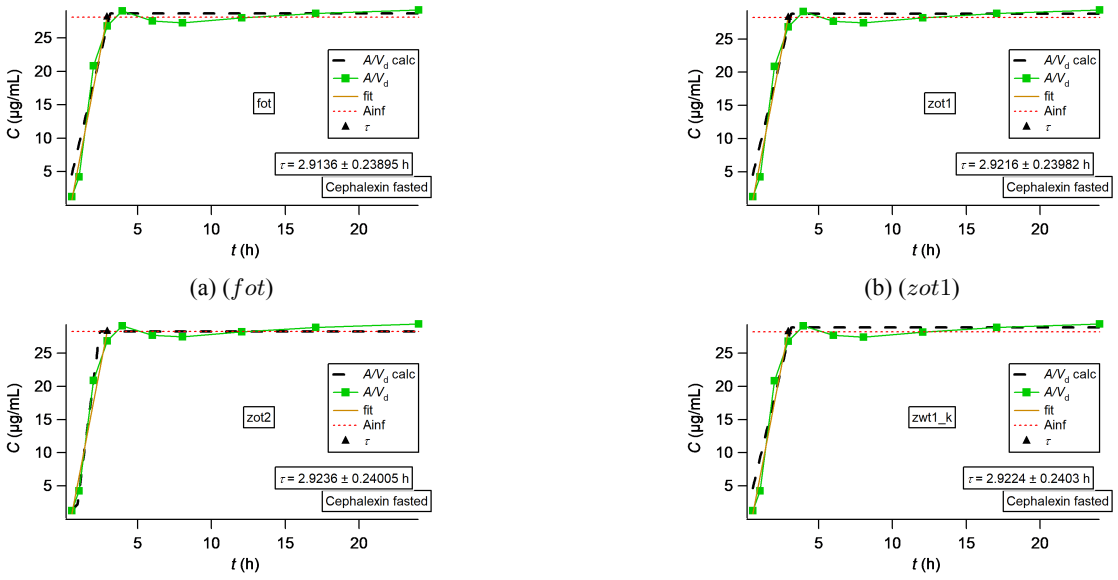

(a) (fot) (b) $(zot1)$

(c) $(zot2)$ (d) $(zwt1\_k)$

Figure 4.21: Percent absorbed (expressed as apparent absorbed concentration) $versus$ time plot (green squares and solid line) for cephalexin monohydrate (fasted) derived from the various PBFTPK model fittings [44]. The black triangles denote the termination of drug absorption, i.e., τ. The black dashed line is the simulation based on the modified models, while the solid brown line is the fit of this model to the ascending limb data. The dashed red lines are the average levels of the plateau values.

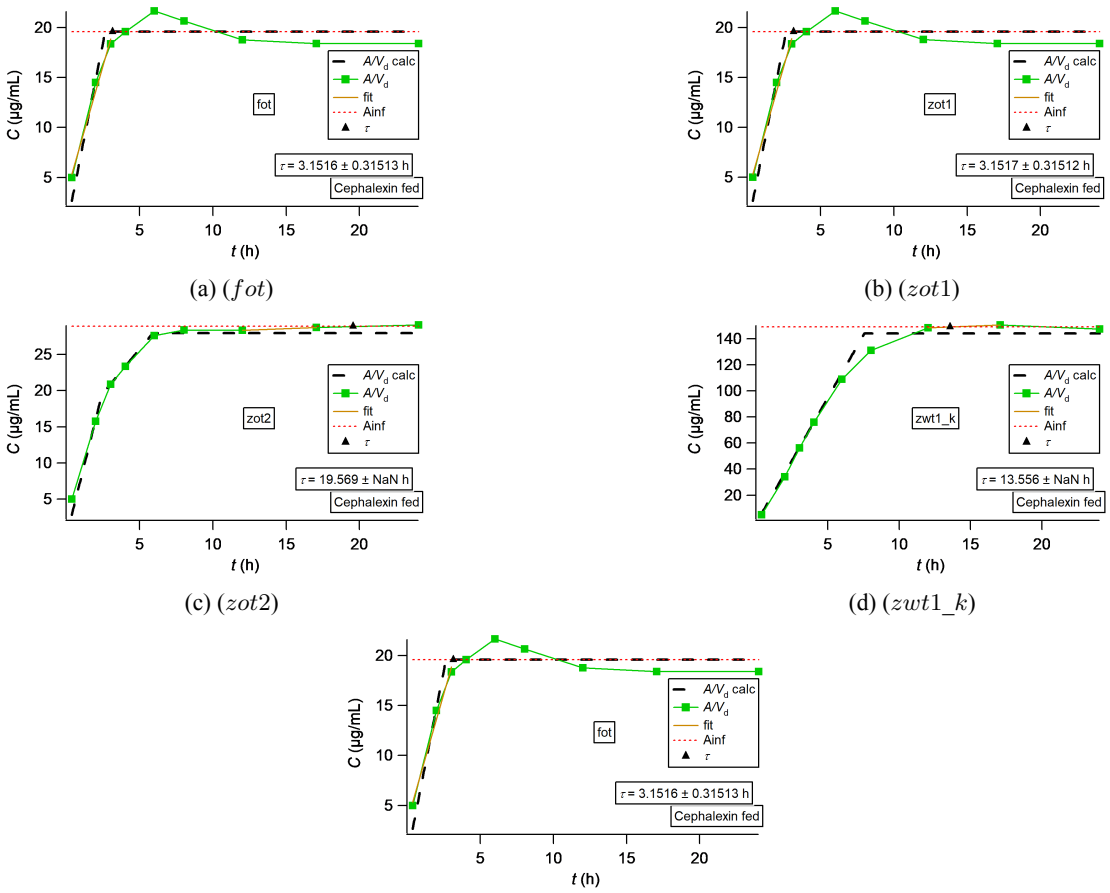

(a) (fot) (b) $(zot1)$

(c) $(zot2)$ (d) $(zwt1\_k)$

(e) (fwt_k)

Figure 4.22: Percent absorbed (expressed as apparent absorbed concentration) $versus$ time plot (green squares and solid line) for cephalexin monohydrate (fed) derived from the various PBFTPK model fittings [44]. The black triangles denote the termination of drug absorption, i.e., τ. The black dashed line is the simulation based on the modified models, while the solid brown line is the fit of this model to the ascending limb data. The dashed red lines are the average levels of the plateau values.

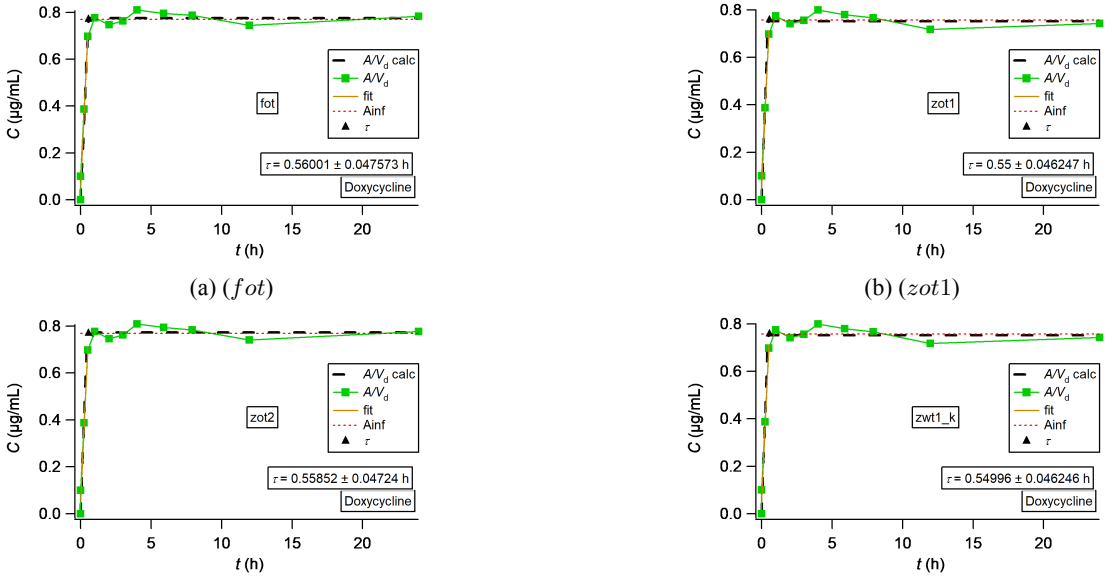

(a) (fot) (b) $(zot1)$

(c) $(zot2)$ (d) $(zwt1\_k)$

Figure 4.23: Percent absorbed (expressed as apparent absorbed concentration) $versus$ time plot (green squares and solid line) for doxycycline hyclate derived from the various PBFTPK model fittings [45]. The black triangles denote the termination of drug absorption, i.e., τ. The black dashed line is the simulation based on the modified models, while the solid brown line is the fit of this model to the ascending limb data. The dashed red lines are the average levels of the plateau values.

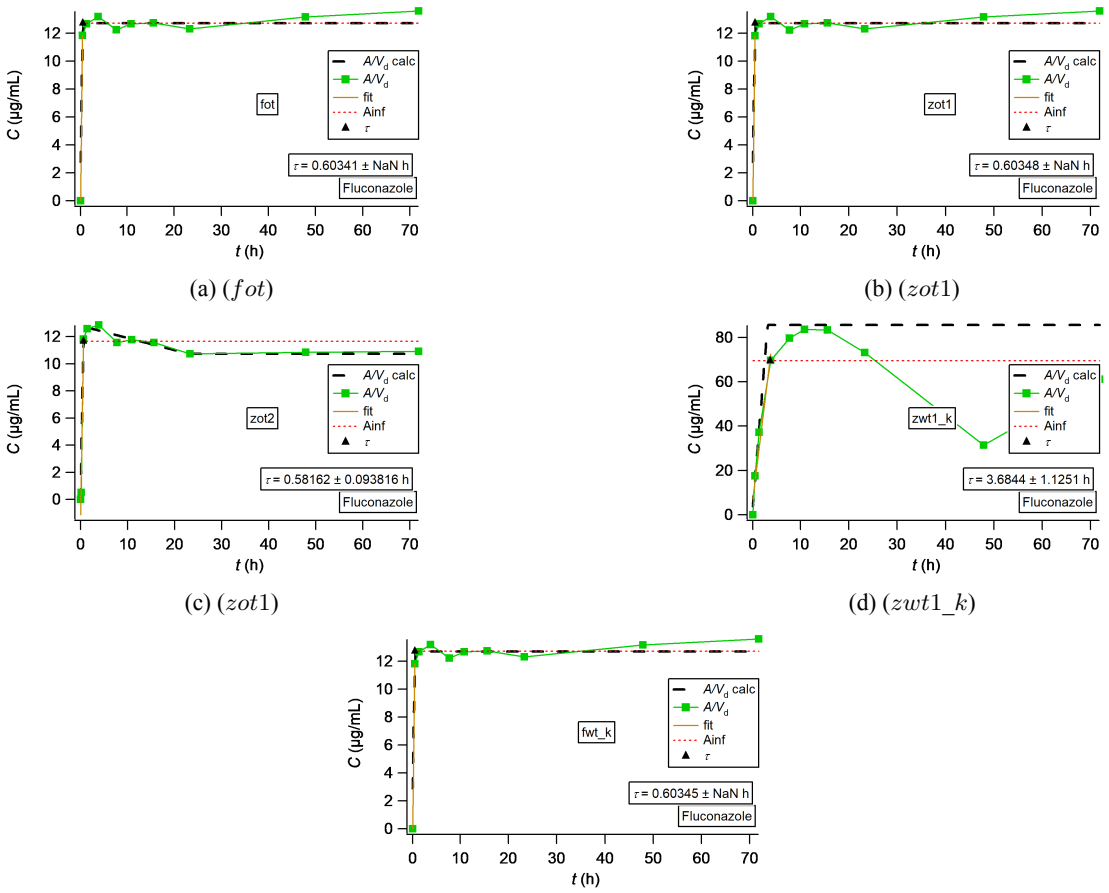

(a) (fot) (b) $(zot1)$

(c) $(zot1)$ (d) $(zwt1\_k)$

(e) (fwt_k)

Figure 4.24: Percent absorbed (expressed as apparent absorbed concentration) $versus$ time plot (green squares and solid line) for fluconazole derived from the various PBFTPK model fittings [46]. The black triangles denote the termination of drug absorption, i.e., τ. The black dashed line is the simulation based on the modified models, while the solid brown line is the fit of this model to the ascending limb data. The dashed red lines are the average levels of the plateau values.

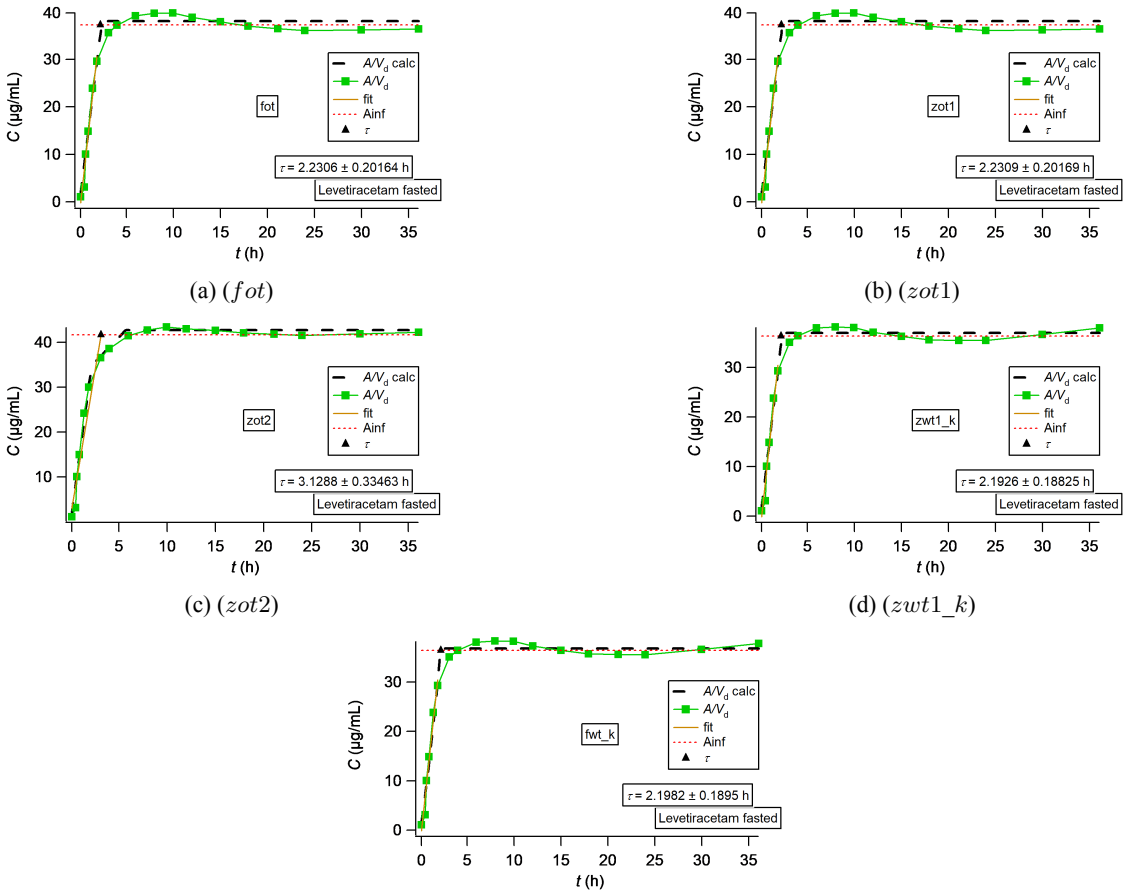

(a) (fot) (b) $(zot1)$

(c) $(zot2)$ (d) $(zwt1\_k)$

(e) (fwt_k)

Figure 4.25: Percent absorbed (expressed as apparent absorbed concentration) $versus$ time plot (green squares and solid line) for levetiracetam (fasted) derived from the various PBFTPK model fittings [47]. The black triangles denote the termination of drug absorption, i.e., τ. The black dashed line is the simulation based on the modified models, while the solid brown line is the fit of this model to the ascending limb data. The dashed red lines are the average levels of the plateau values.

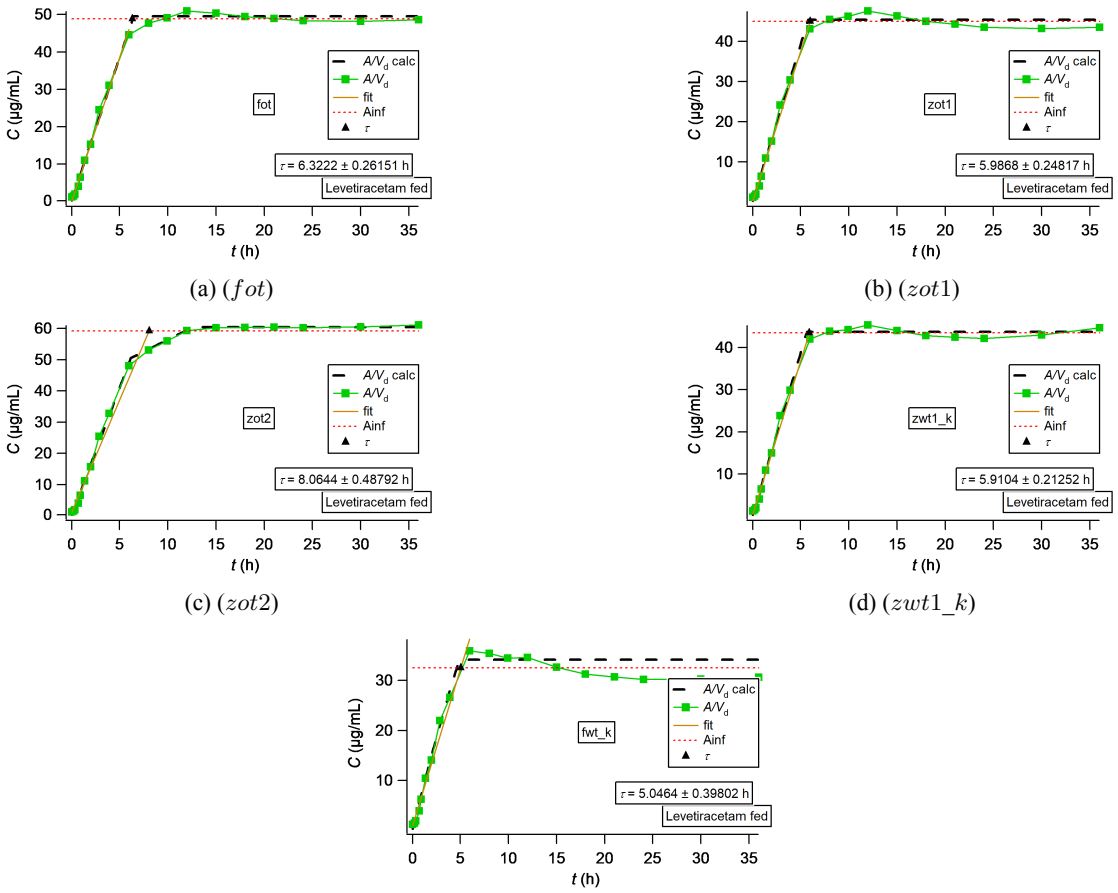

(a) (fot) (b) $(zot1)$

(c) $(zot2)$ (d) $(zwt1\_k)$

(e) (fwt_k)

Figure 4.26: Percent absorbed (expressed as apparent absorbed concentration) $versus$ time plot (green squares and solid line) for levetiracetam (fed) derived from the various PBFTPK model fittings [47]. The black triangles denote the termination of drug absorption, i.e., τ. The black dashed line is the simulation based on the modified models, while the solid brown line is the fit of this model to the ascending limb data. The dashed red lines are the average levels of the plateau values.

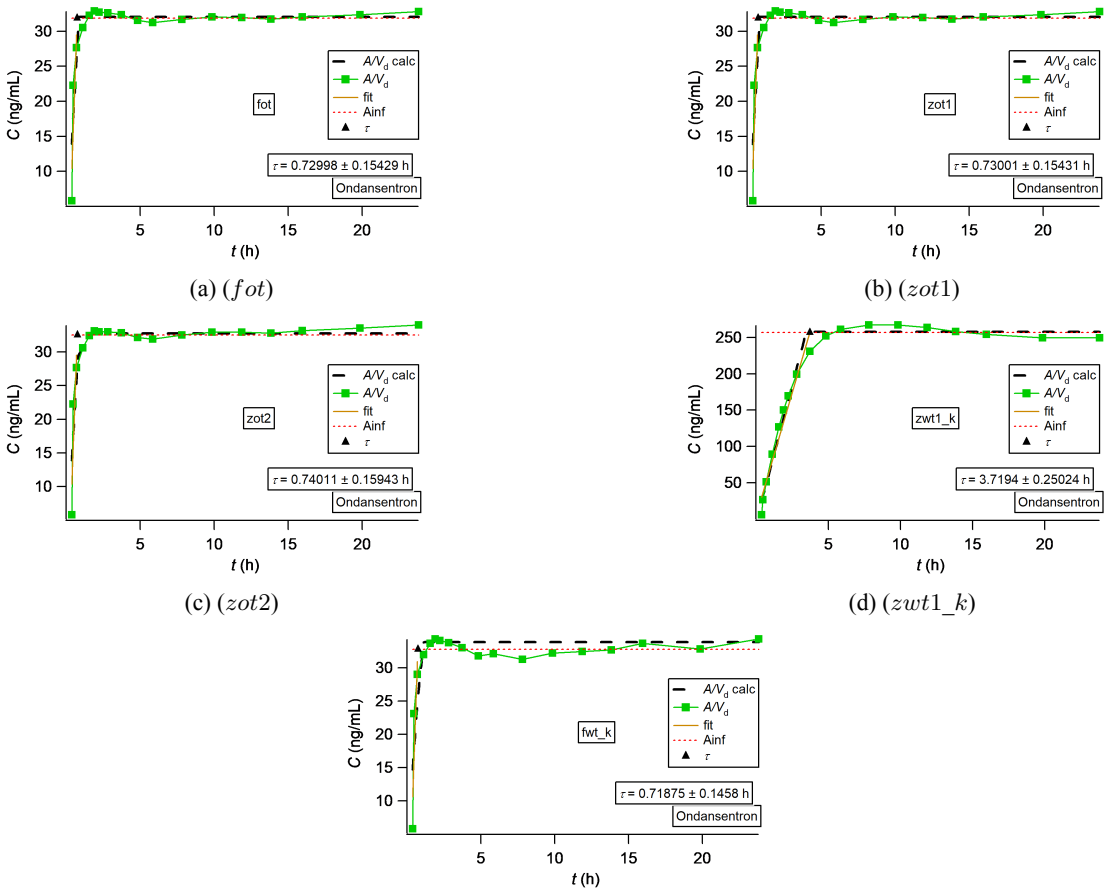

(a) (fot) (b) $(zot1)$

(c) $(zot2)$ (d) $(zwt1\_k)$

(e) (fwt_k)

Figure 4.27: Percent absorbed (expressed as apparent absorbed concentration) $versus$ time plot (green squares and solid line) for ondansetron derived from the various PBFTPK model fittings [48]. The black triangles denote the termination of drug absorption, i.e., τ. The black dashed line is the simulation based on the modified models, while the solid brown line is the fit of this model to the ascending limb data. The dashed red lines are the average levels of the plateau values.

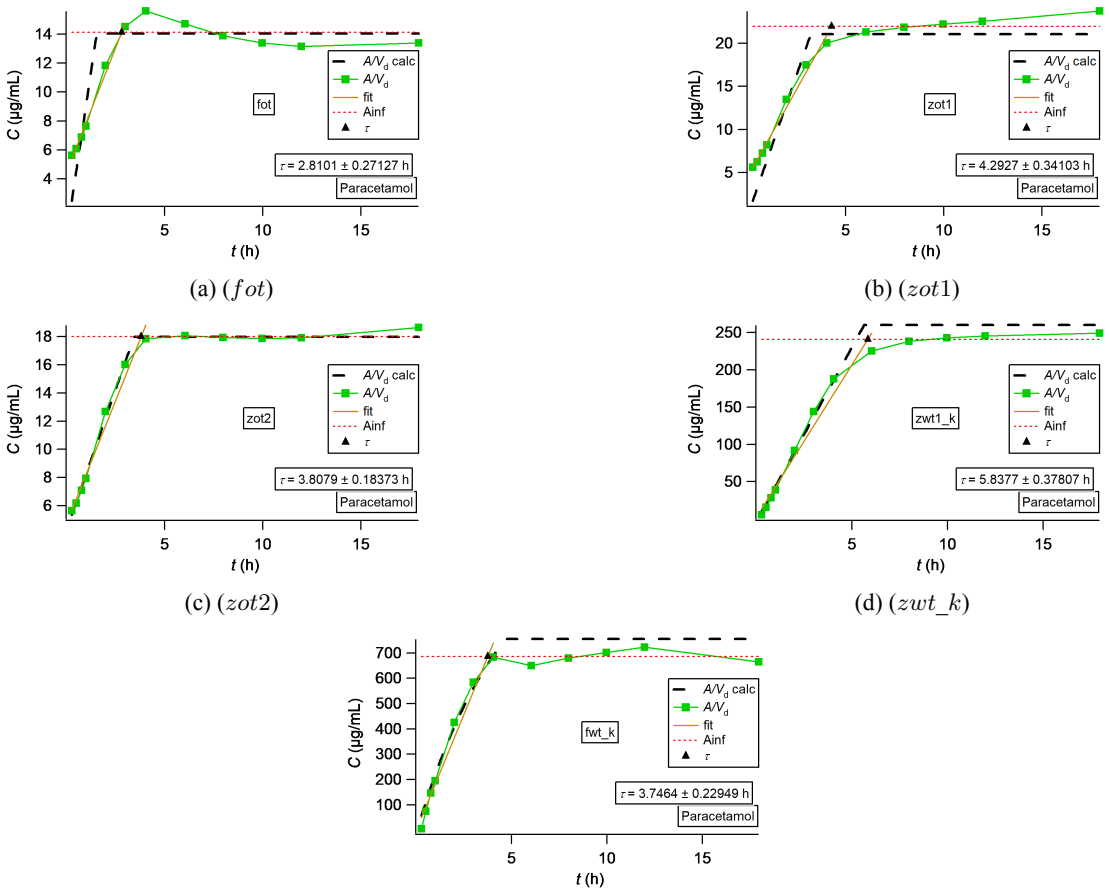

(a) (fot) (b) $(zot1)$

(c) $(zot2)$ (d) (zwt_k)

(e) (fwt_k)

Figure 4.28: Percent absorbed (expressed as apparent absorbed concentration) $versus$ time plot (green squares and solid line) for acetaminophen (paracetamol) derived from the various PBFTPK model fittings [49]. The black triangles denote the termination of drug absorption, i.e., τ. The black dashed line is the simulation based on the modified models, while the solid brown line is the fit of this model to the ascending limb data. The dashed red lines are the average levels of the plateau values.

Last but not least, Table 4.8 summarizes the estimates for the termination of the absorption phase, i.e., τ, from every model depicted in Figure 4.17 through 4.28.

Table 4.8: Displays τ estimates for each PBFTPK model, derived from the percent absorbed versus time plots depicted in Figures 4.17 - 4.28.

Drug Name	PBFTPK model	τ (± SD) (h)
Amitriptyline Hydrochloride [40]	fot	3.0984 ± 0.44309
	zot1	3.101 ± 0.44342
	zot2	3.1296 ± 0.44754
	zwt1_k	3.2581 ± 0.43981
	zwt2_k	3.4301 ± 0.46902
	fwt_k	3.2547 ± 0.43914
Amoxicillin Trihydrate [41]	fot	1.0053±0.19988
	zot1	1.0053 ± 0.19989
	zot2	1.1794 ± 0.28219
	zwt1_k	4.7064 ± 0.73743
	fwt_k	4.6285 ± 0.68905
Acetylsalicylic Acid [42]	fot	1.9235±0.18022
	zot1	1.9237 ± 0.18023
	zot2	1.7974 ± 0.19007
	zwt1_k	1.9308 ± 0.17788
	fwt_k	1.9244 ± 0.17826
Bisoprolol Fumarate [43]	fot	1.9641±0.32414
	zot1	1.9642 ± 0.32414
	zot2	2.0421 ± 0.34308
	zwt1_k	-
	fwt_k	3.2183 ± 1.1764
Cephalexin Monohydrate (fasted) [44]	fot	2.9136±0.23895
	zot1	2.9216 ± 0.23982
	zot2	2.9236 ± 0.24005
	zwt1_k	2.9224 ± 0.2403
Cephalexin Monohydrate (fed) [44]	fot	3.1516±0.31513
	zot1	3.1517 ± 0.31512
	zot2	-
	zwt1_k	-
	fwt_k	-

Drug Name	PBFTPK model	τ (± SD) (h)
Doxycycline Hyclate [45]	fot	0.56001±0.047573
	zot1	0.55 ± 0.046247
	zot2	0.55852 ± 0.04724
	zwt1_k	0.54996 ± 0.046246
Fluconazole [46]	fot	0.60341±0.000654
	zot1	0.60348 ± 0.000625
	zot2	0.58162 ± 0.093816
	zwt1_k	3.6844 ± 1.1251
	fwt_k	0.60345 ± 0.000624
Levetiracetam (fasted) [47]	fot	2.2306±0.20164
	zot1	2.2309 ± 0.20169
	zot2	3.1288 ± 0.33463
	zwt1_k	2.1926 ± 0.18825
	fwt_k	2.1982 ± 0.1895
Levetiracetam (fed) [47]	fot	6.3222±0.26151
	zot1	5.9868 ± 0.24817
	zot2	8.0644 ± 0.48792
	zwt1_k	5.9104 ± 0.21252
	fwt_k	5.0464 ± 0.39802
Ondansetron [48]	fot	0.72998±0.15429
	zot1	0.73001 ± 0.15431
	zot2	0.74011 ± 0.15943
	zwt1_k	3.7194 ± 0.25024
	fwt_k	0.71875 ± 0.1458
Acetaminophen (Paracetamol) [49]	fot	2.8101±0.27127
	zot1	4.2927 ± 0.34103
	zot2	3.8079 ± 0.18373
	zwt1_k	5.8377 ± 0.37807
	fwt_k	3.7464 ± 0.22949

In all of these plots, the continuous lines represent the effective concentration, while the dashed lines depict the absorption profiles based on the Finite Absorption Time (F.A.T.). Figures 4.17-4.28 illustrate the percent absorbed versus time plots for the drugs listed in Table 4.1, derived from the fitting results described in Figures 4.3 – 4.14. Specifically, for the amitriptyline dataset, which aligns better with a zero-order/two-compartment model with two successive input stages (τ_1=1.6595 h and τ_2=1.3992 h, as detailed in Table 4.4), Figure 4.17 depicts the percent absorbed versus time plot. In this plot, the end of the absorption phase is estimated at τ=3.4301 h. The graph reveals two distinct ascending limbs, each consisting of two data points, leading to a horizontal plateau. This pattern persists throughout Figures 4.18-4.28, with sporadic major deviations attributed to potential inaccuracies in τ estimation.

2. Temporal Biopharmaceutics Classification System: Coupling Drug Dissolution with BCS

In a recent article we introduced the concept of Finite Dissolution Time (F.D.T.) as an intuitive extrapolation of Finite Absorption Time (F.A.T.) concept. This is a plausible extrapolation since drug dissolution takes place under $in\ vivo$ conditions for a finite time regardless of the complete or incomplete dissolution of the dose administered. The finite character of both terms, F.A.T.and F.D.T. is physiologically sound since drug absorption does not take place beyond the absorptive sites while drug dissolution is also not important beyond the absorptive sites. Accordingly, the inception of the F.A.T. and F.D.T. concepts are linked with the physiological constraints of the dissolution and absorption processes under $in\ vivo$ conditions. However, it is not uncommon to see $in\ vitro$ dissolution profiles reaching a plateau value of 100% of dose dissolved at finite time. In this particular case, the term F.D.T. denotes the time needed for the complete dissolution of the drug dose. Besides, the F.D.T. is, in essence, included in the today's regulatory biowaiver guidelines ; this is so since the rapid (<30 min) or very rapid (<15 min) dissolution criterion for the biowaivers imply completion of the dissolution process in finite time. Intuitively, the F.D.T estimate, τ_d, considered under $in\ vivo$ conditions is equal or shorter than the F.A.T. estimate τ, namely, $\tau_d \leq \tau$. For Class II drugs, $\tau_d = \tau$, for Class I and III drugs $\tau_d < \tau$ while for Class IV drugs both relationships i.e., $\tau_d = \tau$ and $\tau_d < \tau$ are possible. We should note that a Class II drug with basic properties can be completely dissolved in the stomach, not precipitate and be absorbed in the intestine and essentially behave like BCS Class I drug.

So far, the mean dissolution behavior of solid drug particles has been quantified with the mean dissolution time (M.D.T.) and the mean dissolution time for saturation (M.D.T.s.) for drugs whose dose is completely or not completely dissolved at the end of the dissolution process, respectively . Both terms correspond to a stochastic interpretation of the dissolution process since the profle of the accumulated fraction of drug amount dissolved from a solid dosage form gives the probability of the residence times of the drug molecules in the dissolution medium. The fraction of drug dissolved is always a distribution function, and therefore it can be characterized by its frst (statistical) moment, which is the M.D.T. The latter term holds only when the entire available drug dose is dissolved completely. When drug particles remain undissolved at the end of the dissolution

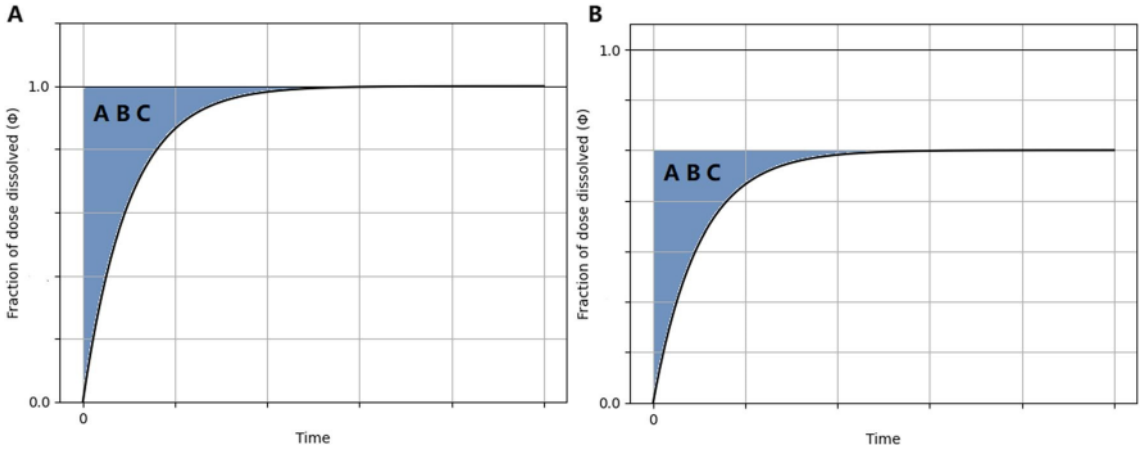

Figure 4.29: Graphical estimation of M.D.T. (A) and M.D.T.s. (B) from the experimental fraction of dose dissolved (Φ)-time data. The shaded region denotes the Area Between the Curves (ABC).

process, the M.D.T. is not defined since it is equal to infinity. In this case, the Mean Dissolution Time for saturation (M.D.T.s.) is coined and refers only to the portion of the dose that is actually dissolved . Unfortunately, the clear distinction between (M.D.T.) and (M.D.T.s.) has neither been recognized nor adopted in the literature so far. In this work, we show that the three parameters, (F.D.T.), (M.D.T.) and (M.D.T.s.), lie in the heart of the biopharmaceutic classification system (BCS); this allowed us to couple dissolution time considerations with BCS. A dissolution-based temporal version of BCS, the so-called T- BCS was developed.

2..1 Theoretical background

The temporal classification of Class I and III drugs whose dose is completely dissolved in the dissolution medium are based on the M.D.T. values, while Class II and IV drugs whose dose is not completely dissolved in the dissolution medium are classified according to their M.D.T.s. values using the time axis $(M.D.T.)^{-1}$ or $(M.D.T.s.)^{-1}$, respectively. In addition, drugs/ formulations which exhibit finite dissolution time (F.D.T.) for complete dissolution of the drug dose can be also classified in Class I or III using the $(F.D.T.)^{-1}$ axis. The dimensionless dose/solubility ratio, q, normalized in terms of the volume (900 mL) of dissolution medium, Eq. 4.1.

$$q = \frac{Dose}{C_s V} \tag{4.1}$$

Graphical estimation of M.D.T. or M.D.T.s

The mean dissolution time (M.D.T.) corresponds to the first moment that can be determined from the experimental dissolution data using the following equation:

$$M.D.T. = \frac{\int_0^{W_\infty} t\, dW(t)}{\int_0^{W_\infty} dW(t)} \tag{4.2}$$

where W(t) is the cumulative amount of drug dissolved at time t. Estimates for M.D.T. or M.D.T.s. can be obtained graphically by calculating the area (ABC) between the fraction of dose dissolved (Φ) – time curve and the plateau level, Fig. 4.29. When the plateau level is equal to one (Φ_∞ =1) an estimate for M.D.T. can be derived from Eq. 4.3, Fig. 4.29a. Similarly, an estimate for M.D.T.s. can be derived from Eq. 4.3 when the plateau level is Φ_∞ <1, Fig. 4.29b.

$$M.D.T.\ or\ M.D.T.s. = \frac{ABC}{\Phi_\infty} \tag{4.3}$$

The Noyes Whitney Equation Model

Since the very first experiment in 1897, dissolution is mathematically described by the Noyes-Whitney equation; the integrated form of the dissolved drug concentration C, as a function of time t indicates that the dissolution profile is exponentially reaching the plateau value, the saturation solubility C_s at infinite time, Eq. 4.2

$$C = C_s[1 - e^{-kt}] \tag{4.4}$$

where k is the dissolution rate constant. This equation can be expressed as a function of the fraction of dose dissolved Φ when q≥1 as follows,

$$\Phi = \frac{1}{q}[1 - e^{-kt}] \tag{4.5}$$

which means that only a portion of the dose is dissolved, and the drug reaches the saturation level 1/q. In this case, the corresponding M.D.T.s. is equal to 1/k. On the contrary, when

q<1, which means that the entire dose is eventually dissolved, the dissolution follows the usual exponential form only until it reaches the value Φ=1, i.e., 100% of the drug is dissolved, in a fnite dissolution time, τ_d and thereafter remains constant,

$$\Phi = \frac{1}{q}[1 - e^{-kt}], for\ t < \tau_d \tag{4.6}$$

and

$$\Phi = 1, for\ t \geq \tau_d \tag{4.7}$$

where:

$$\tau_d = -\frac{ln(1-q)}{k} \tag{4.8}$$

In this case (q<1), the M.D.T. is as follows,

$$M.D.T. = \frac{q - (q-1) - ln(1-q)}{kq} \tag{4.9}$$

which for q=1, i.e., when the dose is equal to the drug amount required to saturate the dissolution medium, collapses to M.D.T.=1/k.

The Weibull Function Model

The Noyes-Whitney equation is distinguished by the assertion that a constant, denoted as the dissolution rate constant k, governs the dissolution rate throughout the process. This foundational premise has faced scrutiny in the literature, leading to the emergence of models featuring time-dependent rate coefficients, which are considered to have greater physical relevance with the time-dependent phenomena that occur as dissolution progresses. In this vein, similar analysis has been published for the Weibull function, which is used extensively for the kinetic description of drug dissolution and release data. Therefore, by replacing the dissolution rate constant, k, with a time-dependent coefficient, namely, $k = k_1 t^{-h}$ in the differential Noyes-Whitney equation expressed in terms of Φ, we end up with:

$$\frac{d\Phi}{dt} = k_1 t^{-h}(\frac{1}{q} - \Phi) \tag{4.10}$$

where k_1 is a constant with $time^{h-1}$ units and h is a dimensionless constant. Solving Eq. 4.10 and replacing $a = \frac{k_1}{1-h}\ and\ b = 1-h$, we get a function of the fraction of dose dissolved Φ when q≥1:

$$\Phi = \frac{1}{q}(1 - e^{at^b}) \tag{4.11}$$

which also means that only a portion of the dose is dissolved, and the drug reaches the saturation level 1/q. The corresponding M.D.T.s. is equal to:

$$M.D.T.s. = a^{-\frac{1}{b}}\Gamma(\frac{1}{b} - 1) \tag{4.12}$$

Where Γ(·) is the complete and Γ(·,·) is the incomplete gamma function.

When q<1, the solution takes a branched form as follows:

$$\Phi = \frac{1}{q}(1 - e^{at^b}), for\ t < \tau_d \tag{4.13}$$

and

$$\Phi = 1, for\ t \geq \tau_d \tag{4.14}$$

where:

$$\tau_d = (-\frac{ln(1-q)}{a})^{(\frac{1}{b})} \tag{4.15}$$

In this case (q<1), where 100% of the initial dose is dissolved, the M.D.T. is given by:

$$\frac{1}{bqa^{1/b}}[b(q-1)(-ln(1-q)^{1/b} - \Gamma(\frac{1}{q}, -ln(1-q)) + \Gamma(\frac{1}{b})] \tag{4.16}$$

which for q=1 turns into:

$$M.D.T. = a^{-\frac{1}{b}}\Gamma(\frac{1}{b} - 1) \tag{4.17}$$

The Reaction - Limited Dissolution Model

The reaction limited model, which relies on a bidirectional chemical reaction involving the undissolved drug species, the freely available solvent molecules, and the resulting drug-solvent complex

was also used for the computational work. It's important to note that this study's foundation relies upon two earlier studies, i.e., conducted by Dokoumetzidis and Macheras in 1997 and by Lansky and Weiss in 1999 [19]. The fundamental differential equation expression describing the rate of the dissolution process, is as follows [17]:

$$\frac{dC}{dt} = k_1^*(\frac{D}{V} - C)^\lambda - k_{-1}C \tag{4.18}$$

where $k_1^* = k_1'[molecularweight]^{(1-\lambda)}$ ($k_1' = k_1[w_0]^b$), where $[w_0]$ is the initial concentration of the free species), D is the initial quantity (dose) in mass units and λ is a dimensionless constant. Equations 4.19-4.21 provide the mathematical foundation for understanding drug dissolution under various conditions, encompassing scenarios with both homogeneous (λ=1) (Eq. 4.19) and solvent-abundant ($\lambda \neq 1$) conditions(Eq. 4.20-4.21):

$$\Phi = \frac{1}{q_{ss}}(1 - e^{(-(k_1^* + k_{-1})t)}) \tag{4.19}$$

$$\frac{dC}{dt} = k_1^*(\frac{D}{C})^\lambda \tag{4.20}$$

$$C = \frac{D}{V} - [(\frac{D}{V})^{1-\lambda} - (1-\lambda)k_1^* t]^{1/(1-\lambda)} \tag{4.21}$$

Equation 4.21 has the form of a power-law and can be fitted to experimental dissolution data. Unlike the Noyes-Whitney and Weibull models, a formula for the M.D.T. and M.D.T.s. can not be derived, and can only be computed through numerical methods for both λ=1 and $\lambda \neq 1$ cases . Consequently, a numerical calculation for the M.D.T. and M.D.T.s., employing Eq. 4.2 at its basis, was the sole method used for estimation of these parameters.

2..2 Results of the analysis of the dissolution data

The drugs/drug products are listed in Table 4.10 alongside with their BCS classification according to various literature references.

Once the F.D.T. and M.D.T. (for Class I and III drugs) and the M.D.T.s. (for Class II and IV) values (h) were estimated graphically as described above in the Methods section, they were plotted with the normalized Dose/ Solubility ratio, q, which was calculated for each drug product individually using Eq. 2.50. The dose that was utilized was the highest dose (mg) and the solubility C_s (mg/mL) corresponding to the three pH values (1.2, 4.5 and 6.8) that all the dissolution tests were carried out. For the volume of the dissolution medium, V (mL), we employed the actual volume of the medium that was used in the dissolution tests in the literature (900 mL). It is important to note that within the context of the biopharmaceutics classification system (BCS), the specified volume is set at 250 mL, aligning with the typical volume of gastrointestinal fluids. The calculation of the M.D.T. and M.D.T.s. value was feasible only for the dissolution curves that unequivocally attained a plateau. Despite our efforts to obtain M.D.T. and M.D.T.s. values for each of the pH levels across all drug products, this was not achievable in certain instances. Similarly, the estimation of the F.D.T. values for Class I and III drugs was not feasible in cases where the dissolution medium led to a plateau less than 100% dissolved. Plotting the 1/M.D.T. or 1/F.D.T. values with the normalized q for Class I and III drugs and the 1/M.D.T.s. values again with their corresponding q values, in the lines of the T-BCS frame, we obtain 4.31. In a similar vein, we plotted the M.D.T., M.D.T.s. and τd that were obtained through the Noyes-Whitney and Weibull fittings with the corresponding normalized Dose/ Solubility ratios, q, resulting in 4.31.

Table 4.9: BCS classification of drugs used in our dissolution analysis. The categorization primarily relies on their respective monograph classifications as documented in the literature. Drugs marked with an asterisk (*) signify dual classifications.

Drug name-Product	BCS Classification
Moxifloxacin Hydrochloride - (Avelox/Moxiflox)	Class I
Zidovudine (Azidothymidine) - (Virex/Lazid/Combivir)	Class I
Sitagliptin Phosphate Monohydrate	Class I
Stavudine	Class I
Primaquine Phosphate	Class I
Amoxicillin Trihydrate - (Innovator/Generic A)	Class I/IV*
Lamivudine - (Epivir/Aspen)	Class I/III*
Enalapril Maleate - (Vasotec)	Class III
Proguanil Hydrochloride - (Paludrine)	Class III
Metformin Hydrochloride	Class III
Acyclovir - (Zovirax)	Class III/IV*
Cimetidine - (Tagamet)	Class III
Paracetamol - (Panadol Extra)	Class I/III*
Metoclopramide	Class III
Ketoprofen - (Test/Reference Product)	Class II
Efavirez - (Sustiva)	Class II/IV*
Rifampicin	Class II
Ibuprofen	Class I/II*
Nifedipine	Class I/II*
Piroxicam	Class I/II*
Carbamazepine	Class II
Amodiaquine Hydrochloride	Class III/IV*
Ciprofloxacin Hydrochloride	Class II/IV*
Folic Acid	Class II/IV*
Furosemide	Class III/IV*

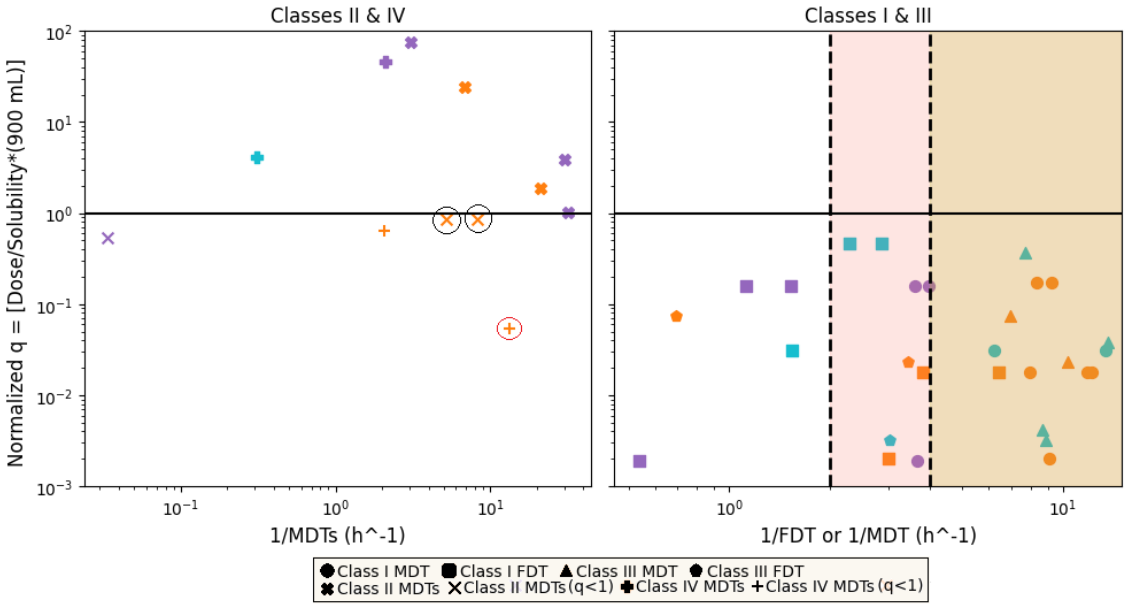

Figure 4.30: Temporal Biopharmaceutics Classification System (T-BCS) with scattered experimental data from the drugs listed in Table II. For both subplots, the ordinate axis indicates the normalized dose/solubility ratio, q, in term of the volume of dissolution medium (900 mL), corresponding to the lowest solubility. On the left subplot, the horizontal time axis (h^{-1}, logarithmic scale) corresponds to (1/M.D.T.s.) values for Class II and IV drugs. On the right subplot, the horizontal time axis (h^{-1}, logarithmic scale) corresponds to (1/M.D.T.) or (1/F.D.T.) values for Class I and III drugs. The shaded regions indicate the areas for drugs exhibiting rapid (30 min, pink shade at the 2 h^{-1} mark) or very rapid (15 min, beige shade marked at the 4 h^{-1} mark) dissolution in terms of the biowaiver's criteria. Orange data points correspond to dissolution medium of pH 1.2, purple data points correspond to dissolution medium of pH 4.5 and blue data points correspond to dissolution medium of pH 6.8.

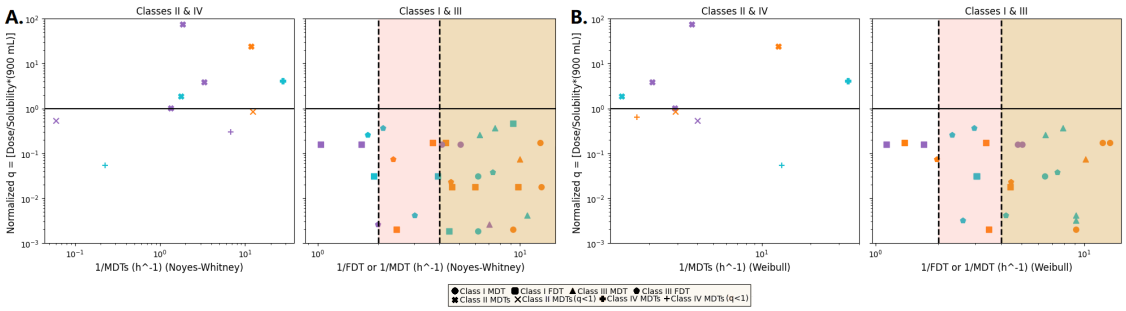

Figure 4.31: Temporal Biopharmaceutics Classification System (T-BCS) with scattered experimental data from the drugs listed in Table II. For both plots, the ordinate axis indicates the normalized dose/solubility ratio, q, in term of the volume of dissolution medium (900 mL), corresponding to the lowest solubility. On the left subplots, the horizontal time axis (h^{-1}, logarithmic scale) corresponds to (1/M.D.T.s.) values for Class II and IV drugs whereas on the right subplots, the horizontal time axis (h^{-1}, logarithmic scale) corresponds to (1/M.D.T.) or (1/F.D.T.) values for Class I and III drugs. The M.D.T., τ_d and M.D.T.s. values were calculated according to the expressions of Table I based on the Noyes-Whitney equation (Plot A) and Weibull function (Plot B). The shaded regions indicate the areas for drugs exhibiting rapid (30 min, pink shade at the 2 h^{-1} mark) or very rapid (15 min, beige shade marked at the 4 h^{-1} mark) dissolution in terms of the biowaiver's criteria. Orange data points correspond to dissolution medium of pH 1.2, purple data points correspond to dissolution medium of pH 4.5 and blue data points correspond to dissolution medium of pH 6.8.

Regarding Fig. 4.30, theoretically, one would anticipate q values for Class I and III drugs to be less than 1 because their solubility in the pH range should enable them to fully dissolve the highest dose in the given volume (900 mL). In fact, all Class I and III drugs satisfy the inequality q<1 while most of the data points lie beyond the 2 h^{-1} mark (>80% of the total Class I and III data points) (less than 30 min-rapidly dissolved limit for biowaiver status granting), Fig. 4.30. In parallel, q values for Class II and IV drugs should exceed 1 due to their solubility limitations, resulting in a saturated solution at the end of the dissolution process. However, some observations deviated from this expectation, Fig. 4.30. In this vein, enclosed data points for Class II and IV drugs with q<1 are noted. Black circles highlight drugs (ketoprofen and piroxicam) previously classifed in Classes I and II of the BCS. Red circle mark drug (amodiaquine hydrochloride) previously classified in Classes III and IV of the BCS. It should be noted that the classification in Fig. 4.30 relies on a fixed volume of 900 mL and reveals that less than 50% of the Class II and IV dataset (5 out of 12, accounting for 41.67%) is positioned below the threshold of q=1 and almost all are positioned within the range of q=0.1 to q=1, as evident when considering the logarithmic scale, Fig. 4.30.

The exact location of the drug in the x-axis coupled with the q value quantifies the Class II or IV character within each T-BCS region, individual points are defined by their specific q and M.D.T./M.D.T.s. values. This implies that the positioning of these data points reflects the heterogeneous nature of compounds within the same class. When considering Class II and IV data points, it becomes crucial to account for two factors: the q value, which directly stems from the solubility of the compound, and the M.D.T.s. values, particularly their relative placement in relation to the borderline with the M.D.T. values. The precise coordinates of these data points serve as a quantitative measure that sheds light on the compound's behavior and the interplay between the two dissolution mechanisms. As elaborated before, it's important to note that under both $in\ vitro$ and $in\ vivo$ conditions, a single mechanism does not exclusively operate. The inadequacy of the reaction-limited mechanism is intricately linked to the complexity arising from the simultaneous involvement of multiple dissolution mechanisms in these scenarios.

As evident from Figs. 4.31A and 4.31B, the data points conform to the same pattern observed in Fig. 4.30. Most of the Class I and III drugs are positioned beyond the 2 h^{-1} threshold, indicating that they exhibit mean dissolution and finite dissolution times of less than 30 min, which is the time limit for rapidly dissolved drugs. Similarly, an equivalent number of data points pertaining

to Class II and IV drugs are situated below the q=1 line, as previously explained in the context of Fig. 4.31. When compared, Figs. 4.30, 4.31A and 4.31B show a slightly different data point distribution. Noteworthy data points in Figs. 4.30 and 4.31, beyond the 10 h^{-1} threshold and below the q=1 threshold, belonging to either Class I/II or III/IV, exhibited release and dissolution profiles that are akin to drugs from Class I/III that reach % dissolved profiles>85% in 30 min. In fact, similar dissolution profiles for ketoprofen piroxicam and amodiaquine hydrochloride in dissolution media 1.2 were reported. Thus, analysis of the dissolution data revealed that, these drugs exhibit dissolution profiles exceeding 86% dissolved within approximately 45 min for piroxicam, less than 30 min for ketoprofen, and less than 60 min for amodiaquine hydrochloride. This underscores the substantial influence of their dual classification (Class I/II for ketoprofen, piroxicam and III/IV for amodiaquine hydrochloride) on their dissolution profiles, particularly evident in the case of ketoprofen.

Our next goal was to explore potential relationships between the various M.D.T. and M.D.T.s. values, estimated using the Noyes-Whitney equation, the Weibull function, and the reaction-limited model of dissolution with those calculated from the graphical method, which simply relies on the experimental data using Eq. 2.51. To visualize and quantify the relationships among these three sets of models, we generated a correlation plot, Fig. 4.32; the inspection of the plots reveals that the Weibull function has the best performance since in both plots the slope of the regression lines is close to unity and the intercept is close to zero. The corresponding correlation coefficients, R^2 are 0.83 for Class I/III drugs and 0.56 for Class II/IV drugs. These values are supportive for the correlation of the variables (parameters) analyzed if one considers the diversity of data in terms of inter-and intraclass variation (both q>1 and q<1 Class II/IV drugs are included) and the longer (double) time span of the Class II/ IV drugs' data in comparison with the Class I/III drugs' data. It seems that the Weibull function captures much better the dynamics of the dissolution process across all data analyzed since the fundamental differential equation (Equation 2.59) describes a first-order process with a time dependent coefficient driving the dissolution rate. In fact, the analytical power of the Weibull function for the discernment of dissolution-release process in homogeneous /heterogeneous media have been previously depicted in. Regarding the Noyes Whitney model for both Classes I/III and II/IV drugs the intercept is close to zero, the slopes are 0.61 and 1.10 and the correlation coefficients are 0.63 and 0.58, respectively. These results show that the Noyes Whitney

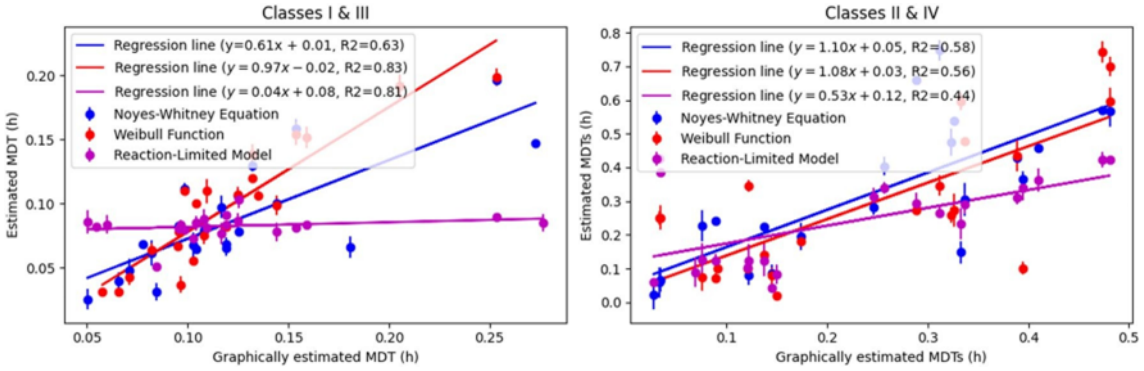

Figure 4.32: Temporal parameters correlation plot: The left and right subplots contain experimental data (h) for Class I/III and estimated values (h) using the Noyes-Whitney (blue), Weibull function (red), and reaction-limited model (purple), while the abscissa presents graphically calculated M.D.T. values (h). Each model's color-coded trendline derived from linear regression analysis is also shown in the legends.

model has comparable performance with the Weibull model only for Classes II/IV drugs. This can be associated with recent findings, which indicate that soluble compounds follow the diffusion limited model, while sparingly soluble drugs follow the reaction limited model of dissolution. In the same vein, for the reaction-limited model, the most noticeable observation is the lack of correlation for Class I/III drugs, with a correlation coefficient of only 0.04.

Although the better performance of the Weibull model is perhaps not surprising given it provides a more "flexible" fit compared to Noyes Whitney, the poor performance of the reaction-limited model even for BCS II/IV drugs requires consideration in the light of the dissolution mechanisms operating under $in\ vitro$ and $in\ vivo$ conditions. After so many years of drug dissolution research, the prevailing dissolution mechanism relies on the diffusion layer model; however, there are many reports in literature which justify the reaction-limited dissolution model. For example, in a 2022 study, Sleziona et al. discussed the particle dissolution behavior of a highly soluble and a sparingly soluble compound using a theoretical geometrical phase-field approach. They confirmed that the prevailing mechanism in the case of the highly soluble compound was indeed the diffusion layer model whereas the reaction limited, in their case surface-reaction limited, case was the prevailing model for the sparingly soluble compound. This theoretical work is related to two previously published studies. In the former study, carried out under hydronamically controlled in vitro conditions, the two mechanisms seem to operate simultaneously. The latter study links the supersaturated phenomena, which are usually encountered with Class II and IV drugs with the reaction-limited model of drug dissolution. Overall, there has not been a single case where a com-

pound follows only a single mechanism to the full extent under in vitro and $in\ vivo$ conditions. It is obvious that easily dissolved drugs (like Class I and III drugs) have much shorter finite dissolution time values and more simple dissolution profiles in comparison with sparingly soluble drugs which have much longer M.D.T.s and more complex dissolution profiles (s-shaped). This means that when we attempt to correlate $in\ vitro$ and $in\ vivo$ results, it is much more difficult to predict Class II and Class IV behavior instead of the other two classes. Finally, it should be noted that all phenomena stated above are a function of the agitation rate which are dramatically different under $in\ vitro$ and $in\ vivo$ conditions. Based on all above,the poor performance of the reaction limited model of dissolution, using various drugs from different BCS classes under $in\ vitro$ and $in\ vivo$ conditions is a plausible result.

The mean and median estimates and their standard deviation and range, respectively, of the M.D.T., M.D.T.s. and τ_d parameters are listed in Table III for Class I/III and Class II/ IV drugs. A comparison of mean with the median estimates reveals their similarity except for the M.D.T.s. graphical and Noyes Whitney estimates and to a lesser degree reaction limited estimates for Class II and IV drugs. For these three sets of results the median is more appropriate as a measure of the central tendency of the data. In all other cases, the mean describes the data adequately. It should be also noted that the Weibull function had the best performance in terms of statistical performance since for all parameters studied for Class I/III and II/IV drugs the mean estimates were associated with small standard deviations and the corresponding median values were very similar. Although the sample is small (see Table II), the magnitude of the parameters roughly follows the expected ranking M.D.T.$<\tau_d<$M.D.T.s. It should be noted that the inequality M.D.T.$<\tau_d$ is reasonable since M.D.T. reflects the mean behaviour of solid particles in terms of the time scale of the dissolution process while τ_d refers to the time for the completion of the dissolution process of the solid drug particles. In this vein, the M.D.T. estimates being 2–3 folds shorter than τ_d should not be used as metrics for the rapid or very rapid dissolving drug classification. Nevertheless, the M.D.T. and τ_d estimates are useful if contrasted with the F.A.T. estimates derived from the analysis of blood concentration time data or the percent absorbed versus time plots for the development of $in\ vitro$ - $in\ vivo$ correlations.

Table 4.10: Mean (± SD) and median (range) time parameters estimates using the graphical and modeling approaches for Class I/III and Class II/IV drugs listed in Table 2.

Model	Temporal parameter	Class I/III	Class II/IV
Graphical	τ_d (h)	0.28 (± 0.4)[mean] 0.33 (0.086-1.86)[median]	-
	M.D.T. (h)	0.13 (± 0.06)[mean] 0.109 (0.050-0.373)[median]	-
	M.D.T.s. (h)	-	2.3 (± 7) [mean] 0.32 (0.027-30) [median]
Noyes-Whitney	τ_d (h)	0.35 (± 0.2)[mean] 0.29 (0.084-0.97)[median]	-
	M.D.T. (h)	0.098 (± 0.05)[mean] 0.083 (0.026-0.24)[median]	-
	M.D.T.s. (h)	-	2.7 (± 6) [mean] 0.42 (0.018-24) [median]
Weibull	τ_d (h)	0.33 (± 0.16)[mean] 0.29 (0.084-0.88)[median]	-
	M.D.T. (h)	0.11 (± 0.05)[mean] 0.106 (0.031-0.21)[median]	-
	M.D.T.s. (h)	-	0.27 (± 0.2) [mean] 0.25 (0.018-0.74)[median]
Reaction-limited	τ_d (h)	-	-
	M.D.T. (h)	0.07917 (± 0.00882) [mean] 0.08093 (0.05143-0.10293) [median]	-
	M.D.T.s. (h)	-	0.46 (± 0.7)[mean] 0.29 (0.034-3.2)[median]

Chapter 5

Conclusions

In conclusion, the accurate estimation of τ holds paramount significance, especially when considering its relative magnitude in relation to gastrointestinal (GI) transit time, alongside the biopharmaceutical classification of the studied drugs. This crucial information is indispensable for the proper treatment and interpretation of data in the context of oral drug absorption. The concept of finite absorption time (F.A.T.) emerges as a physiologically sound framework in this study. The derived estimate of τ, obtained through the analysis of oral data using an immediate release formulation, stands out as a distinctive characteristic of each drug. It becomes evident from this investigation that oral drug absorption is inherently terminated within a finite time frame. This achievement relies on the physiologically relevant first-order under sink conditions absorption principle, emphasizing the rate-limiting role of BCS Class-dependent parameters such as solubility and permeability. The developed PBFTPK models, rooted in the finite time absorption concept, exhibit promising results, opening avenues for their application in various pharmaceutical research domains. The PBFTPK models, mark the dawn of a new era in both scientific and regulatory aspects of biopharmaceutical sciences. This paradigm shift extends its influence beyond fundamental topics like bioavailability and bioequivalence, impacting areas such as $in\ vitro - in\ vivo$ correlations and interspecies pharmacokinetic scaling. Notably, the exclusive reliance on oral data for estimating absolute bioavailability may lead to significant regulatory considerations. In essence, this study not only advances our comprehension of oral drug absorption but also prompts a reevaluation of established practices with broader implications for pharmaceutical research and development.

An immediate implication of the Finite Absorption Time (F.A.T.) concept is the consideration of $in\ vivo$ drug dissolution within the confines of physiological time constraints. Specifically, $in\ vivo$ drug dissolution operates within a finite dissolution time (F.D.T.), denoted as τ_d [51], which is either equal to or shorter than the F.A.T., expressed as $\tau_d \leq \tau$. This inequality, along with the concepts of mean dissolution time (M.D.T.) and mean dissolution time for saturation (M.D.T.s.), was recently investigated in a separate study, culminating in the development of a quantitative classification framework known as the Temporal-Biopharmaceutics Classification System (T-BCS) [51]. Although BCS is fundamentally a qualitative system used for categorizing drugs based on their solubility and permeability characteristics, the T-BCS introduces a novel dimension by complementing and expanding a previously reported quantitative biopharmaceutical classification system. This approach enables the establishment of correlations, the assessment of

magnitudes of time dissolution parameters, and the comparison of different drugs, offering valuable insights into the classification of drugs within the BCS framework.

The central message conveyed by our study is that the calculations of the percentage of absorbed drug are both physically and physiologically accurate. Consequently, their incorporation into the construction of In Vitro-In Vivo Correlations ($IVIVC$) stands on solid scientific ground. Simultaneously, the gradual application of physiologically based time constraints for the percentage of drug dissolved, as outlined in the preceding paragraph, is anticipated to enhance $IVIVC$, thereby improving the predictability of both published and, notably, unpublished $IVIVC$. In alignment with this perspective, Alimpertis et al. (2024) [52] reevaluated $IVIVC$, integrating the physiologically sound F.A.T. and F.D.T. concept. This revision led to the creation of a modified Levy plot, offering enhanced physiological insights into $in\ vivo$ and $in\ vitro$ drug dissolution/absorption processes [52].

Lastly, the inherently ”top-down” nature of Physiologically Based Finite Transit-Compartment Perfusion-Permeation Kinetic (PBFTPK) models, rooted in the F.A.T. concept, can complementary be employed with physiologically based pharmacokinetic (PBPK) models, characterized as ”bottom-up.” This combined approach facilitates a more comprehensive understanding of drug absorption phenomena. The integration of PBFTPK models enhances the analytical power of population analysis in addressing various aspects of drug absorption phenomena.

Bibliography

[1] P. Macheras, *Στοιχεία Βιοφαρμακευτικής Φαρμακοκινητικής*. Αθήνα: Ιδιωτική Έκδοση, 1984.

[2] P. Macheras, 'On an unphysical hypothesis of Bateman equation and its implications for pharmacokinetics', *Pharmaceutical research*, vol. 36, pp. 1–3, 2019.

[3] P. Macheras and P. Chryssafidis, 'Revising pharmacokinetics of oral drug absorption: I models based on biopharmaceutical/physiological and finite absorption time concepts', *Pharmaceutical Research*, vol. 37, pp. 1–13, 2020.

[4] P. Chryssafidis, A. A. Tsekouras, and P. Macheras, 'Re-writing oral pharmacokinetics using physiologically based finite time pharmacokinetic (PBFTPK) models', *Pharmaceutical Research*, vol. 39, no. 4, pp. 691–701, 2022.

[5] P. Chryssafidis, A. A. Tsekouras, and P. Macheras, 'Revising pharmacokinetics of oral drug absorption: II bioavailability-bioequivalence considerations', *Pharmaceutical Research*, vol. 38, pp. 1345–1356, 2021.

[6] P. Macheras and C. Reppas, *Βιοφαρμακευτική*. Αθήνα: Ιδιωτική Έκδοση, 1992.

[7] D. Wu, A. A. Tsekouras, P. Macheras, and F. Kesisoglou, 'Physiologically based pharmacokinetic models under the prism of the finite absorption time concept', *Pharmaceutical Research*, vol. 40, no. 2, pp. 419–429, 2023.

[8] P. Macheras and A. A. Tsekouras, 'Columbus' egg: Oral drugs are absorbed in finite time', *European Journal of Pharmaceutical Sciences*, p. 106265, 2022.

[9] A. A. Tsekouras and P. Macheras, 'Re-examining digoxin bioavailability after half a century: Time for changes in the bioavailability concepts', *Pharmaceutical Research*, vol. 38, no. 10, pp. 1635–1638, 2021.

[10] N. Alimpertis, A. A. Tsekouras, and P. Macheras, 'Revising the assessment of bioequivalence in the light of finite absorption time (FAT) concept: the axitinib case', in *30th PAGE meeting Ljubljana*, 2022, vol. 28.

[11] N. Alimpertis, A. A. Tsekouras, and P. Macheras, 'Revamping Biopharmaceutics-Pharmacokinetics with Scientific and Regulatory Implications for Oral Drug Absorption', *Pharmaceutical Research*, vol. 40, no. 9, pp. 2167–2175, 2023.

[12] A. Charalabidis, M. Sfouni, C. Bergström, and P. Macheras, 'The biopharmaceutics classification system (BCS) and the biopharmaceutics drug disposition classification system (BDDCS): beyond guidelines', *International journal of pharmaceutics*, vol. 566, pp. 264–281, 2019.

[13] R. H. Manzo, M. E. Olivera, G. L. Amidon, V. P. Shah, J. B. Dressman, and D. M. Barends, 'Biowaiver monographs for immediate release solid oral dosage forms: Amitriptyline hydrochloride', *Journal of pharmaceutical sciences*, vol. 95, no. 5, pp. 966–973, 2006.

[14] D. Thambavita *et al.*, 'Biowaiver monograph for immediate-release solid oral dosage forms: amoxicillin trihydrate', *Journal of pharmaceutical sciences*, vol. 106, no. 10, pp. 2930–2945, 2017.

[15] J. B. Dressman *et al.*, 'Biowaiver monograph for immediate-release solid oral dosage forms: acetylsalicylic acid', *Journal of pharmaceutical sciences*, vol. 101, no. 8, pp. 2653–2667, 2012.

[16] N. A. Charoo *et al.*, 'Biowaiver monograph for immediate-release solid oral dosage forms: bisoprolol fumarate', *Journal of pharmaceutical sciences*, vol. 103, no. 2, pp. 378–391, 2014.
[17] G. F. Plöger *et al.*, 'Biowaiver monographs for immediate release solid oral dosage forms: cephalexin monohydrate', *Journal of Pharmaceutical Sciences*, vol. 109, no. 6, pp. 1846–1862, 2020.
[18] E. Jantratid *et al.*, 'Biowaiver monographs for immediate release solid oral dosage forms: Doxycycline hyclate', *Journal of pharmaceutical sciences*, vol. 99, no. 4, pp. 1639–1653, 2010.
[19] N. Charoo *et al.*, 'Biowaiver monographs for immediate release solid oral dosage forms: Fluconazole," *Journal of pharmaceutical sciences*, vol. 103, no. 12, pp. 3843-3858, 2014, 2014.
[20] M. Petruševska *et al.*, 'Biowaiver monographs for immediate release solid oral dosage forms: levetiracetam', *Journal of Pharmaceutical Sciences*, vol. 104, no. 9, pp. 2676–2687, 2015.
[21] G. S. Rajawat *et al.*, 'Biowaiver monograph for immediate-release solid oral dosage forms: ondansetron', *Journal of pharmaceutical sciences*, vol. 108, no. 10, pp. 3157–3168, 2019.
[22] L. Kalantzi *et al.*, 'Biowaiver monographs for immediate release solid oral dosage forms: Acetaminophen (paracetamol)', *Journal of pharmaceutical sciences*, vol. 95, no. 1, pp. 4–14, 2006.
[23] C. A. S. Bergström, S. B. E. Andersson, J. H. Fagerberg, G. Ragnarsson, and A. Lindahl, 'Is the full potential of the biopharmaceutics classification system reached?', *European Journal of Pharmaceutical Sciences*, vol. 57, pp. 224–231, 2014.
[24] Y. Zhai *et al.*, 'Bioequivalence Study of Amitriptyline Hydrochloride Tablets in Healthy Chinese Volunteers Under Fasting and Fed Conditions', *Drug Design, Development and Therapy*, pp. 3131–3142, 2020.
[25] M. Kandeel, 'Pharmacokinetics and oral bioavailability of amoxicillin in chicken infected with caecal coccidiosis', *Journal of Veterinary Pharmacology and Therapeutics*, vol. 38, no. 5, pp. 504–507, 2015.
[26] H. A. Elsheikh, A. A. Taha, A. E. Khalafalla, I. A. M. Osman, and I. A. Wasfi, 'Pharmacokinetics of amoxicillin trihydrate in Desert sheep and Nubian goats', *Veterinary Research Communications*, vol. 23, pp. 507–514, 1999.
[27] J. Autmizguine *et al.*, 'Pharmacokinetics and pharmacodynamics of oral cephalexin in children with osteoarticular infections', *The Pediatric infectious disease journal*, vol. 32, no. 12, pp. 1340–1344, 2013.
[28] A.-S. Malmborg, 'Bioavailability of doxycycline monohydrate: a comparison with equivalent doses of doxycycline hydrochloride', *Chemotherapy*, vol. 30, no. 2, pp. 76–80, 1984.
[29] L. A. Meijer, K. G. F. Ceyssens, B. De Greve, and W. De Bruijn, 'Pharmacokinetics and bioavailability of doxycycline hyclate after oral administration in calves', *Veterinary Quarterly*, vol. 15, no. 1, pp. 1–5, 1993.
[30] J. L. Davis, J. H. Salmon, and M. G. Papich, 'Pharmacokinetics and tissue distribution of doxycycline after oral administration of single and multiple doses in horses', *American journal of veterinary research*, vol. 67, no. 2, pp. 310–316, 2006.
[31] J. B. Bogardus and R. K. Blackwood Jr, 'Solubility of doxycycline in aqueous solution', *Journal of pharmaceutical sciences*, vol. 68, no. 2, pp. 188–194, 1979.

[32] S. Strauch, E. Jantratid, and J. B. Dressman, ‘Comparison of WHO and US FDA biowaiver dissolution test conditions using bioequivalent doxycycline hyclate drug products’, *Journal of Pharmacy and Pharmacology*, vol. 61, no. 3, pp. 331–337, 2009.
[33] E. M. Nash and K. S. Sangha, ‘Levetiracetam’, *American journal of health-system pharmacy*, vol. 58, no. 13, pp. 1195–1199, 2001.
[34] F. Roila and A. Del Favero, ‘Ondansetron clinical pharmacokinetics’, *Clinical pharmacokinetics*, vol. 29, no. 2, pp. 95–109, 1995.
[35] P. V. Colthup, C. C. Felgate, J. L. Palmer, and N. L. Scully, ‘Determination of ondansetron in plasma and its pharmacokinetics in the young and elderly’, *Journal of pharmaceutical sciences*, vol. 80, no. 9, pp. 868–871, 1991.
[36] M. D. Rawlins, D. B. Henderson, and A. R. Hijab, ‘Pharmacokinetics of paracetamol (acetaminophen) after intravenous and oral administration’, *European journal of clinical pharmacology*, vol. 11, pp. 283–286, 1977.
[37] R. B. Raffa *et al.*, ‘Pharmacokinetics of oral and intravenous paracetamol (acetaminophen) when co-administered with intravenous morphine in healthy adult subjects’, *Clinical Drug Investigation*, vol. 38, pp. 259–268, 2018.
[38] L. R. Shaw, W. J. Irwin, T. J. Grattan, and B. R. Conway, ‘The effect of selected water-soluble excipients on the dissolution of paracetamol and ibuprofen’, *Drug development and industrial pharmacy*, vol. 31, no. 6, pp. 515–525, 2005.
[39] B. Ameer, M. Divoll, D. R. Abernethy, D. J. Greenblatt, and L. Shargel, ‘Absolute and relative bioavailability of oral acetaminophen preparations’, *Journal of pharmaceutical sciences*, vol. 72, no. 8, pp. 955–958, 1983.
[40] C. Norkus, D. Rankin, and B. KuKanich, ‘Pharmacokinetics of intravenous and oral amitriptyline and its active metabolite nortriptyline in Greyhound dogs’, *Veterinary anaesthesia and analgesia*, vol. 42, no. 6, pp. 580–589, 2015.
[41] G. Paintaud, G. Alván, M. L. Dahl, A. Grahnen, J. Sjövall, and J. O. Svensson, ‘Nonlinearity of amoxicillin absorption kinetics in human’, *European journal of clinical pharmacology*, vol. 43, pp. 283–288, 1992.
[42] S. Ito, R. Oka, A. Tsuchida, and H. Yoshioka, ‘Disposition of single-dose intravenous and oral aspirin in children’, *Developmental pharmacology and therapeutics*, vol. 17, no. 3–4, pp. 180–186, 1991.
[43] A. Sairaku *et al.*, ‘Head-to-head comparison of the heart rate variability between the bisoprolol transdermal patch and bisoprolol fumarate tablet’, *Cardiovascular Therapeutics*, vol. 36, no. 3, p. e12325, 2018.
[44] A. Chicoine, W. Cox, L. Huang, G. Wang, and P. Dowling, ‘Bioavailability and pharmacokinetics of a novel cephalexin oral paste formulation in fed and fasted dogs’, *Journal of veterinary pharmacology and therapeutics*, vol. 32, no. 4, pp. 400–402, 2009.
[45] E. A. Abu-Basha, N. M. Idkaidek, and T. M. Hantash, ‘Pharmacokinetics and bioavailability of doxycycline in ostriches (Struthio camelus) at two different dose rates’, *Journal of veterinary science*, vol. 7, no. 4, pp. 327–332, 2006.
[46] F. G. Latimer, C. M. H. Colitz, N. B. Campbell, and M. G. Papich, ‘Pharmacokinetics of fluconazole following intravenous and oral administration and body fluid concentrations of fluconazole following repeated oral dosing in horses’, *American journal of veterinary research*, vol. 62, no. 10, pp. 1606–1611, 2001.

[47] M. J. Beasley and D. M. Boothe, ‘Disposition of extended release levetiracetam in normal healthy dogs after single oral dosing’, *Journal of Veterinary Internal Medicine*, vol. 29, no. 5, pp. 1348–1353, 2015.
[48] J. M. Quimby, R. C. Lake, R. J. Hansen, P. J. Lunghofer, and D. L. Gustafson, ‘Oral,subcutaneous, and intravenous pharmacokinetics of ondansetron in healthy cats’, *Journal of veterinary pharmacology and therapeutics*, vol. 37, no. 4, pp. 348–353, 2014.
[49] H. C. Atkinson, I. Stanescu, C. Frampton, I. I. Salem, C. P. H. Beasley, and R. Robson, ‘Pharmacokinetics and bioavailability of a fixed-dose combination of ibuprofen and paracetamol after intravenous and oral administration’, *Clinical Drug Investigation*, vol. 35, pp. 625–632, 2015.
[50] G. Charkoftaki, A. Dokoumetzidis, G. Valsami, and P. Macheras, ‘Elucidating the Role of Dose in the Biopharmaceutics Classification of Drugs: The Concepts of Critical Dose, Effective In Vivo Solubility, and Dose-Dependent BCS’, *Pharmaceutical Research*, vol. 29, pp. 3188-3198, 2012.
[51] A. Simitopoulos, A. A. Tsekouras, and P. Macheras, ‘Coupling Drug Dissolution with BCS’, *Pharmaceutical Research*, Accepted for Publication, 2024.
[52] N. Alimpertis, A. Simitopoulos, A. A. Tsekouras, and P. Macheras, ‘IVIVC Revised], *Pharmaceutical Research*, pp. 1-12, 2024.